Michael Oberaigner, BSc

Specimen preparation for electron tomography by electrochemical thinning

MASTER'S THESIS

to achieve the university degree of

Diplom-Ingenieur

Master's degree programme: Technical Physics

submitted to

Graz University of Technology

Supervisor

Ao.Univ.-Prof. Dipl.-Ing. Dr.techn. Gerald Kothleitner

Co – Supervisor

Dipl.-Ing. Dr. Georg Haberfehlner, BSc

Institute of Electron Microscopy and Nanoanalysis

Graz, November 2019

AFFIDAVIT

I declare that I have authored this thesis independently, that I have not used other than the declared sources/resources, and that I have explicitly indicated all material which has been quoted either literally or by content from the sources used. The text document uploaded to TUGRAZonline is identical to the present master‘s thesis.

_____ _____

Date Signature

Kurzfassung

Elektronentomographie ermöglicht eine qualitative und quantitative Analyse von dreidimensionalen Strukturen im Nanobereich. Dazu wird eine Bilderserie aus unterschiedlichen Kippwinkeln in einem Transmissionselektronmikroskop aufgenommen, woraus das dreidimensionale Objekt rekonstruiert werden kann. Um dieses Verfahren anwenden zu können, werden hohe Anforderungen an das Präparat gestellt. Die Probendicke muss von jedem gemessenen Kippwinkel unterhalb des maximal erlaubten Wertes sein und hängt unter anderem vom verwendeten Signal sowie Material ab. Die Elektronenenergieverlustspektroskopie stellt dabei die höchste Anforderung mit einer typischen maximalen Dicke von 100 nm. Die optimale Form der Probe ist daher eine Nadel mit einem maximalen Durchmesser von 100 nm, in Form einer sogenannte Nanospitze. Solche Nanospitzen können unter anderem durch elektrochemischen Abtrag hergestellt werden. Dazu wird eine Probe mit symmetrischem Querschnitt als Anode in einer Elektrolysezelle verwendet und durch das Abtragen der Durchmesser bis zur Nanospitze geätzt.

Diese Arbeit beschäftigt sich mit der Implementierung eines Arbeitsablaufs zur Erzeugung von Nanospitzen durch elektrochemischen Abtrag. Dies beinhaltet die Vorbereitung des Ausgangsmaterial für den Ätzprozess, den Aufbau des dafür benötigten Geräts, sowie die Charakterisierung der Spitzen. Der Einfluss des Querschnitts und der angelegten Spannung bei den einzelnen Schritten auf die Qualität der Spitze werden anhand einer nickelbasierten Legierung ermittelt, um auch allgemeine Erkenntnisse für die Präparation zu ziehen. Schlussendlich wird eine tomographische Serie einer derart präparierten nickelbasierten Spitze aufgenommen. Des Weiteren wird gezeigt wie eine Wolframnadel nachgespitzt werden kann, um diese wieder als in-situ Mikromanipulator in einer Focused Ion Beam Anlage verwenden zu können.

Abstract

Electron tomography enables a three-dimensional qualitative and quantitative analysis of structures in the nanoscale regime. The object can be reconstructed from a tilt angle series taken with a transmission electron microscope. This method requires a special shape of the specimen. The thickness has to be below a maximum allowed value from any direction. This specific value depends for example on the used detector signal as well as on the type of material. Energy electron loss spectroscopy has the highest requirements on the sample with a maximal thickness of 100 nm. The optimal shape for the samples is a needle-shaped specimen with a thickness below 100 nm, a so called nanotip. Such tips can be prepared by electrochemical polishing. This is accomplished by using a specimen with a symmetric cross section run as an anodic electrode in an electrolytic cell. The diameter of the specimen is thinned as long as only a nanotip remains.

This work focuses on the implementation of a workflow to fabricate nanotips by electrochemical polishing. This includes the preparation of the initial material for the polishing process, the development of the device required for this, as well the characterisation of the tips. The influences of the symmetric cross section and the applied voltage at each step on the quality of the tip are examined by experiments with a nickel-based alloy. From these results, general conclusions are tried to be given. Finally, tomography is performed with such a nickel-based nanotip to demonstrate the usage from the obtained nanotips. Furthermore, a tungsten needle is attempted to be re-sharpened to re-use it as an in-situ micromanipulator for a focused ion beam instrument.

Acknowledgements

First, I would like to thank Professor Ferdinand Hofer, the head of the institute, providing the opportunity to write my master thesis at the institute of *Electron Microscopy and Nanoanalysis.*

A special thanks goes to Professor Gerald Kothleitner for supervising me, and to my second supervisor Georg Haberfehlner. Both of you taught me a lot of scientific work and improved the quality of this work substantially.

My gratitude also goes to the full FELMI-ZFE team for supporting me during my thesis, especially Cornelia, David and Martina, who is unparalleled at specimen preparation. I appreciate also Dr. Francisca Mendez-Martin from the *Montanuniversität Leoben* for giving me first insights into nanotip preparation techniques.

I would like to thank my office colleagues, the *Neoncrew,* for all the funny moments at *FELMI*, as well for our fabulous *Diplomanden*-dinners. I hope such delicious meetings will go on.

Furthermore, I would like to thank all my friends from my hometown, still being friends like I had never left, and my flatmates for 5 funny years including enormous cooking projects as well as some crazy projects distracting me from my study.

I would like to thank my lovely girlfriend, Jacqui, who turned the last few semesters of my study into the best. Thanks for the countless times you helped me and cheered me up, particularly during the final months.

Last, but definitely not least, I thank my wonderful family, especially my parents, Hermann and Barbara, for supporting me my whole life long no matter what I wanted to do. You and my siblings, Christina and Johannes, have given and still give me valuable advice concerning my professional and personal life, which made me to the person who I am now.

Contents

1. Introduction

Transmission electron microscopy (TEM) offers great possibilities for the analysis of nanostructures down to atomic resolution. The requirements on specimen preparation are strict, especially for advanced TEM methods, like electron energy loss spectrum (EELS) or high resolution TEM (HRTEM) and scanning TEM (HRSTEM). The sample thickness is a crucial point and has to be typically smaller than a few hundred nanometres. For example, to measure high quality EELS spectra, the transmitted electron should not scatter more than once. The preparation of TEM-samples is therefore an effortful process in order to obtain samples of such small thicknesses. Several techniques have been developed, for example ion beam based techniques like FIB (Focused Ion Beam) milling or sample thinning using a PIPS (Precision Ion Polishing System).

Similar to computed tomography, known from medicine, TEM offers also the possibility to reconstruct an object from many single images taken at different tilt angles. For such experiments of electron tomography, the requirements for the specimen become even more severe. Ideally, the sample should have the same thickness for any angle it is observed from. Therefore, a needle-shaped specimen is optimal, which has a diameter below the critical thickness over a long length. Such nanotips are required also for atom probe tomography, another method that allows for a 3D-reconstruction with atomic resolution. Focused ion beam (FIB) systems are often used for this kind of sample preparation, but this technique is less cost efficient, time consuming and can produce artifacts caused by ion implantation. In comparison, a much simpler approach is electrochemical polishing.

By electrochemical polishing, any metallic sample with a symmetric cross section can be etched to a nanotip. This is done by electrolysis, where the specimen acts as the anodic electrode. If a voltage is applied, the oxidation process produces cations from the specimen, which are soluble in the solution and can react further with the electrolyte. This removal reduces the diameter of the specimen until a nanotip is achieved.

This thesis focuses on the implementation of a workflow to prepare nanotips by electrochemical polishing at the “Austrian Centre for Electron Microscopy and Nanoanalysis”. The method is tested for two different types of materials (Inconel 718 and Tungsten). The thesis starts with a short theoretical introduction of electron microscopy, nanoscale tomography and electrochemistry, followed by a closer look on the methods for preparing nanotips. The practical part describes the setup of the equipment in general, as well as the preparation of the used materials and the nanotip fabrication itself. Afterwards, the nanotips are characterised and the impact of different parameters on the quality of nanotips are determined. For the evaluation and comparison of the tips, a MATLAB-script has been written, which automatically detects the characteristics of the tips out of an image. Finally, electron tomography on a tip of Inconel 718 is performed to demonstrate their suitability. The summary and the outlook recapitulate the thesis, its findings and discuss potential improvements.

2. Principles

2.1. Electron microscopy

2.1.1. Fundamentals

Diffraction imposes a resolution limit, regardless of lens quality. If a point is imaged with a chromatic light source and a perfect lens, a bright central point, which is surrounded by several rings, is obtained. These rings fade the further they are away from the central point, forming an Airy disk. The Abbe equation (1) gives the closest distance of two points, which can be distinguished due to overlapping Airy disks. (Rayleigh criterion) [1]

$$d = \frac{0.612 * \lambda}{n * \sin \alpha} \tag{1}$$

The resolution can be improved by increasing the index of refraction *n* and the half-aperture angle α. The index of refraction can be influenced by filling the space between the lens and the point source with a medium of higher optical density. The aperture angle can be increased by reducing the distance from the specimen to the objective lens. The resolution limit of a typical light microscope with an ultraviolet source is around some hundred nanometres. [1]

Another way to improve the resolution is the usage of lower wavelengths for imaging. According to de Broglie, electrons have wave-like properties and can be described by a so called de Broglie wavelength The wavelength decreases with increasing kinetic energy, which is described by following equation (2): [1], [2]

$$\lambda = \frac{h}{m * v} \tag{2}$$

From equation (2) it follows, that if a particle is accelerated high enough (gaining speed), the resolution of a classical microscope can be exceeded. For example, considering relativity, an electron has a wavelength of 0.122 Å at an energy of 10 keV. [3]

When using electrons for imaging, they have to overcome the work function of a metal to be able to leave it and move freely in vacuum. Electron sources should provide high brightness and a small energy spread. One type is a thermal field emission gun (FEG). Due to thermal excitation and an applied electric field, electrons can escape the metal. After emission, the electrons are accelerated to high energies and are focused by magnetic lenses. [3], [4]

These electrons should reach the sample without any scattering process. The long mean free paths of the electrons are obtained by applying high vacuum from the source to the sample and detectors. [2]–[4]

Depending on the scale and information that is needed from the specimen, two different microscopes are used: scanning electron microscope (SEM) and transmission electron microscope (TEM). The main differences between them are their type of sample preparation, the detectors, and the scattering signal used for imaging. [2], [4]

These two microscopes will be briefly explained in the next sections.

2.1.2. Scanning electron microscopy

The SEM is typically operated with an acceleration voltage from 0.1 keV up to 30 keV. Lenses and apertures focus the electrons to a beam to a diameter of about one nanometre, and the beam is scanned across the sample. When the primary electrons encounter the specimen, the complex physical processes are categorised in two events: elastic and inelastic scattering processes. Monte Carlo simulations can be used to visualize the size of those interaction volumes for different primary electron energies and materials. The elastic and the inelastic scattering processes lead to two different signals, which are frequently used for the characterisation: [4]

- secondary electrons (SE)
- back-scattered electrons (BSE)

Additionally, X-rays created in the sample are used for energy dispersive X-rays (EDX) analysis. Figure 1 schematically shows the interaction volumes, which are probed using different signals. [4]

Each of these signals is measured with a special detector and contains different information about the sample, like topographic features (SE), composition (EDX) and crystal structure (BSE). [4]

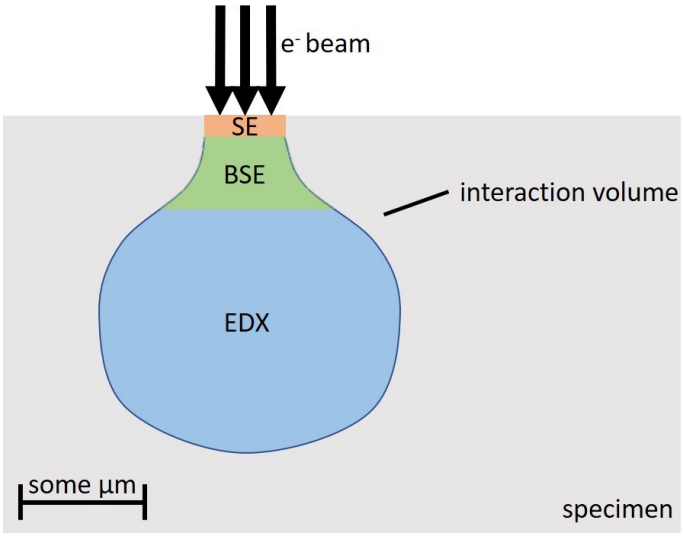

Figure 1: Detected interaction volumes of the different signals. (after [5]*)*

Secondary electrons

SEs are weakly bound valence electrons or conduction band electrons, which are emitted due to excitation by an inelastic scattering process. The energy transferred from the primary electrons is very small compared to their kinetic energy. The kinetic energy of SEs is in the range of some tens of eV and they can be completely reabsorbed within the specimen. Due to this, only a few secondary electrons from a low depth reach the surface of the sample and have enough energy to exceed the surface barrier energy. Mean escape depths are in the range of a few nanometres. [4]

SEs can be separated in different classes according to their appearance. When the primary beam encounters the specimen, the first order SEs are created. These electrons are carrying high-resolution information. The second class is caused by back-scattered electrons when leaving the specimen. These electrons have enough energy to generate other SEs. These two classes contain information about the specimen. Furthermore, BSEs can travel to parts of the microscope and create SEs. Detection of this third class and the fourth class of SEs, stemming from pre-specimen instrumental sources depending on the instrumental construction, should be avoided. Considering this, the detector has to be carefully constructed. [4]

The approximate shape of the volume, from which SEs are escaping the specimen, is a cylinder. The diameter of this cylinder limits the lateral spatial resolution. [4]

Due to their low escape depth, the amount of electrons leaving the sample depends on the local surface inclination. An easy geometric explanation is that, at a tilt angle, the primary beam moves longer within the escape depth of the SEs and thus generates a higher number of measurable SEs. This effect is used to obtain topographic contrast. [4]

Back-scattered electrons

The primary electron can reverse its initial direction after enough scattering events. An elastic scattering process occurs in the electric field of the positively charged nuclei without any energy transfer, called Rutherford scattering. These interactions lead to a deviation of the primary path up to angles of 180°, and the electrons can escape the specimen again near their entrance area. These electrons are called back-scattered electrons (BSE). This process also depends on the inclination of the local surface. Due to their high energy, BSEs can leave the sample even after penetrating far into the specimen. Therefore, they do not deliver topographical contrast as well as SEs and have a higher radial distribution. Depending on the type of material measured, the lateral spreading can degrade the lateral resolution to some hundred nanometres. However, BSEs contain information about the material composition. The higher the atomic number of the elements in the specimen, the higher the probability of an elastic scattering event in the electric field of the nuclei, resulting in a higher rate of BSEs. Besides the mass contrast, a crystallographic contrast appears also due to the Bragg diffraction as used in electron backscatter diffraction (EBSD). [4], [6]

X-ray spectroscopy

Two different kinds of radiation are obtained if the specimen is hit by high-energy electrons: Characteristic X-rays and a Bremsstrahlung continuum. An inner shell electron can be ionized in an inelastic scattering process, leaving a hole. For this to occur, the ionization energy has to be overcome by the energy of primary electrons. After the electron is removed, an electron from an outer shell can fill the hole. The difference between the initial and final energy state of the electron will be emitted as an X-ray photon or as an Auger electron. Therefore, the emitted X-rays have discrete energies, depending on the initial and final shell of the inter-shell transition. Every type of element has different shell energies (K, L and M). Therefore, each element emits photons with its characteristic energies, the so-called characteristic X-rays. These can be used for qualitative and quantitative elemental analysis. [4]

Bremsstrahlung is a continuous X-ray spectrum, which is emitted by the deceleration of charged particles. This underground signal reaches from a few eV to the highest energies of the primary electrons. The low energy X-rays are re-absorbed within the specimen, before they are able to leave it. Characteristic X-rays with low intensities can vanish in the Bremsstrahlung background. [4]

Detectors

For BSEs, passive detectors can be used, as no post-specimen acceleration is needed to detect this kind of electrons. Two principal types of detectors are common: scintillator based solid state detectors. [4]

The most frequently used detector for SEs is an Everhart-Thornley (E-T) scintillator detector. SEs are accelerated beforehand by a high potential to have enough kinetic energy. This potential would also influence the primary electron beam, which is why the scintillator is shielded. A weak potential is applied to the cage to attract the low energy SEs. Depending on the inclination of the E-T detector to the measured area, less or more SEs can be collected. Areas facing towards the detector are brighter than areas pointing away, leading to an easy interpretation of the signal [4]

A second type of detector for SEs is the Through-the-Lens (TTL) detector. It uses the magnetic field of the objective lens, which reaches into the vacuum chamber. The SEs spiral up the magnetic field through the lens to an E-T detector. Because of the detector's central position, the TTL detector does not have the high topographic contrast of an E-T detector. The advantage is that the third class of SEs, which does not contain information about the specimen, is not absorbed. [4] The two detectors are compared in Figure 2.

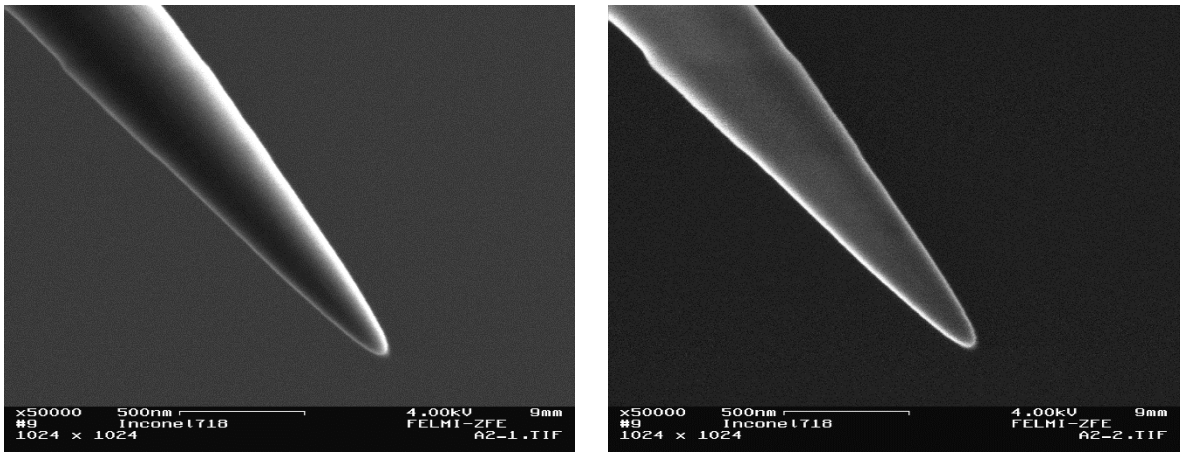

(a) ET-Detector *(b) TTL detector*

Figure 2: Comparison between the E-T detector in the vacuum chamber and the TTL detector of a nanotip.

The X-Ray spectrum is measured most commonly by an energy dispersive detector. The EDX spectrum is measured by a semiconducting crystal. Each incoming X-ray excites a number of electron-hole pairs proportional to its primary X-ray energy. This effect can be used to measure the whole spectrum simultaneously. The semiconductor needs to be cooled, and an extremely sensitive electronic system is necessary to obtain a good spectrum. [4], [7]

Sample preparation

According to Kirchhoff's current law, the sum of all currents is zero. The remaining electrons, which do not leave the specimen, e.g. as BSEs and SEs, have to flow to the electric ground. If the connection from the specimen to the ground is interrupted, a charging of the sample occurs. In the worst case, the electric field caused by the charging will deaccelerate and reflect the primary electrons. As a result, not the specimen is imaged, but instead the vacuum chamber, detector and apertures. Usually, charged areas appear bright, surrounded by a dark halo. The detectors attract low energy SEs through a weak electric field. The negatively charged area increases the efficiency of this collection process, because the local electric field of charged areas is much higher than the electric field of the detector. The emission of SEs at the surrounding area will be diminished, because the electric force will attract the SEs back in the specimen. [4]

This has to be avoided for non-conductive materials. A method to eliminate such charging effect is to coat the sample with some conductive layers, which must cover all the complex structures. This is achieved with deposition of a conductive layer by thermal evaporation (electron beam heating, resistive heating) or sputtering with ions. Frequently used materials are gold, palladium or carbon. [4]

2.1.3. Transmission electron microscopy

A better resolution than with the scanning electron microscope is achieved by the transmission electron microscope (TEM) or scanning transmission electron microscope (STEM). As the name already indicates, the specimen has to be transparent for the electrons of the electron source. Those are accelerated to much higher energies than in the SEM, to around 100-300 keV, in order to pass through the sample. The thickness of the sample should be typically around a few ten nanometres of nanometres. The allowed value depends on the used detector, composition of the specimen, the acceleration voltage and the required resolution. [2]

As in the SEM, electrons scatter elastically or inelastically in the specimen. This results in different contrasts, which can be used for imaging. Electrons, which do not scatter and are not intercepted by an objective aperture (diffraction contrast) and can interfere with the incident wave (phase contrast), are used for bright-field imaging. Dark-field imaging measures larger angle scattered electrons, for example with a high-angle annular dark-field (HAADF) detector in STEM. The specimen can also be imaged in reciprocal space, giving information about the crystal structure and orientation via diffraction. [2]

For analytical measurements, again the characteristic X-rays can be used. Due to the lower thickness of samples, the analysed volume is broadened only slightly. Another possibility for doing analytical measurements is electron energy loss spectroscopy (EELS). For this, transmitted inelastic electrons are separated by their energy loss after with a magnetic prism. The EELS spectrum has characteristic edges from inner shell ionizations of each element. Additionally, the energy loss near edge structure contains information about the chemical bonding and band structure. The extended energy loss fine structure far from the edge include information about the coordination of neighbouring atoms. Near the zero-loss peak, dielectric information can be derived and plasmon excitations can also be detected. [2]

As already mentioned, the specimen thickness is a crucial point in TEM. In material science, several techniques have been developed, like electrochemical polishing and ion-beam milling, to obtain such thin specimens. [2] The requirements for the specimen thickness become even more restricted in electron tomography.

2.2. Nanoscale tomography

Two different techniques are mainly used to reconstruct 3D-objects in the nanometer and atomic regime. On one hand, a reconstruction can be made from a series of tilted 2D images taken with the TEM. This is known as electron tomography. On the other hand, atom probe tomography (APT) can be used, which removes atom by atom from the specimen and analyses each atom. [8], [9]

2.2.1. Electron tomography

In electron tomography, the 3D-object is reconstructed from a series of two-dimensional TEM projection images acquired at different angles. The reconstruction process is mostly done by real-space back-projection. Different methods have been developed to achieve better reconstruction of the object. Weighted back-projection uses a weighting filter to reduce the problem of over-sampling at low frequencies and the under-sampling at high frequencies. The method can be enhanced further by iterative reconstruction methods. At each iteration, the re-projections and the measured projections are compared until they match best. [8]

In material science, the signals of HAADF, EDX or EELS are used mainly because of their insensitivity to diffraction contrast (thickness fringes or bend contours). Depending on which signal is used, the specimen thickness has to be below a specific maximum thickness for all tilt angles. For EELS, multiple inelastic scattering must be avoided. Therefore, the specimen thickness must be smaller than the mean inelastic free path. A typically thickness of the specimen for EELS is around 100 nm. For acquiring the series of tilted images, a needle-shaped specimen with a diameter smaller than 100 nm is optimal. [2], [3], [8]

Eventually, electron tomography can be correlated with the atom probe tomography. Either technique benefits from the other, when compared quantitatively.

2.2.2. Atom probe tomography

Atom probe tomography enables a 3D-reconstruction with atomic resolution. The principle is shown in Figure 3. Atoms are removed layer by layer of the apex of a needle shaped specimen. The removal happens by field evaporation. A very intense electric field is achieved by applying a high voltage and an appropriate radius at the end of the specimen. The electric field can pull away the atoms at the surface. If these ions are spatially projected, the nanotip can be reconstructed out of this signal. The species of the atom can be identified by the measurement of the time-of-flight. Instead of the electric field evaporation, or in addition, a laser pulse can be used to remove the atoms. This enables the analyses of semiconductors and insulators. [9]

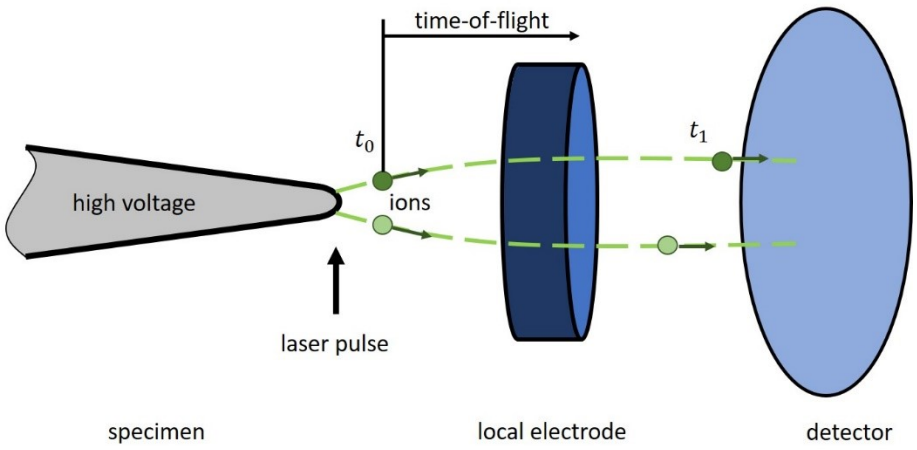

Figure 3: Principle of APT. (after [9]*)*

The needle shaped specimen needs to fulfill some requirements to be suitable for an APT: [9]

- Radius of curvature (ROC) of the apex between approximately 50 nm and 150 nm.
- Smooth surface free from protrusions, grooves or cracks.
- Circular cross section
- Region of interest within approximately 100 nm of the apex
- Sufficient specimen length and tip clearance
- Appropriate tip angle

The preparation of such a specimen can be difficult. The most commonly used methods are focused ion beam milling and electrochemical polishing.

2.2.3. Sample preparation

Focused ion beam

The focused ion beam (FIB) system operates like a scanning electron microscope, but instead of using electrons for imaging, it uses gallium ions. These ions are much heavier than electrons and can sputter atoms away from the specimen. The systems also often have an additional scanning electron microscope to image in-situ while milling. Nanotips are obtained from the FIB system by annular milling and several techniques have been evolved to prepare the specimen for this process. These methods are also performed in the FIB, for example the moat method, wedge method, lift-out method, micropost release technique and so on. They can be time consuming, like the moat method, or need an additional in-situ micromanipulator, like the lift-out method. [9], [10]

The last step in this milling process is always the annular milling, shown in Figure 4. For this purpose, the ion beam is directed antiparallel to the tip axis. The pattern is ring-shaped with an outer diameter, which is slightly larger than the needle, and an inner diameter, which is larger than the required tip. No material is removed within the inner diameter. The process is repeated, lowering the ion current and the inner radius until the required tip is obtained. The outer diameter often stays constant to avoid protrusions. [9], [10]

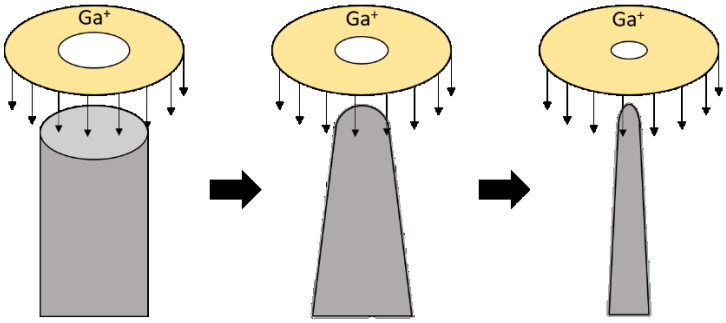

Figure 4: Principle of annular milling. (after [9]*)*

The FIB system offers the possibility to prepare nanotips from semiconductors and insulators. The additional SEM enables the selection of the region of interest. However, it can be time consuming and the appropriate equipment is needed. A disadvantage of the FIB system is that the structure and the chemical composition of the material are changed due to the ion bombardment. The generated amorphous layer can reach a depth of 30 nm and gallium can be implanted up to 50 nm in the specimen. A “cleaning” step with low energy ions can partly remove this layer. Nevertheless, an amorphous layer up to 5 nm and gallium implantation up to 10 nm is still possible. [9], [10]

2.3. Electrochemistry

Nanotips can be prepared by dissolving material from the electrode in an electrolytic cell. The fundamentals of electrochemical polishing and the used methods to prepare nanotips are the main topic of this thesis, and explained in detail in this section.

2.3.1. Fundamentals

Electrochemistry deals with the electron transfer at the solution-electrode interface. Figure 5 shows a typical electrochemical cell. Due to the applied voltage *U*, chemical reactions are enforced in an electrolytic cell. If the voltage source is exchanged with an electric consumer, chemical reactions are spontaneous, called a galvanic cell as applied in batteries. The cathode in a galvanic cell is positive with respect to the anode, but in an electrolytic cell, the anode is the positive electrode. [11], [12]

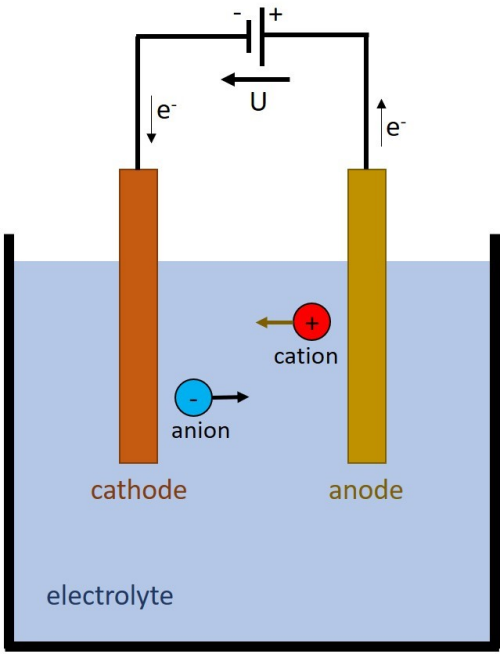

Figure 5: Electrochemical cell, electrolytic. (after [11]*)*

In the solution, two flows of particles can be observed. The anodic current consists of anions, which are negatively charged particles. These particles diffuse to the anode. In the opposite direction, cations are diffusing to the cathode, the electrode with the negative potential. The charge equilibrium is established by electrons, which are moving from the anode to the cathode via the electric connection of the electrodes. The chemical reactions at the electrodes are called redox reaction, consisting of the oxidation at the anode and the reduction at the cathode. At the oxidation reaction, the element loses at least one electron; the reduction describes the reverse process. The fundamental equation for redox process is given in equation (3): [11]

$$O + n * e^{-} \rightleftharpoons R \tag{3}$$

O is the oxidized species, *n* is the number of electrons and *R* is the reduced species.

A further fundamental equation of electrochemistry is Faraday's law of electrolysis. This equation given in (4) states that the material, which passes through the electrochemical cell, is proportional to the total charge. This can be used to calculate the deposited or removed material. [11], [13]

$$Q = n * F * N \tag{4}$$

Q denotes the total transferred charge, *F* is the Faraday's constant ($F = 96{,}5\,\frac{C}{mol}$), *n* is the number of electrons transferred per mole of product and *N* is the amount of transferred product. [11]

In an electrochemical cell, the current can be divided into two types, the faradic and the non-faradic current. The current, which is involved in chemical reactions, oxidation and reduction, is called faradic i_F. The non-faradic current $i_{non\text{-}F}$ is related to Ohm's law but the resistance has to be considered as impedance *Z* because of the capacitances present in the cell. [11]

Faradic: $$i_F = \frac{dQ}{dt} = n * F * \frac{dN}{dt} \tag{5}$$

Non-faradic: $$i_{non-F} = \frac{V}{Z} \tag{6}$$

A reason for the non-faradic current is the capacitance, which is caused by an electrical double layer. Several layers are formed at the electrode-solution interface, if an electrostatic potential is applied. The first layer, the Thomas-Fermi layer, is located on the solid side of the electrode. If the electrode is conducting, the thickness of this layer is smaller than one Ångström. The counterpart of these charges is the double layer at the electrolyte side. This can be seen in Figure 6. In the double layer two layers can be distinguished, the inner Helmholtz plane and the outer Helmholtz plane. The inner layer consists of specifically adsorbed ions and solvent molecules. In the adsorption process, charges can be exchanged. The inner layer limits the closest distance of the non-specifically adsorbed ions to the electrode, the outer Helmholtz plane. These ions are independent of chemical properties of the surface and influence the electrode surface only by long-range electrostatics. The ions of the outer Helmholtz plane are less compact than the ions from the inner Helmholtz plane. They can spread out in the three-dimensional region by thermal agitation in the solution. This region is called the diffusive layer and reaches from the outer Helmholtz plane into the bulk electrolyte. The thickness depends on the total ionic concentration in the solution. [11], [12], [14]

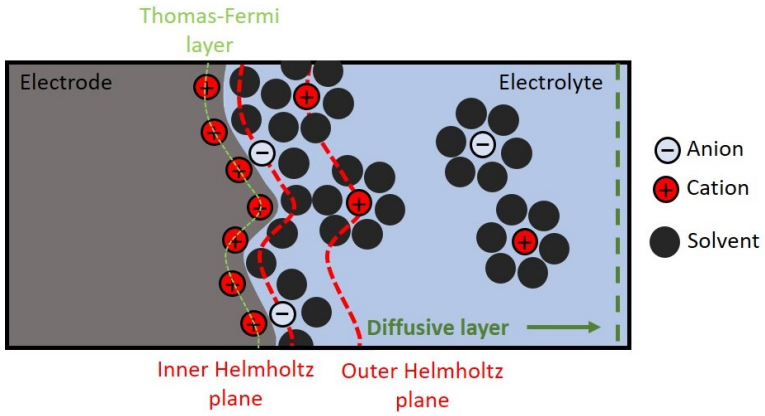

Figure 6: Formation of the double layer and the Helmholtz planes at the anode. The diffusive layer can intrude further in the elecrolyte. (after [11], [15]*)*

The diffusive layer has a uniform thickness. Due to the uneven surface of the electrode, the ohmic resistance between cathode and anode is location-dependent. The resistance at valleys is higher than at protruded areas. This is the basis of electrochemical polishing. Due to Ohm's law, higher currents at hills occur and therefore more material is removed, resulting in a smooth surface. [13], [15]

The Gouy-Chapman-Stern model provides a detailed mathematical description of the double layer and diffusive layer formation at the electrode-electrolyte interface. The model considers the Boltzmann

energy distribution, the diffusion of a point charge (Fick's law) and the immobile layer (inner Helmholtz layer). Typical lengths are from a few to a several hundred Ångström. [12]

Figure 7 shows the ion concentration at the electrode-electrolyte interface at limited current with the adsorbate acceptor model. The first step is the oxidation of the metal *M* at the electrode surface to adsorbed ions M_{ads}^{+Z}. The oxidation state is given by *Z* and it depends on the used metal. The acceptor *A* (solvent) dissolves these adsorbed ions from the surface (see Figure 6). If the concentration of the acceptors at the interface is near zero, the current is limited. Hence, the diffusion of the acceptors to the electrode surface limits the corrosion rate, rather than the diffusion of the metal cations away from the surface. [13]

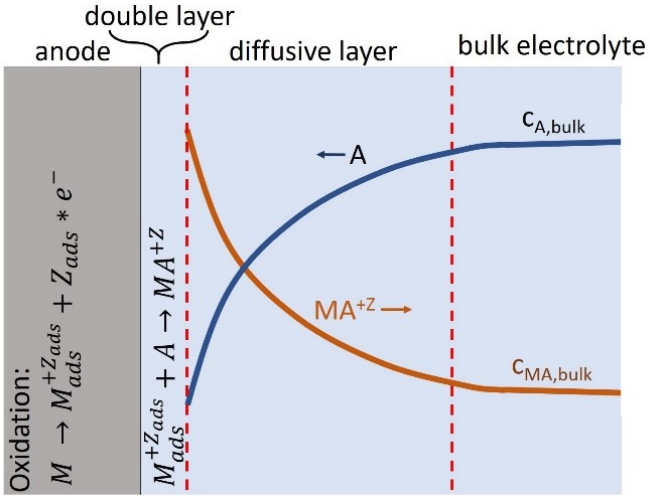

Figure 7: Adsorbate acceptor model: Anodic dissolution of a metal with the diffusion into the bulk electrolyte. (after [15]*)*

A second model of the anodic dissolution is the salt film model shown in Figure 8. In this theory, two films are formed: a compact film and a porous salt film. The compact film consists of the oxide states of the material through which the cations are transported by solid-state ionic conduction. The thickness of this layer is in the range of 10 nm. The pores of the salt film are filled with the saturated electrolyte solution and the charges are transported by the anions and cations by migration in the pores. This layer generally has a high electric resistance caused by low porosity and a layer thickness of several microns. [15]

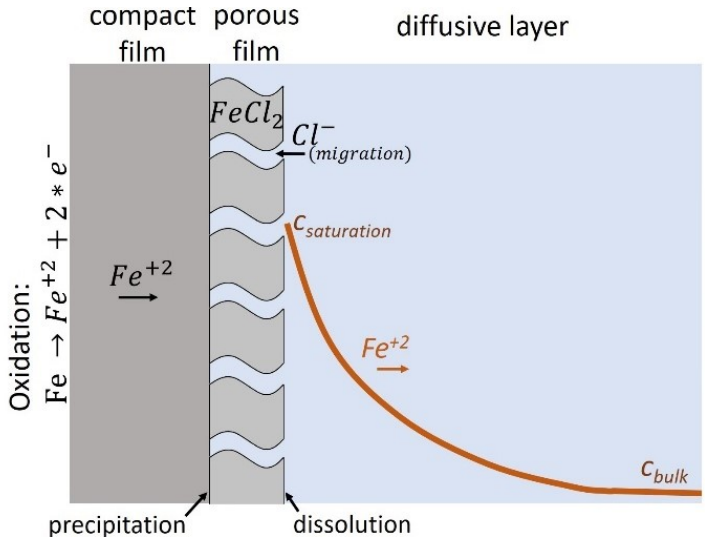

Figure 8: Salt film model: Anodic dissolution of a metal, as example iron, into the bulk electrolyte. (after [15]*)*

Depending on the metal and on the used electrolyte, the metal ions can remain dissolved in the solvent, or they can react with parts of the solvent. [11], [12]

The cathode material is usually not involved in reactions in the electrolytic cell, the reduction only takes place at the electrode surface. However, the reaction can cause depositions at the cathode. Using an aqueous solution, hydrogen and hydroxide anions are generated at the cathode. This chemical reaction is given by equation (7). The hydroxide ion forms a layer around the cathode. [11]

$$2H_2O + 2e^- \rightarrow H_{2(g)} + 2OH^- \quad (7)$$

2.3.2. Electrochemical polishing

As already mentioned, the location-dependent faradic current due to differences of the ohmic resistance in an electrochemical cell can be used to enhance the surface properties. The specimen acts as electrode (anode), therefore only metals can be electrochemically polished [13]

The electrochemical polishing process depends on a large number of variables: [12]

- Electrode: material, surface area, surface condition, geometry
- Solution: bulk concentration of the electroactive species, concentration of other species, solvent
- Electrical: voltage, current, total transferred charge
- Mass transfer: adsorption, surface concentration, diffusion, convection
- External: temperature, pressure, time

In the following sections, the most important parameters and their impact on the polishing process are explained. Due to the high number of parameters influencing the polishing process, an overall recipe cannot be given for achieving a good nanotip. Nevertheless, some rules and approaches can be extracted. Ultimately, the voltage and the electrolyte are the parameters, which have to be adapted for every different type of material.

Voltage

Figure 9 shows a general polarisation curve. The curve can be subdivided into four regimes. The offset potential E_d represents the onset of the general electrochemical reactions, which can be derived from the Nernst equation (equation (8)). This equation describes the correlation between concentration and potential of an electrochemical cell. Here [O] is the concentration of the oxidized species and [R] the concentration of the reduced species. The standard potential E^0 is the measured voltage of the individual electrode to the hydrogen standard electrode potential at given standard conditions. [11], [13], [15], [16]

$$E = E^0 + \frac{R * T}{n * F} ln \frac{[O]}{[R]} \tag{8}$$

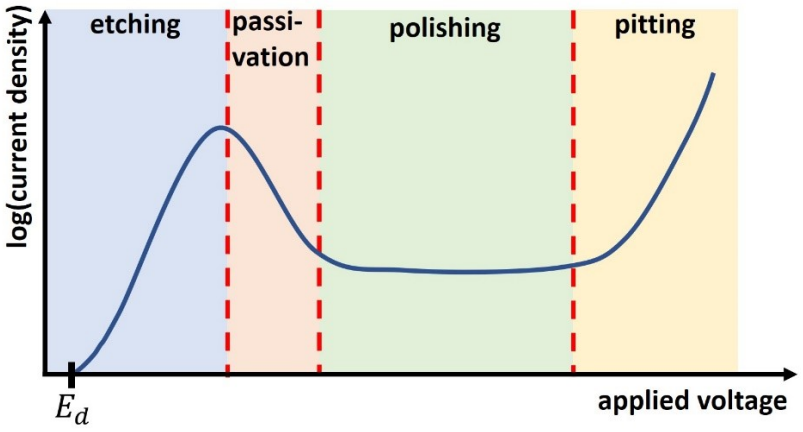

Figure 9: General polarisation curve. The curve is subdivide in four regimes; etching, passivation, polishing and pitting. (after [13]*)*

A nearly linear increase of the current is observed above E_d in the first regime, the etching regime. Due to the low current, enough acceptors are available at the electrode-electrolyte interface. The metal ions can therefore be dissolved directly into the bulk electrolyte. The most electroactive species is dissolved first, with electroactivity depending for example on the type of element, crystallographic orientation and site. This selective dissolution results in a non-uniform etching. [13], [15]–[17]

Differences of the electroactivity of different elements in an alloy result in non-uniform etching rates. An important value for the potential is the so-called critical potential. Above this point, a macroscopic three-dimensional de-alloyed structure develops, whilst below the critical potential the surface remains smooth. A possible explanation for the smoothening effect is that the less noble metal dissolves and first leads to a rough surface of the noble metal. This high curving causes a curvature-driven surface diffusion. Thus, the noble metal covers the active dissolution sites. As a result, the sample has a smooth surface consisting of the noble metal. If the applied voltage is above the critical voltage, the dissolution overcomes the surface diffusion and roughening occurs. The critical potential is kinetically determined and depends on the alloy and the electrolyte. [18]

If the applied voltage is increased further, the current density decreases. The passivation regime is reached. This regime can be explained with the two different dissolution models, adsorbate acceptor model and salt film model. Within the adsorbate acceptor model, the concentration of the acceptors begins to decrease at the electrode-electrolyte interface. This limits the current because not all oxidized metal cations can be dissolved anymore, and they form a transient passive layer. This layer of oxidized ions has a higher electric resistance. With the salt film model, the decrease of the current density can be explained by the thickening of the salt film. The salt film precipitation starts at the passivation regime, and the kinetic limitation (oversaturation) at this onset leads to the current density peak in the passivation regime. [13], [15], [16], [19]

The polishing regime is defined by the plateau in the U-I curve. The explanation with the adsorbate acceptor model is the enhancement of the transient passive layer, which has a high ohmic resistance. The salt film model explains the plateau by the thickening of the high ohmic resistance layer. The smoothest surfaces are obtained in the polishing regime due to the diffusive layer and its different ohmic resistance of protrusions and valleys at the anode surface. The different electroactive atoms are protected by the passive layer or the salt film and the dissolution depends nearly only on the thickness of the diffusive layer above it. [13], [15], [16], [19], [20]

At the pitting regime, the voltage is high enough to pull-off the oxide layer or the salt film. This reveals a larger unprotected surface area for electrochemical reactions. The evolution of oxygen can also start at this regime. The bubbles, which are trapped on the anode surface, avoid further dissolution at this area. These two effects can result in a non-uniform etching rate, called pitting. [15]

The applied voltage for a smooth surface should be in the polishing regime. However, a problem in the nanotip production is the blunting of the tip. After finishing a nanotip, the residual current of the electrolytic cell decreases the sharpness of the tip. Blunting can be reduced by lowering the etching rate, equivalent to a smaller current. [21], [22]

Electrolyte

A crucial part of every electrochemical cell is the electrolyte, which contains dissolved ions. These mobile charge carriers support the current flow. A requirement for the electrolyte is a good solvating power to dissolve reactants from the electrode. [11] Electrolytes are often concentrated acid or alkaline solutions, and the composition of the used solution has therefore a big influence on the polished material. Furthermore, agents can be used for increasing the conductivity, bath stability, activating the surface, improving levelling or metal distribution. [13]

The correct electrolyte depends on many parameters; recipes can be found in many papers and books. A good summary e.g. is appendix B in reference [9].

Temperature

The current limit at the plateau of the polishing regime increases with higher temperature. This was shown for electrochemical polishing of niobium [23] and stainless steel [24]. This can be explained by the diffusion of the ions, which limits the mass transfer. The dependence of the diffusion coefficient on temperature can be seen in equation (9). It shows an exponential behaviour, which also acts exponential on the current increase. The temperature influences also the viscosity of the diffusive layer at the anode. The viscosity decreases with higher temperature, but is essential for a good surface quality. [13]

$$D = D_0 * e^{-\frac{Q_a}{R*T}} \tag{9}$$

D_0 is the initial diffusion coefficient and Q_a the activation energy for diffusion.

Electrodes

The cathode should ideally be a noble metal to avoid unwanted chemical reactions with parts of the electrolyte. Typical materials are gold or platinum. [11]

The anode is the specimen and cannot be chosen arbitrarily. The electrolyte has to be adapted to the material of the specimen.

Geometry

The geometry of the electrodes is important for the macroscopic current density distribution. This distribution determines the localized dissolved or deposited material. The ohmic resistance between two electrodes is smallest at the electrode edges. This increases the current density at the edges, called edge effect. [25] If an electrode with a symmetric cross section is placed in a ring that acts as counter electrode, the shape of the symmetric cross section will be etched to a circle due to the edge effect. In the end, the current density distribution is uniform.

Especially for preparing nanotips, a square or a circular cross section of the anode is important, as an asymmetric cross section will lead to blade-shaped tips. [26]

Mass transfer

The mass transfer is given by the movement of material in the solution. Three different types of mass transfer exist: migration, diffusion and convection. The gradient of the electric potential applies a force on charged particles, called migration. Diffusion originates from a concentration gradient, and convection can be caused for example by stirring or thermal agitation. The flux, which is the sum of the three different types, determines the Faradic current in the cell. Equation (10) gives the mass transfer J of one species in one dimension: [12]

$$J(x) = \underbrace{-D\frac{\partial C(x)}{\partial x}}_{diffusion} - \underbrace{\frac{zF}{RT}DC\frac{\partial \phi(x)}{\partial x}}_{migration} + \underbrace{Cv(x)}_{convection} \tag{10}$$

D is the diffusion coefficient, C the concentration, ϕ the potential and v the velocity.

Migration dominates over diffusion in the bulk electrolyte because the concentration gradient is quite low. There are some possibilities to enhance the transfer. Migration and diffusion can be influenced by adding agents into the electrolyte. Convection can be introduced by stirring or vibrations. [12]

2.3.3. Methods for fabricating nanotips

Electrochemical polishing is used to remove material from the electrode to enhance the surface quality of the workpiece, which acts as the anode, in an electrolytic cell. [13] Material is taken from the sample until it gets thinner and thinner. If the sample has a symmetric cross section at the beginning, a tip is created in the end. With the right techniques, nanotips with a diameter down to 10 nm are possible. There is already some literature about the different procedures, which can be found in [17], [21], [22], [26]–[35].

In the following, the fundamentals of nanotip preparation and different techniques are described. In addition, the influence of some parameters like electrolyte concentration, applied voltage or *Cut-Off* time for the current are explained.

The basis of the nanotip fabrication (see Figure 10) is almost the same for every method. The sample is immersed in the electrolyte and is connected to the positive potential. Material is removed continuously from the sample. Due to capillary forces, a meniscus is formed at the electrolyte-air interface, which determines the final shape of the tip at static etching. At the meniscus, the specimen gets thinner than at other positions, this is called the *Neck-In*. It is assumed, that at the meniscus a vortex is formed, which removes the electrochemical reaction products of the oxidation away from the surface. This results in a smaller diffusive layer and therefore a higher current density is possible. The form of the meniscus depends on the diameter of the specimen, which gets smaller during etching. The change in etching conditions leads to a shift of the meniscus. This movement happens stepwise, leading to a tip shape as shown in Figure 11. This can cause problems for the reproducibility of nanotips. A mass flow occurs downwards along the anode surface due to heavier metal anions. The saturation of the flux with metal anions increases along the surface and reduces the diffusion-limited current as well as the etching rate. The cross section gets smaller and smaller until the tensile stress due to the mass of the lower part gets too high and the lower part breaks off. This is called the *Drop-Off*, which leaves a very sharp tip at the breaking point. [17], [21], [22], [33]–[37]

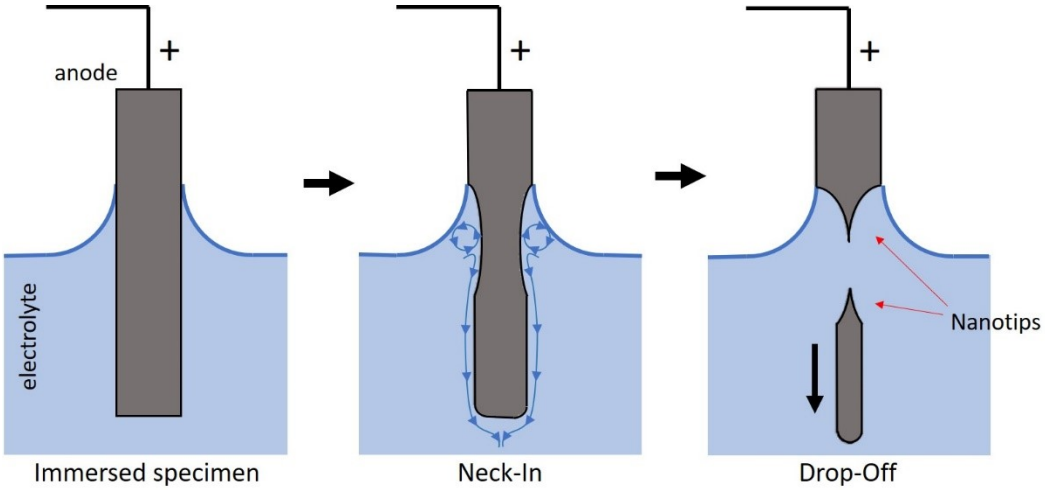

Figure 10: The basic principle of making a nanotip. (after [28]*)*

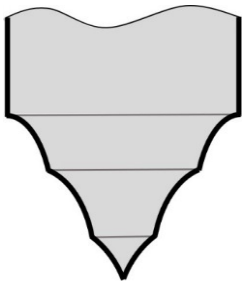

Figure 11: Meniscus shift leading to a step by step tip. (after [35]*)*

The method in Figure 10 shows the simplest technique. Some modifications are explained in the next chapters. Many of them can be combined to get a sharp tip.

Cathode geometry

The shape and position of the cathode can influence the tip shape and quality. The cathode is sometimes shielded from the anode to reduce vibrations caused by hydrogen. The immersed surface area of the anode can be shrunk to a very small area with special shapes of the cathode, such as with an open loop. For this geometry, the open loop contains a bubble of electrolyte and the specimen can be etched only at the bubble surface. [17]

Nevertheless, the most common shape of the cathode for making nanotips is a ring or cylinder. With cylindrical cathodes, longer tips can be made than with a ring. If the cylinder is only partially immersed in the electrolyte, the capillary forces form a meniscus, like at the anode. A top layer is formed, where the etching rate is reduced, which increases the length of the tip. The diameter of the cathode cylinder affects the ion transfer. The smaller the diameter, the steadier the etching process. This leads to a reduced *Neck-In* effect at the electrolyte-air interface and therefore a longer tip. [38]

If a ring is used instead of a cylinder, the immersion depth of the ring can shift the *Neck-In* position due to the electrical-field distribution. The smaller the ring, the more the position of the *Neck-In* can be influenced. However, the diameter of the ring should not be too small as the bubbles of hydrogen formation and thermal heat at the cathode interface can disturb the tip during the *Drop-Off*. [38]

Buoyancy force assistance

The *Drop-Off* happens when the tensile stress is higher than the allowed tensile strength of the material. The critical cross section can be reduced by minimizing the resulting force, which acts on the falling part. The buoyancy force of a denser inert liquid can be used to support the part. This can be calculated with equation (11). The minimum radius depends on the gravitational force F_G, the surface tension F_S, the buoyant force F_B and the maximal tensile strength of the material. Thus, the dropping part should be as short as possible and the inert liquid as dense as possible. The down-falling part also has a nanotip and, due to the lost electric connection to the power supply, there is no problem with blunting the tip. An additional advantage is the reduced consumption of electrolyte. This method is shown in Figure 12. [33]

$$r_{min} = \sqrt{\frac{F_G - F_S - F_B}{\pi * \sigma_W}} \tag{11}$$

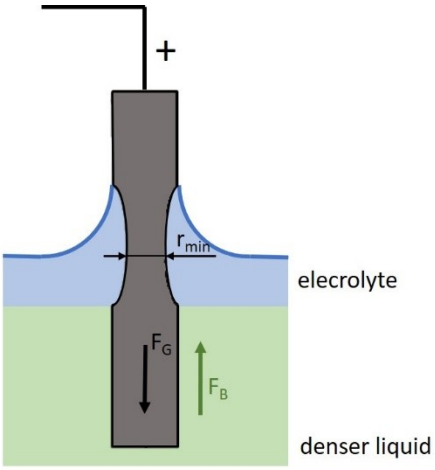

Figure 12: Etching with a denser and inert liquid. (after [17]*)*

Moving anode

As mentioned, the highest etching rates are obtained at the meniscus at the electrolyte-air interface and the meniscus can arbitrary shift due to the shrinking diameter of the anode. This can be controlled by constantly moving the anode to shift the interface over a long range along the specimen. Then, the meniscus moves continuously and does not jump step by step. Another advantage is that the tip shape can be controlled, for example to get high aspect ratios and small tip angles. At higher velocities of the anode, the diffusive layer can be disturbed, therefore a higher current density appears at the whole immersed area of the specimen leading to an increased aspect ratio. However, the high velocities require high accelerations. The acceleration force induces more stress on the specimen, which acts on the cross section at the *Neck-In*, and therefore breaks earlier at bigger radii. [33]–[35]

Setting the amplitude *A* and the frequency *f* of a vibration, the tip shape can be controlled with this method, shown in Figure 13. The aspect ratio can be enhanced by increasing the amplitude and the frequency, but the diameter at the *Drop-Off*, which affects the end radius of the nanotip, increases. [34]

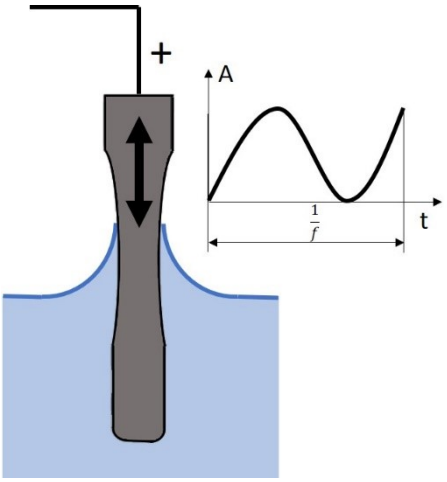

Figure 13: Etching with a induced vibration of the anode. (after [34]*)*

Cut-Off time

A problem at the nanotip fabrication is the blunting of the tip. Directly after the *Drop-Off*, the residual current blunts the tip. This blunting effect is shown in Figure 14. With a fast *Cut-Off* circuit, this can be reduced or even avoided. [22]

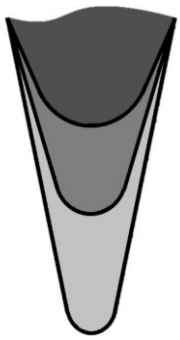

Figure 14: Blunting of the tip. (after [22]*)*

The current curve for such an etching process is depicted in Figure 15. At the beginning, a high current flows due to the capacitance of the double layer at the electrodes. Then, the current decreases slightly over time because the surface of the anode gets smaller, therefore with a limited current density, the total current decreases. The *Drop-Off* induces a rapid drop of the current because the electric connection to the surface area of the dropping part is lost. After this event, the total charge should be kept as small as possible to avoid blunting by reducing the residual etching time and current. [22]

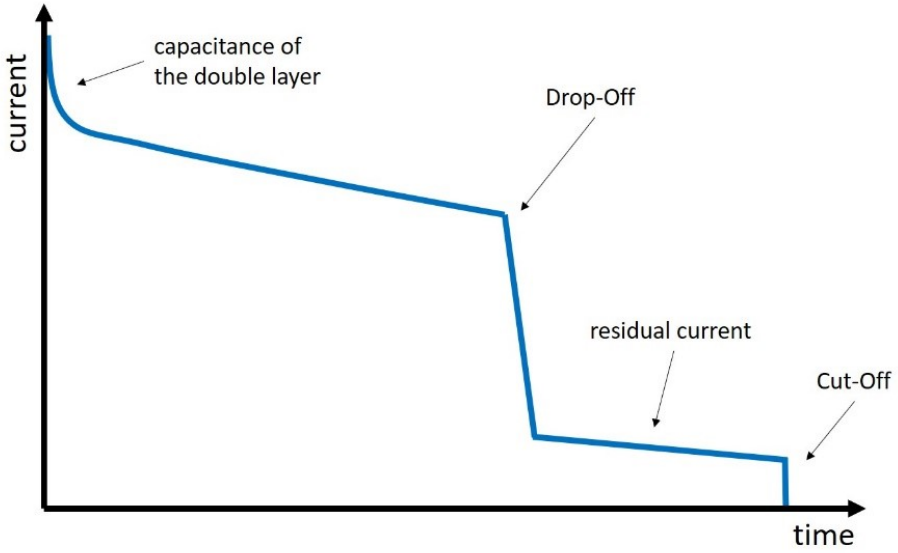

Figure 15: Draft of the etching current over time with Drop-Off and Cut-Off. (after [22]*)*

According to [35], a good and simple *Cut-Off* circuit can be accomplished with a differentiator, which detects the *Drop-Off*, and a flip-flop, which subsequent switches the MOSFET. The MOSFET cuts off the power supply of the electrolytic cell in a short time. *Cut-Off* times below 100 ns are possible with this design. However, several parameters can complicate the detection of the *Drop-Off*. The signal of the current can be very noisy. The vibration of the anode to control the tip shape can induce oscillation of the current. At higher voltages, more hydrogen is produced at the cathode and the electrolyte can evaporate, because of the electric resistance heat. This electrolyte boiling also leads to an unstable current. For this reason, the electric circuit for the *Cut-Off* has to be designed carefully, especially the differentiator to detect the correct slope at the *Drop-Off*. [22], [35]

Even if the voltage is cut off, a natural bias of the potential is present due to the difference between the work functions of the anode and cathode. As long as the anode is immersed in the electrolyte, a small current blunts the nanotip. Thus, only a *Cut-Off* of the voltage may not be enough to get a sharp tip. A better choice is to apply a reversed bias after the *Drop-Off* to avoid the blunting current from the natural potential difference. [30]

The blunting due to the residual current only affects the upper tip, which is connected to the electric circuit. The dropping part is separated immediately after the *Drop-Off* from the electric circuit. Nevertheless, handling the fabricated nanotip should be possible. This requires a certain length, which increases the mass. As discussed previously, a larger mass increases the breaking radius. Therefore, if the lower tip is used, a compromise between tip radius and practicability needs to be found. [22], [33]

A second possible method to avoid blunting is to remove the nanotip from the electrolyte directly after the *Drop-Off*. [26] This is explained in chapter 3.1.

Pulsed-voltage

Instead of applying a DC-voltage, rectangular pulses can be used for etching. The current density distribution at the anode becomes more uniform with a pulsed voltage. The formation of a *Neck-In* is reduced. During the pulse-on time, the concentration of acceptors reduces, and the dissolution products accumulate at the electrode-electrolyte interface, similar to DC-etching. This leads again to the vortex and the flux at the anode. However, during the pulse-off time, the products of the dissolution diffuse away, and the acceptor concentration increases. The vortex and the flux cannot establish. The same etching condition appears for the pulse-on time at every location of the anode, if pulses in the millisecond range are applied. A vibrating anode with pulse etching would be therefore unnecessary. [21]

The blunting of the tip can be reduced by applying only single pulses manually just before the *Drop-Off* happens. If pulse durations in the range of some milliseconds are applied, similar ROCs are accessible as with a *Cut-Off* circuit in the nanosecond range. [21]

By using a combination of first applying a DC voltage and second a pulsed voltage, the tip shape can be controlled. If only pulsed voltages are used, high aspect ratios can be achieved, due to the uniform etching rates. The longer the DC etching time, the shorter the tip length. Post-treatment with single voltage pulses can be used to increase tip angles with a minimal growth of the ROC. [21]

AC-voltage

Electrochemical polishing with AC-voltage can also be used to get nanotips with high aspect ratio. Nevertheless, more gas is generated at the specimen, which can cause more localised electropolishing activity. Furthermore, the passive layer is always removed at the negative potential at each cycle. [17] This is unwanted, as the passive layer ensures a good surface quality, especially for alloys, by keeping a constant etching rate of all elements.

However, with a combination of AC-voltage and pulsed voltage, nanotip radii below 20 Å are possible, but this method often leads to multi tips. [29] These tips can therefore not be used for electron tomography.

3. Experimental methods

This section first describes the preparation of nanotips and the constructed device. Next, the evaluation of nanotips will be explained, where for quick analysis a MATLAB-script has been written. In addition, the algorithm used to characterize the tips is specified. The respective code is attached in the appendix.

3.1. Preparation of nanotips

For the fabrication of nanotips a similar technique, as used in reference [9], is established. The process consists of three steps: *Thinning*, *Neck-In* and *Drop-Off*. Every step is performed using a microloop, which acts as the cathode. Due to the surface tension, the loop can keep a droplet of the electrolyte in between. The anode is moved by a manual manipulator. This method attains good nanotips with a simple construction and small amounts of consumed electrolyte.

In the first step – the *Thinning* step – the specimen is thinned quickly to a smaller diameter, as shown in Figure 16. This step is done at higher voltage to have an elevated etching rate. The specimen is immersed and removed completely from the electrolyte while voltage is applied. This is repeated until a small enough and constant diameter over the whole specimen is obtained. Thereby the initial quadratic circular cross section changes into a circle. If the original shape is not close to a nearly perfect square, an ellipse is etched. This affects the final shape of the nanotip.

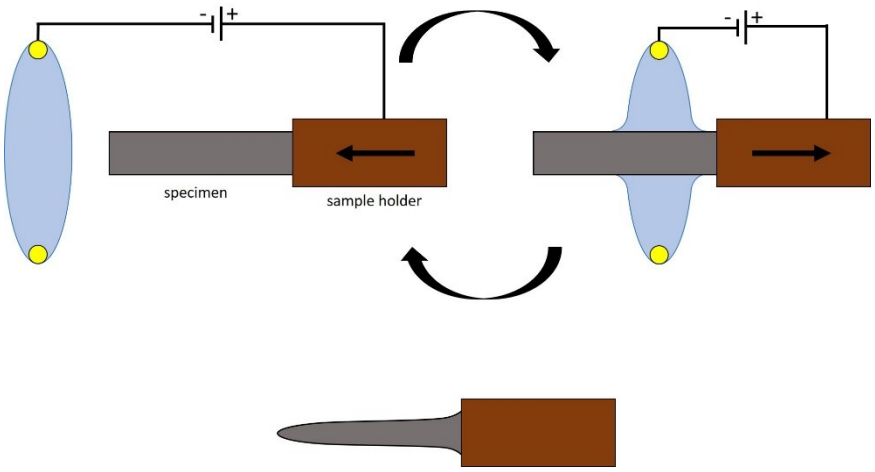

Figure 16: First step of thinning the specimen. (after [26]*)*

After the specimen is changed to a thin circular shape, the *Neck-In* can be created, as shown in Figure 17. The specimen is immersed in the electrolyte, but the front end of the nanotip protrudes from the electrolyte. Then the specimen is moved slightly back and forth while voltage is applied. The end of the tip is never immersed into the electrolyte to get a good *Neck-In*. If the front end starts to wobble, the *Neck-In* is too small to keep the front end straight. Then, the final step, the *Drop-Off*, can be performed.

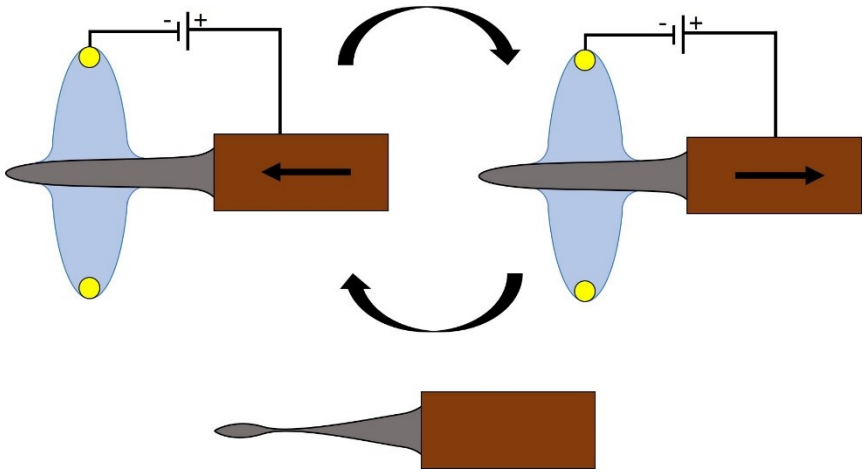

Figure 17: Forming the Neck-In. (after [26]*)*

During this last step, shown in Figure 18, the front end is broken off. For this purpose, the electrolyte-air interface is placed at the narrowest region of the *Neck-In* without any voltage applied. Now, the specimen is moved out of the electrolyte, while at the same time voltage is switched on. The surface tension pulls the front end into the electrolyte, while at the same time the diameter of the *Neck-In* shrinks. If the cross-sectional area falls below a critical value, the force, which is caused by the surface tension, is strong enough to exceed the tensile strength of the material. Thus, the front end breaks off. If this does not happen, the process must be repeated until the end drops off.

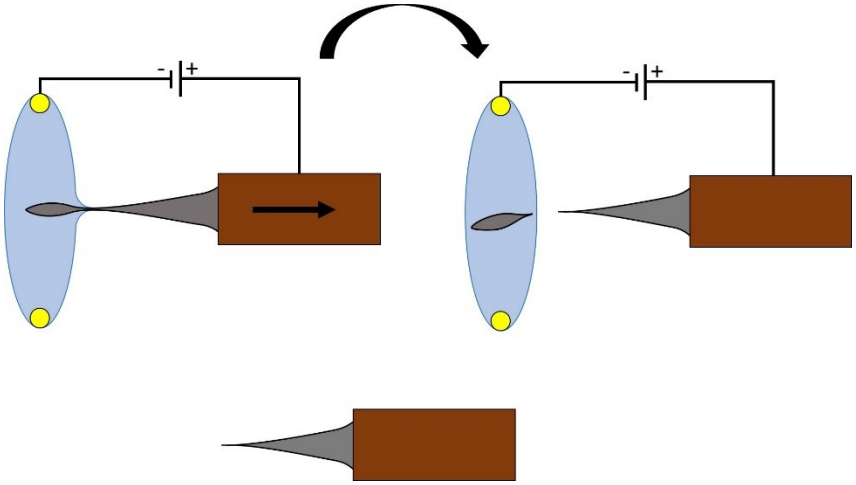

Figure 18: Performing the Drop-Off. (after [26]*)*

The specimen at the *Neck-In* is under tensile stress before the *Drop-Off*. If the front end breaks off, a slight recoil happens which can bend the nanotip. Since the volume of the nanotip is very small, the released energy can be enough to melt the front end. The result is a ball-shaped end of the nanotip. [37]

The specimen cross sections are usually squares with side lengths between 200 µm and 400 µm, because this shape is easier to prepare than e.g. circular geometries. A fast fabrication of the nanotips can be accomplished by using two different solutions. First, a stronger electrolyte is used to ensure high etching rates and thereby obtain tips quickly. With this electrolyte all three steps are performed: *Thinning*, *Neck-In* and *Drop-Off*. Afterwards, a weaker electrolyte is used, and the last two steps, the *Neck-In* step and the *Drop-Off* step are repeated on the previously fabricated tip. The strong electrolyte is used for fast etching processes and the weak electrolyte guarantees a good quality of the nanotip.

An advantage of this method is that blunting of the tips is avoided, because the specimen leaves the electrolyte instantly after the *Drop-Off*. This makes a fast *Cut-Off* circuit unnecessary and a reverse bias is also obsolete.

The setup developed for this method is shown in Figure 19. The single steps of the nanotip fabrication can be observed with a transmitted light microscope (*Wild Heerbrugg M8*). The voltage in use for the etching is applied by a laboratory power supply (*RS Pro RS6005D*). The movement of the specimen is implemented with an XYZ-table (*CHUO PRECISION INDUSTRIAL LT-211-1CL*). The Y- and Z-axis are used to position the specimen exactly in the middle of the microloop. The X-axis moves the specimen back and forth for different etching steps. For the microloop, a gold wire with 0.5 mm diameter from *Goodfellow* is used. The diameter of the loop is approximately 5 mm. The microloop is connected to the negative pole of the power supply with a crocodile clip. The realized apparatus can be seen in Figure 20 and Figure 21.

The specimen is held by a tweezers, which can be locked, and has a good corrosion resistance to acids. The tweezers can be fixed by a screw on the manipulator and is electrically isolated from it. The tweezers are then connected to the positive pole of the power supply with a crocodile clip. A button is used to close the electric connection from the electrolytic cell to the positive pole. The electrolytic cell stays at ground potential with opened switch. The setup is now ready to start the etching process.

The electrolyte is dripped from a height of approximately 5 mm above the microloop with a pipette. Due to the surface tension, the microloop is able to hold the liquid. The thickness of the droplet in the loop can be controlled by varying the height from which the electrolyte is dripped. A thin electrolyte layer is often used at the *Neck-In* step in order to avoid immersion of the sample holder, if the specimen length is already too short. A beaker is placed under the microloop to collect the dripping solution.

The device must be cleaned properly after finishing the fabrication of the nanotip. Especially the microloop has to be rinsed with ethanol and distilled water. If precipitates are visible on the gold cathode, they can easily be wiped away with cleaning paper.

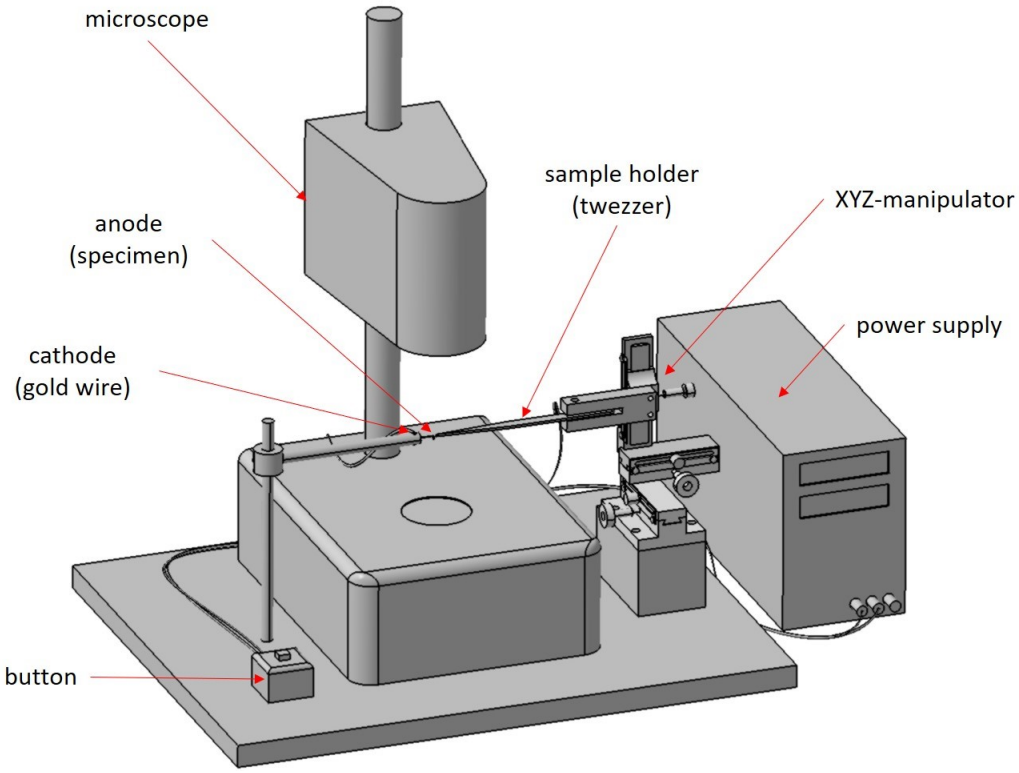

Figure 19: Planned construction for the nanotip etching.

Figure 20: Overview of the realized apparatus for the nanotip preparation.

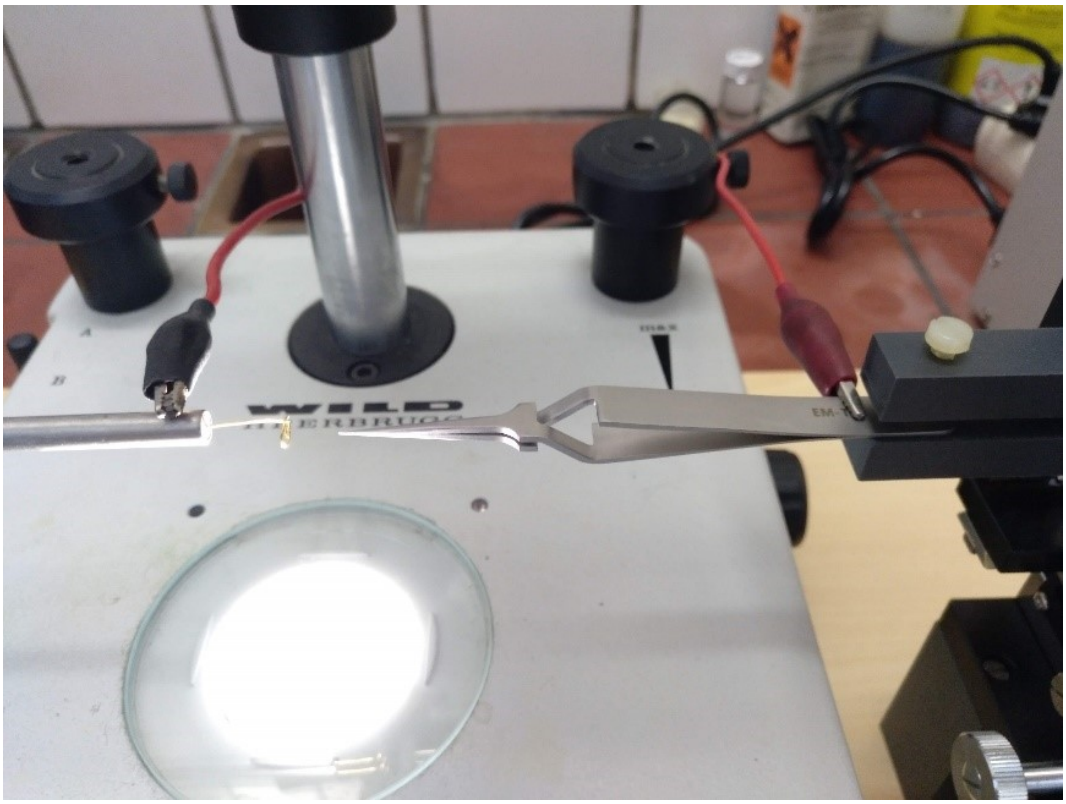

Figure 21: Close-up view of the realized apparatus. On the left side is the goldwire, which contains the electrolyte, and is connected to the negative pole of the power supply. On the right side are the tweezers, which are connected to the positive pole. The tweezers are fixed to the manipulator, which carries out the movement.

3.2. Evaluation of nanotips

A script was developed, which evaluates the angle of the tip α, the radius of curvature (ROC) and the length of the tip, which has a smaller diameter than 100 nm (called the *critical length*). These characteristic parameters of the tip can be seen in Figure 22. For the comparison of nanotips examined in this thesis, only the *critical length* is considered, as the resolution of the used SEM is often not good enough to give reliable values of the ROC. Furthermore, due to the small size of the ROC the script can misinterpret the curvature of other irregularities or protrusions as the ROC of the nanotip. The tip angle depends on how the image is cropped. If only the last few hundred nanometres of the tip are considered, the angle is often bigger than if a longer part of the tip is taken into account. Only the *critical length* does not depend on these parameters and is therefore a reliable measure, which works well for the comparison of different nanotips.

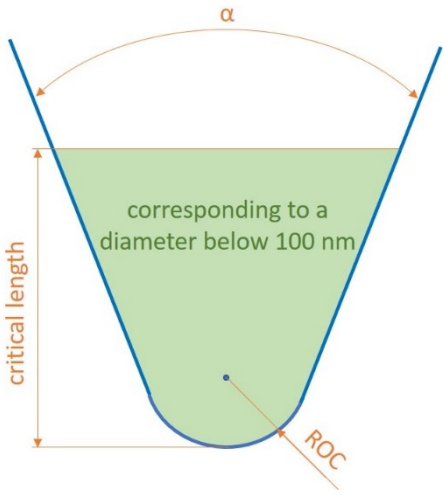

Figure 22: Draft of a tip with its characteristic parameters, which are evaluated with the MATLAB-script.

First, a SEM image of the analysed nanotip is loaded into the script. For this, the path, where the image is saved, and the name of the image have to be entered. Additionally, the correct scale and the size of the image for correct conversion from pixel to nanometres have to be checked. The original image has to be processed first to calculate the values of interest. Figure 23 shows an example of an original image, which is loaded into the script.

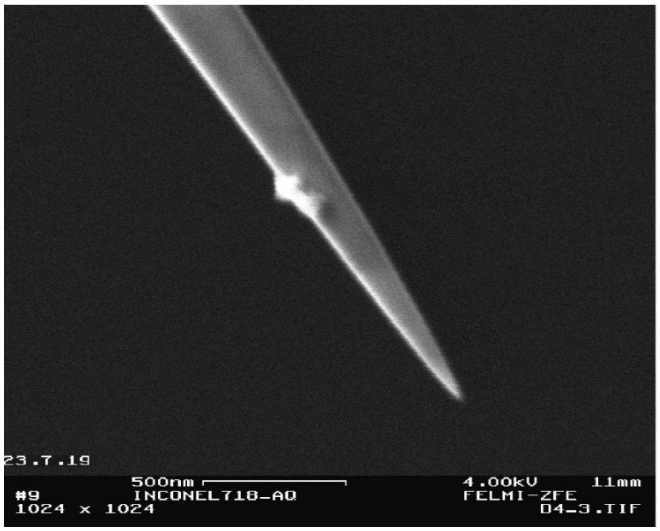

Figure 23: Example for the demonstration of the evaluation of nanotips. This is the original image, which is loaded into the script for further calculations.

After starting the program, it is requested to select the region of interest (Figure 24). For this purpose, a rectangle can be drawn and by clicking the right mouse button, the option to *Crop Image* appears. This area will then be used for further calculations.

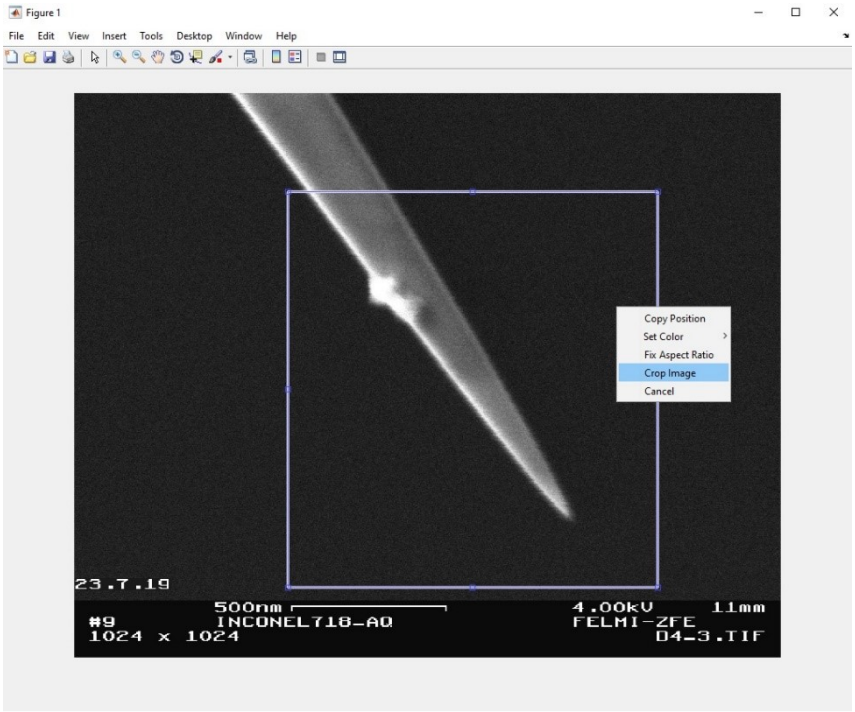

Figure 24: Selection of the area of interest.

The consequent steps of image processing are shown in Figure 25. After the image has been cropped, the contrast is adjusted with a function from the MATLAB-library. The greyscale image is converted into a binary image, consisting of zeros and ones, to enable further calculations. The threshold is evaluated with the Otsu's method, which is already implemented. [39] To avoid failures at this step, the whole tip in the original SEM image should be brighter than the background. Good results were achieved with the TTL detector. Figure 2 shows the difference between the two detectors. For the E-T detector, the center of the tip is darker than the background. This can lead to an error at the calculation. In contrast for the TTL detector, the tip is brighter than the background.

At the next step, small areas in the tip, which are wrongly attributed to the background, are automatically removed. This is realised by deleting connected areas, which have less pixels than a specified number, and, in order to improve the calculations, the boundary of the tip will be smoothed as well. The difference between the original and the smoothed tip is not large, but the curvature of the tip is a little bit flattened. This is also one reason why the ROC is not considered for validating the quality of the tips.

From the smoothed image, the boundary is evaluated with the MATLAB function *bwboundaries*, which traces the border in a binary image, and is needed for further calculations.

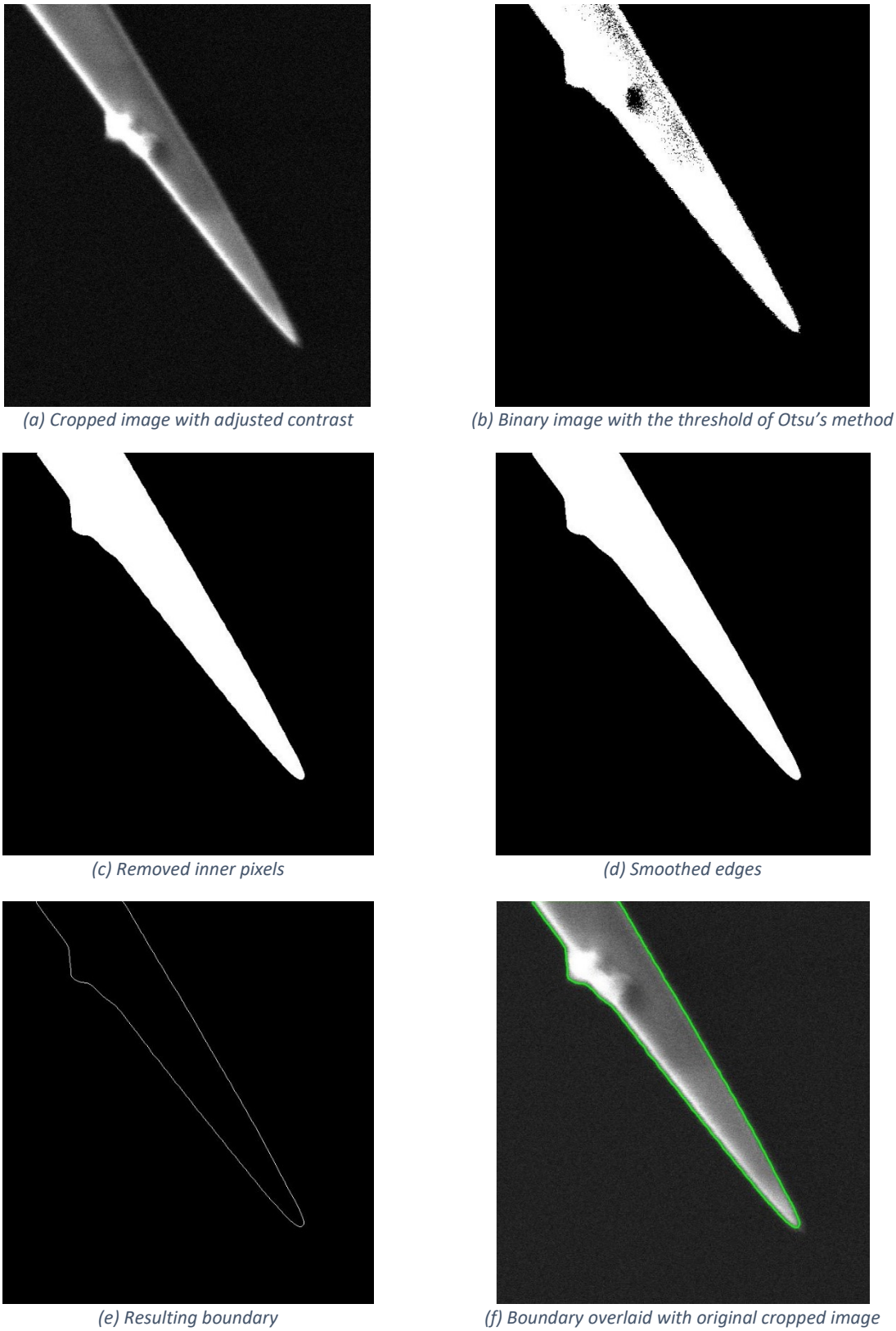

(a) Cropped image with adjusted contrast

(b) Binary image with the threshold of Otsu's method

(c) Removed inner pixels

(d) Smoothed edges

(e) Resulting boundary

(f) Boundary overlaid with original cropped image

Figure 25: Image processing steps to get the boundary of the tip from the cropped image.

Next, the Radon transform is used to detect the two lines of the shaft. This enables the calculation of the tip angle. The calculation of the Radon transform can be done either on the cropped image or on the resulting boundary image. If the original image does not have a bright boundary, it is recommended to do the calculation with the boundary image, as it requires a certain amount of contrast to perform properly.

The Radon transform is a commonly used method for line detection. A line in the original image appears as a point in the Radon space. The mathematical expression for this is given by equation (12). Here, a 2-dimensional function *g(x,y)* is transformed. The Dirac function forces the integration along the line, which is given by equation (13). [40]

$$R(x', \Theta) = \int_{-\infty}^{\infty} \int_{-\infty}^{\infty} g(x, y) * \delta(x' - x * \cos\Theta - y * \sin\Theta)\, dx\, dy \tag{12}$$

$$x' - x * \cos\Theta - y * \sin\Theta = 0 \tag{13}$$

The principle of the Radon transformation is illustrated in Figure 26. The function g(x,y) is summed up along the perpendicular axis of ρ. The result is the function R(ρ). This is done for several angles θ. Figure 27 shows the Radon-transformed function of a nanotip.

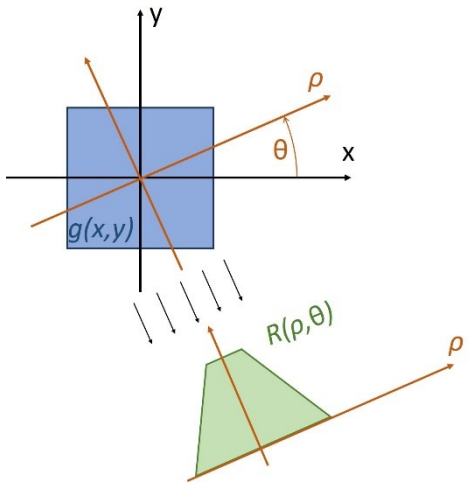

Figure 26: Radon transformation for a 2-dimensional function visualised. (after [40]*)*

A problem is sometimes the selection of the correct peaks. The peak-selection problem can be solved with a mean filter. [40] This problem appears only rarely during nanotip evaluation and can be avoided by selecting a smaller or bigger area at the cropping step. Thus, the peak-selection problem is not considered further.

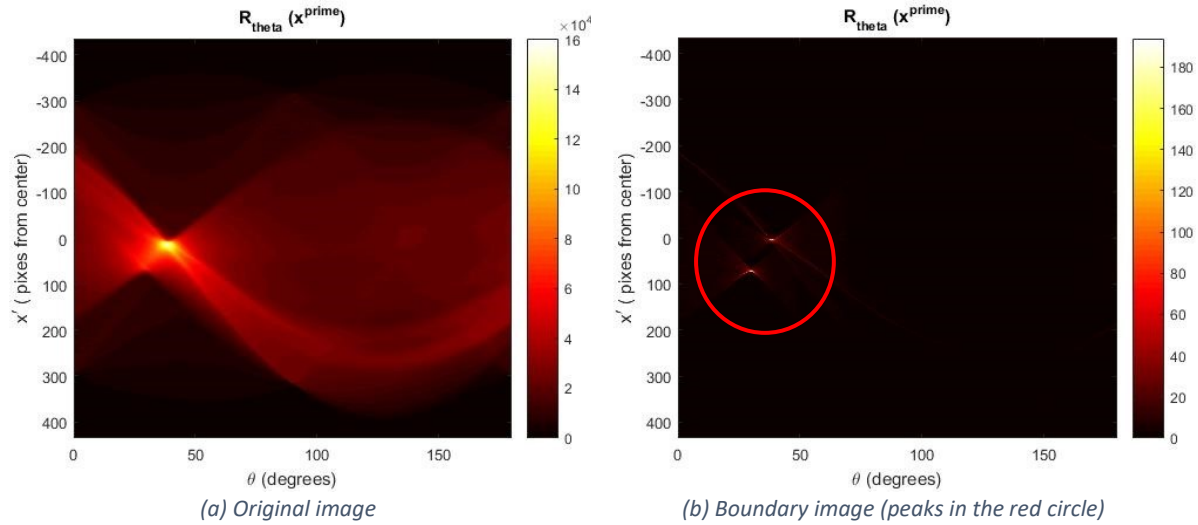

(a) Original image *(b) Boundary image (peaks in the red circle)*

Figure 27: Radon transformation of the nanotip from Figure 23.

Figure 27 shows the difference between the Radon transform of the original and the boundary image. The boundary in the original image is not bright enough, especially the upper edge of the tip, which complicates the detection of the second peak. However, two peaks are clearly visible in the Radon transform of the boundary image. Problems occur only if a side of the tip is not a straight line. If the edge consists for example of two lines, an additional peak appears in the Radon space. This can be solved by adjusting the region of interest or by selecting the peak manually.

If the two peaks are found, the tip angle α can be calculated as the difference of these two corresponding angles:

$$\alpha = |\theta_1 - \theta_2| \tag{14}$$

For the evaluation of the *critical length*, the image (Figure 25 (d)) is rotated clockwise by the angle $\frac{|\theta_1+\theta_2|}{2}$. This way, the tip is orientated vertically. From bottom to top, the width of the tip is checked by the algorithm at each height until it reaches 100 nm. The distance from the apex of the tip to this position (marked as a red line in Figure 28) is the *critical length*.

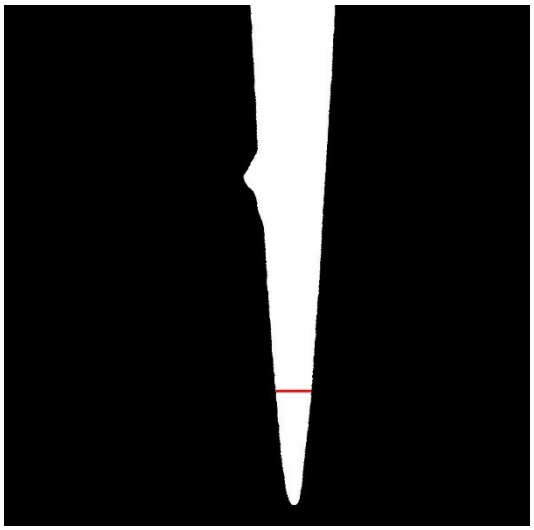

Figure 28: Rotated nanotip with the 100 nm marker (red line), the length below is the critical length.

For the ROC evaluation, the function *imfindcircles* from the MATLAB-library is taken. The function uses the circular Hough transformation, which is explained in [41]. This transform can detect any shape, which can be expressed mathematically, but the computational effort increases drastically because more complex shapes require more dimensions. For a line, two dimensions are necessary (y-intercept and slope), whilst for a circle, even three dimensions are required (x-offset, y-offset, radius). [42]

It is assumed, that the end of the tip is the roundest shape in the image. The algorithm starts with a low sensitivity for the detection, which is increased until one circle is found. This works well for perfect tips, but if they feature irregularities or protrusions, the end of the tip is sometimes misinterpreted. Figure 29 shows such an error. This can be avoided again by selecting a new area of interest or by choosing the circle manually.

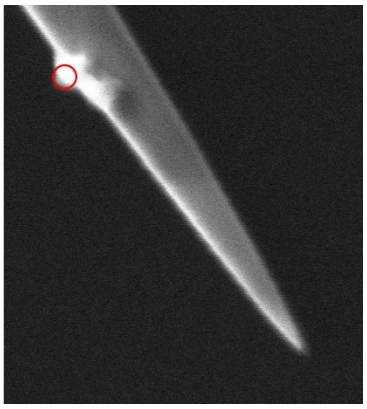

Figure 29: Detection of the wrong circle; irregularities captured instead of the ROC of the tip.

The results of the MATLAB-script are shown in Figure 30. The length of the yellow line is 100 nm and indicates the *critical length*, which runs from this marker to the apex below. The blue lines are the calculated lines for the tip angle α. At the end of the tip, the discrepancy between the calculated lines and the actual nanotip increases. This emphasises the dependence of the calculated tip angle on the selected area. The red circle indicates the ROC, but the calculated radius does not match the actual ROC well. The fluctuations of the tip angle and ROC are the reason why the *critical length* is chosen for comparisons.

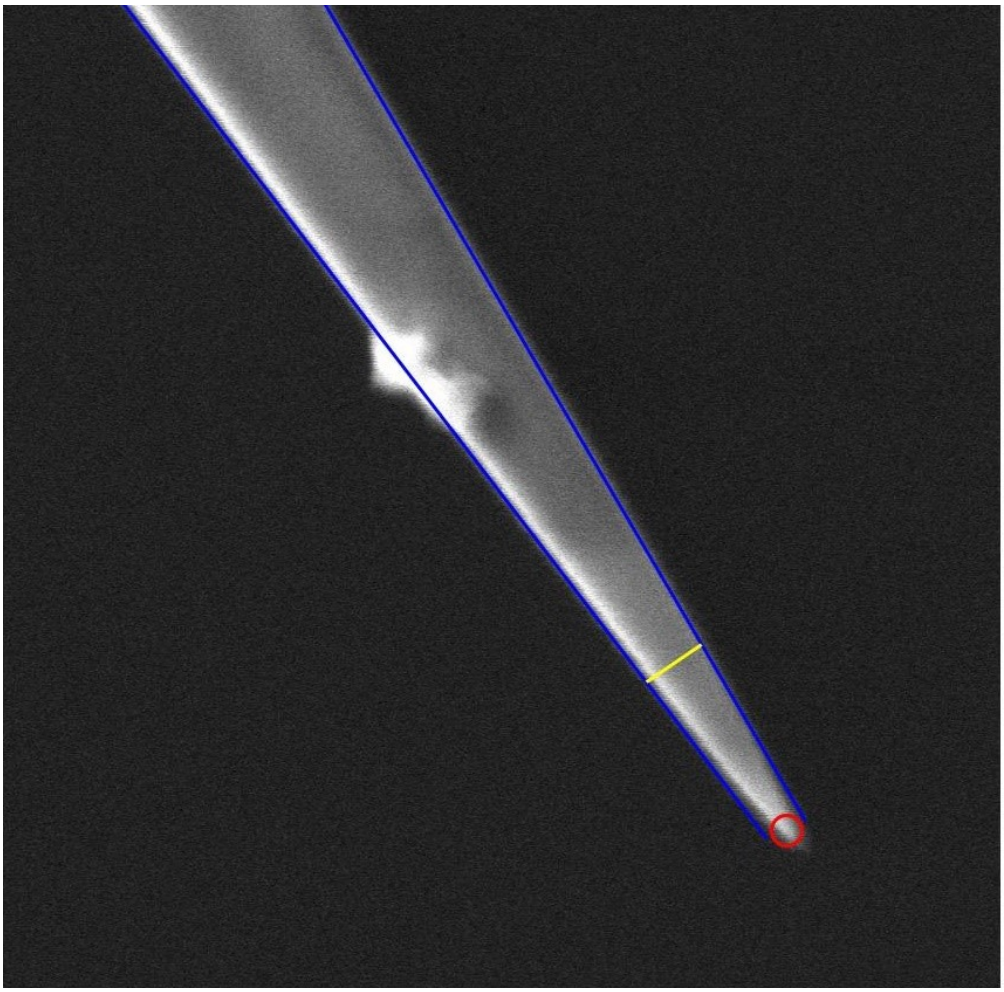

Figure 30: Finished evaluation with the characteristic values (ROC, critical length and tip angle).

4. Materials

In this chapter, the preparation of nanotips made from two different types of materials is described. The first material is a nickel-based alloy. The main focus on this material is to perform electron tomography of this sample, in order to visualize and identify precipitates within the alloy. In addition to that, a second material, a tungsten needle is examined. Here, the aim is to re-sharpen the sample for the re-use as a micromanipulator for FIB applications.

4.1. Inconel 718

The first material is a nickel-based superalloy, called Inconel 718, which features good corrosion resistance and high strength with outstanding weldability. It also provides high creep strength and oxidation resistance up to high temperatures. Due to these properties, the alloy is already a commonly used material in applications of gas turbines, rocket motors, spacecraft and nuclear reactors. [43]

The composition of the Inconel 718 alloy is listed in Table 1. The main parts are nickel, chromium, niobium and molybdenum. The iron ratio is balanced. It has a minimum percentage of around 12 wt% up to nearby 25 wt%. [43]

Table 1: Chemical composition of Inconel 718 in weight percentage.

	Ni	**Cr**	**Fe**	**Nb**	**Mo**	**Ti**	**Al**	**Co**	**C**	**Mn**
Max wt%	55.00	21.00	bal.	5.50	3.30	1.15	0.80	1.00	0.08	0.35
Min wt%	50.00	17.00	bal.	4.75	2.80	0.65	0.20	---	---	---
	Si	**P**	**S**	**B**	**C**					
Max wt%	0.35	0.015	0.015	0.006	0.3					
Min wt%	---	---	---	---	---					

The properties are achieved by precipitation hardening at controlled ageing treatment. Three kinds of different intermetallic precipitations can be distinguished: [44]

- *γ'-phase* has a spherical shape and a chemical composition of $Ni_3(Al,Ti,Nb)$
- *γ''-phase* is disk-shaped and has a chemical composition of $Ni_3(Nb,Ti)$
- *δ-phase* forms from the metastable γ''-phase and is plate-shaped.

The γ'-phase is coherent and the γ''-phase is semi-coherent and both phases are responsible for the precipitation hardening. The incoherent δ-phase is only formed at grain boundaries and therefore it strengthens grain boundaries, but it does not contribute to the precipitation hardening. [44]

The reason why tomography of the alloy becomes interesting, is to investigate the precipitates in 3D detail. [44] From five specimen, which are heat- and pressure-treated differently, nanotips are supposed to be made. Before that, a disk is cut from each specimen for the PIPS preparation. These samples can be investigated preliminary with the TEM. If precipitations are present, a tomography experiment of the nanotips is useful.

The following specimens are investigated:

- Alloy718 (Ref): The reference sample is untreated.
- Alloy718_AC: The sample is forged at 1000°C ($\varepsilon = 0.4$, $\dot{\varepsilon} = 0.015^{-1}$) and air-cooled.
- Alloy718_WQ: The sample is forged at 1000°C ($\varepsilon = 0.4$, $\dot{\varepsilon} = 0.015^{-1}$) and water-quenched.
- Alloy718_DA_WQ: The sample is forged at 1000°C ($\varepsilon = 0.4$, $\dot{\varepsilon} = 0.015^{-1}$), direct-aged and water-quenched.

- Alloy718_ST_DA_WA: The sample is first forged at 1000°C and air-cooled. Afterwards it is heat-treated at 980°C for 10 minutes and air-cooled. Finally, it is again heat-treated at 720°C for 10 minutes and water-quenched. ($\varepsilon = 0.4$, $\dot{\varepsilon} = 0.015^{-1}$)
- Alloy718_ST_P_DA: The sample is treated as the one before, but instead of 10 minutes heat treatments it is heat-treated for 1 h. ($\varepsilon = 0{,}4$, $\dot{\varepsilon} = 0{,}015^{-1}$)

Additionally, an Inconel 718 (Alloy718_HT) specimen was only used for etching tests. This sample received an unknown heat treatment.

For a specific nickel-based superalloy, named CMSX-4, it is recommended to use two different electrolytes. The first one is to achieve high etching rates and the second electrolyte is for a good tip quality. The proposal for the first electrolyte is a solution of 15 % perchloric acid in acetic acid and the second solution consists of 2 % perchloric acid in 2-butoxyethanol. [9]

However, the superalloy CMSX-4 has a different composition than Inconel 718. Good properties for electrochemical polishing of Inconel 718 are offered with a solution of 20 vol% perchloric acid in acetic acid. The polarisation curve of Inconel 718 with this kind of electrolyte shows a stable plateau of the polishing regime. More importantly, the current density increases steadily with increasing potential. This allows higher etching rates, which are relevant for the *Thinning* step. Electrolytes with higher volume ratios of perchloric acid have only small current densities at comparable potentials. [20]

The prepared electrolytes are:

- Electrolyte 1: 20 vol% perchloric acid (60 wt%) in acetic acid
- Electrolyte 2: 2 vol% perchloric acid (60 wt%) in 2-butoxyethanol

This is done by mixing 25 ml of perchloric acid (60 wt%) in 75 ml of acetic acid for electrolyte 1 and 1 ml of perchloric acid (60 wt%) in 49 ml 2-butoxyethanol for electrolyte 2. In reference [20], perchloric acid with 70 wt% is used. Thus, the prepared solution has a lower ratio of perchloric acid than the solution from reference [20]. However, the U-I curve of solutions with 10 vol% and 20 vol% perchloric acid are nearly identical above an applied voltage of 6 V. [20]

The current density is less dependent on the change of concentration in weak electrolytes compared to strong electrolytes. The weak electrolyte operating points are preferred, since the concentration of the solution in the microloop will change during the etching process because of the high surface to volume ratio and temperature increase. The solution consists of acetic acid, perchloric acid and water. Perchloric acid has the highest boiling point with 203°C. [45] Due to the lower boiling point of acetic acid, which is at only 118°C, and water, the concentration of perchloric acid will rise during the etching. [46]

Due to the high number of elements of the alloy and the electrolyte, the chemical reactions in the electrolytic cell are complex. The dissociation of the electrolyte is given in equation (15). [47] The perchlorate acts as anion and diffuses to the anode. Here, it reacts further with the elements of the nickel-based superalloy.

$$HClO_4 + CH_3COOH \rightleftharpoons CH_3COOH_2^+ + ClO_4^- \tag{15}$$

Before the etching process can start, the samples have to be prepared in the correct shape. Due to the high strength of the alloy, the sample preparation is time-consuming. The initial shape of the material is a cylinder with a diameter of 1 cm and a length of 1 cm to 2 cm. The reference sample is shown in Figure 31. The aim is to get pieces with a length of 5 mm to 10 mm and, most importantly, a symmetric cross section. The easiest shape of a symmetric geometry to produce is a square. The length of each square side should be around 300 µm. The area of the cross section is not important for the quality of the nanotip, it only influences the etching time of the *Thinning* step.

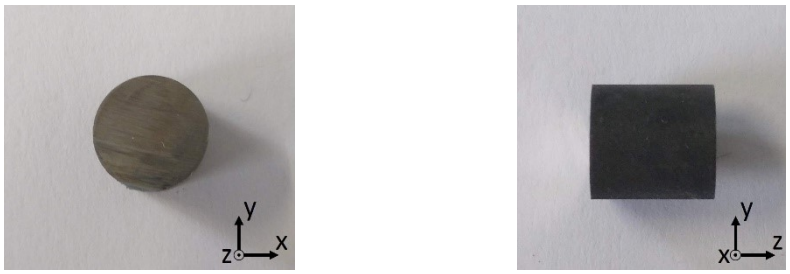

(a) Front view (b) Side view

Figure 31: Starting material of the Inconel 718 alloy. A cylinder with a diameter of 1 cm and length of around 1 cm.

Figure 32 shows how rectangular pins are obtained from the cylinder. First, a disk is cut from the original material with a rotating saw. A diamond-cutting disk is used for the nickel-based alloy. The thickness of the specimen disk should be around 300 µm. The desired thickness is not always obtained, and the sample is often not uniformly thick due to bending of the cutting disk. However, the rotating saw is still used, because it offers a higher cutting speed compared to the wire saw. Two discs are cut from every specimen, one for the PIPS preparation and the other one for the nanotip preparation.

Afterwards, the specimen disk is glued to a ceramic sample holder with a low melting point wax to cut pins out of the disk with the wire saw. Around ten pins can be obtained from a single disk. A rectangular cross section of the pins is beneficial for the grinding process. For this reason, the pins are cut with 500 µm thickness.

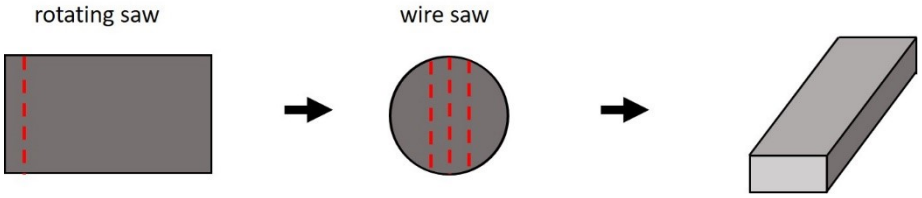

Figure 32: Cutting process: from cylinder to pins.

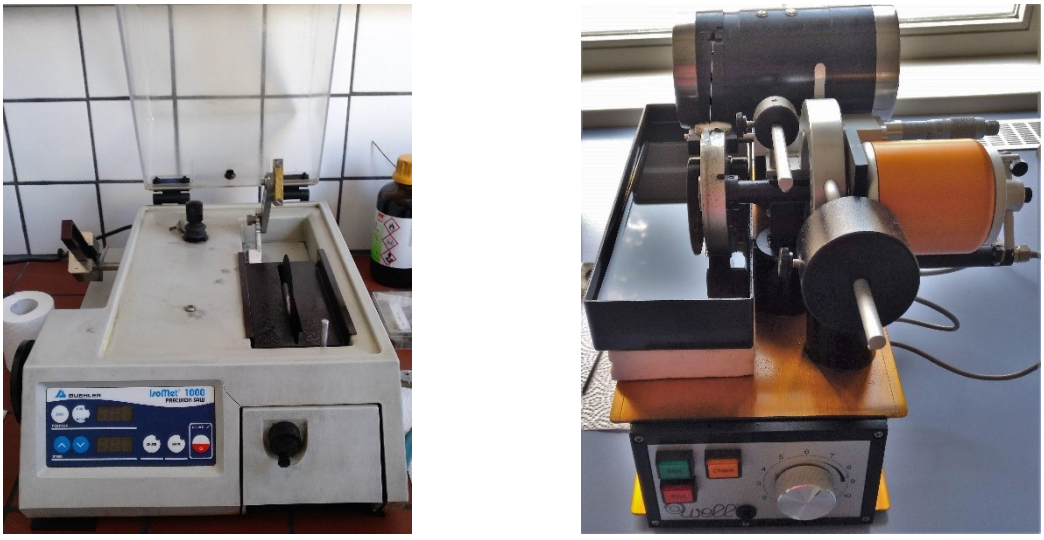

(a) Rotating saw (b) Wire saw

Figure 33: (a) Used rotating saw with a diamond cutting disk (IsoMet 1000 precision saw from Buehler). (b) Used wire saw (diamond wire saw Series 3400 from WELL).

Although the rotating saw and the wire saw work accurately and precisely, they are not good enough to get a sufficiently symmetric cross section. The pins also have burrs caused by the cutting processes.

Therefore, a grinding process is necessary. A rectangular start dimension of the sample of around 300 µm times 500 µm simplifies the handling of the specimen at the grinding process.

For the grinding, the *Disc Grinder 623* from *Gatan* is used, shown in Figure 34. The pins can be fixed with the low melting point wax on the specimen mount. The diameter of the mount is 9 mm. Thus, the pins have to be shortened with the wire saw to the respective maximum length of 9 mm. The specimen mount can be put into the Disc Grinder, where it is possible to adjust the height of the specimen with the micrometer screw. The grinding is performed on the *HandiMet* with water as lubrication and cooling medium. As abrasive paper, the *CarbiMet* strips with a grit size of P1200 from *Buehler* is used.

(a) HandiMet Grinder *(b) Disc Grinder* *(c) Specimen mount*

Figure 34: Used devices for the grinding process.
(a) HandiMet Grinder from Buehler; (b) Disc Grinder 623; (c) specimen mount.

The grinding process is done in four steps to achieve a square cross section and is shown in Figure 35. First, the specimen is observed with a light microscope to examine, which short side has the least burrs. This side is then glued to the specimen mount of the grinder with low melting point wax before the sample gets grinded and polished on the opposite side with more burrs. It is not necessary to remove a large amount of material. Second, the same procedure is done on the long sides. Once again, the side without any or with fewer burrs is identified and glued to the specimen mount. The opposite long side with more burrs is again polished. Afterwards, in the third step, the specimen is flipped and the untreated long side is now polished. Here, the end dimension of the specimen can be chosen by removing more or less material. However, this is not as important as the symmetry of the cross section. The last position of the micrometer screw is noted. The last step is to put the second short side on top and grind the last unpolished side until the sample has a square cross section. This procedure guarantees a high symmetric cross section. The micrometer screw is always adjusted in steps of10 µm.

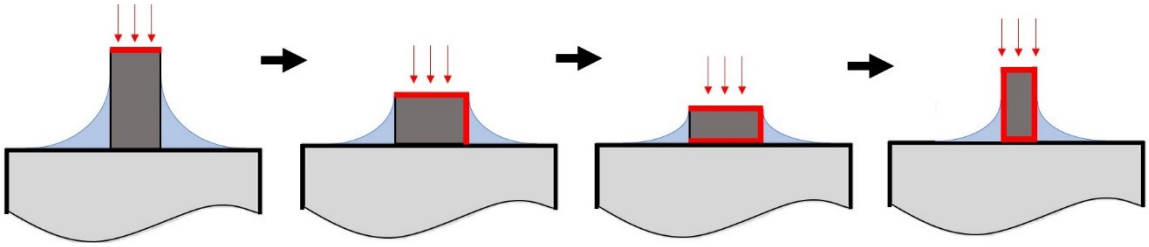

Figure 35: Grinding process, the red lines mark the grinded sides.

The finished specimens are placed in acetone for one hour to remove the residues of the wax. Afterwards, the dimension of the cross section is measured with a measurement probe from *Heidenhain*. Most specimen measurements vary around ±5 µm due to some irregularities of the specimen or uncertainties of the thickness measurement.

The pins are fixed into copper sleeves to handle them during the etching process and to mount them in the sample holder of the TEM. These are commercial copper ferrules. As shown in Figure 36, the

specimen is fixed by crimping the sleeves. They should be well centered to ensure that they are close to the tilt axis of the TEM sample holder.

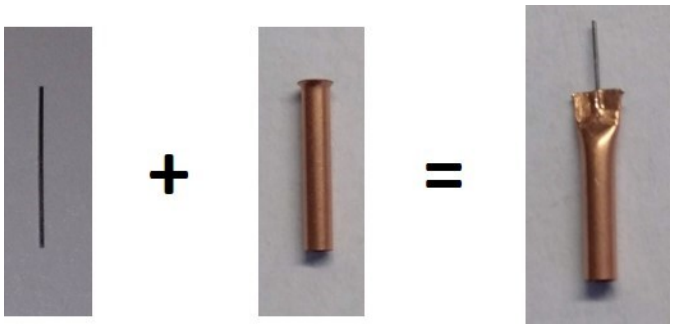

Figure 36: Mounting of the sample in the copper ferrule.

Before etching, the sample is rinsed with isopropanol, ethanol and distilled water. In Figure 37, the specimen is mounted after the cleaning step at the etching device.

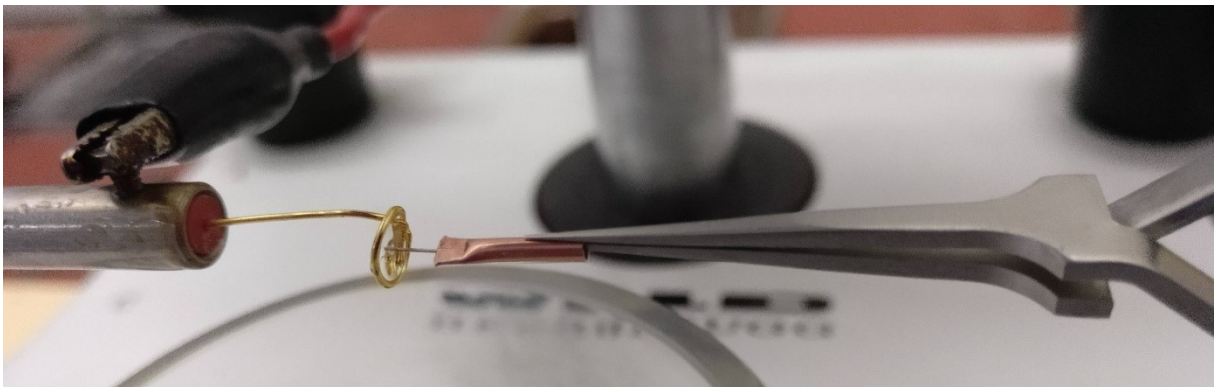

Figure 37: Mounted sample, which is ready to be etched.

The first step is the thinning of the specimen with the electrolyte (solution of perchloric acid in acetic acid). The high concentration of perchloric acid allows a high etching rate. During etching, the solution becomes saturated. This is noticeable by a change in color of the electrolyte. The color of the transparent solution changes to orange. If saturation increases further, the color changes to green. Saturation reduces the etching rate and stops when the electrolyte is fully saturated, which is observable by a dark green color of the solution. The droplet in the microloop should be renewed frequently to maintain good etching rates.

If the sample is thin enough, the *Neck-In* is formed and subsequently the *Drop-Off* is performed.

Afterwards, the electrolyte is changed. For the next steps, electrolyte 2 (solution of perchloric acid in 2-butoxyethanol) is used. The *Neck-In* step is performed on the tip, which was previously prepared with the first electrolyte. Lastly, the *Drop-Off* finalises the nanotip using the weak electrolyte. The specimen is rinsed again with isopropanol, ethanol and distilled water. The liquids are rinsed over the tweezers to the sample. The nanotip should not be immersed directly into a liquid surface, because the surface tension can bend the tip.

For each etching step, different voltages are applied. The parameters for the preparation of nanotips are listed in Table 3. The age of the electrolyte at the time of the tip preparation is noted as well, because a change of the polarisation curve has been detected in reference [48] and could impact the nanotip preparation. The number of pulls necessary for the *Drop-Off* is also recorded.

The effect and interpretation of the different parameters on the specimen is discussed in section 5.1.

Table 2: Parameters of the Inconel 718 etching. Electrolyte 1 is the solution perchloric acid in acetic acid. Electrolyte 2 is the solution perchloric acid in 2-butoxyethanol.

				Electrolyte 1				Electrolyte 2			
No.	**Age**	**Material**	**Dimension**	**Thinning**	**Neck-In**	**Drop-Off**	**Pulls**	**Neck-In**	**Drop-Off**	**Pulls**	**Duration**
1	1 d	Alloy718_HT	(280 x 300) µm²	25 V	25 V	25 V	---	15 V	15 V	1	---
2	7 d	Alloy718_HT	(220 x 230) µm²	25 V	25 V	---	0	15 V	10 V	3	---
3	36 d	Alloy718_AC	(195 x 200) µm²	20 V	20 V	---	0	15 V	16 V	40	30 min
4	36 d	Alloy718_AC	(195 x 205) µm²	20 V	20 V	---	0	15 V	8 V	21	30 min
5	36 d	Alloy718_AC	(190 x 205) µm²	20 V	20 V	20 V	1	15 V	24 V	13	20 min
6	36 d	Alloy718_AC	(185 x 185) µm²	20 V	20 V	---	0	15 V	4 V	6	15 min
7	36 d	Alloy718_AC	(190 x 190) µm²	20 V	20 V	20 V	3	15 V	2 V	31	15 min
8	36 d	Alloy718_AC	(190 x 190) µm²	20 V	20 V	20 V	1	15 V	20 V	23	15 min
9	36 d	Alloy718_AC	(180 x 190) µm²	20 V	20 V	20 V	1	15 V	12 V	9	15 min
10	36 d	Alloy718_AC	(190 x 220) µm²	35 V	35 V	35 V	1	15 V	2 V	5	15 min
11	51 d	Alloy718 (Ref)	(190 x 200) µm²	20 V	20 V	20 V	2	15 V	4 V	11	20 min
12	51 d	Alloy718 (Ref)	(210 x 240) µm²	30 V	25 V	20 V	2	15 V	4 V	5	20 min
13	51 d	Alloy718_DA_WA	(290 x 480) µm²	20 V	20 V	20 V	1	15 V	4 V	5	30 min
14	56 d	Alloy718 (Ref)	(185 x 190) µm²	20 V	20 V	20 V	3	15 V	4 V	20	30 min
15	69 d	Alloy718 (Ref)	---	20 V		Only thinning					
16	69 d	Alloy718 (Ref)	---	35 V		Only thinning					
17	84 d	Alloy718 (Ref)	(165 x 175) µm²	20 V	20 V	---	---	15 V	4 V	15	20 min
18	84 d	Alloy718 (Ref)	(200 x 215) µm²	20 V	20 V	20 V	1	15 V	4 V	2	15 min
19	92 d	Alloy718 (Ref)	(170 x 180) µm²	35 V	35 V	35 V	1	15 V	4 V	5	20 min
20	92 d	Alloy718 (Ref)	(165 x 175) µm²	Only re-sharpening				15 V	4 V	12	10 min
21	92 d	Alloy718 (Ref)	(200 x 215) µm²	Only re-sharpening				15 V	4 V	11	10 min
22	92 d	Alloy718 (Ref)	(185 x 190) µm²	Only re-sharpening				15 V	4 V	18	10 min
23	92 d	Alloy718 (Ref)	(210 x 240) µm²	Only re-sharpening				15 V	4 V	2	10 min
24	98 d	Alloy718 (Ref)	(170 x 180) µm²	Only re-sharpening				15 V	4 V	3	10 min
25	98 d	Alloy718 (Ref)	(185 x 190) µm²	Only re-sharpening				15 V	15 V	4	10 min
26	98 d	Alloy718_HT	(175 x 180) µm²	4 V	4 V	4 V	6	4 V	4 V	3	30 min

4.2. Tungsten

The second material, from which nanotips are prepared, is shown in Figure 38. It is a tungsten needle, which is used for in-situ micromanipulation or for electric measurement. This needle has to be re-sharpened for re-using old needles. It does not have to fulfill the high requirements for electron tomography like the nickel-based alloys. The aspect ratio should not be too high to ensure mechanically stability.

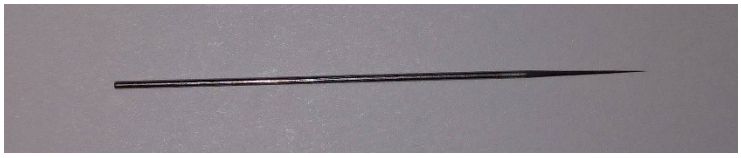

Figure 38: Tungsten tip, which has to be re-sharpened.

Most papers, which deal with electrochemical polishing of nanotips, consider tungsten wires. A lot of information about this matter can be found in the references [21], [22], [28], [34], [35], [37].

The most common electrolyte for electrochemical polishing of tungsten is an aqueous base with potassium hydroxide, called caustic potash. A correlation between electrolyte concentration to the ROC can be found. The lower the concentration, the smaller the ROC. [22] Since only single tips have to be re-sharpened, fast etching rates are not necessary. Thus, an electrolyte with a low concentration of 1 mol/l is prepared by dissolving 5.7 g of potassium hydroxide pellets in 100 ml distilled water.

The chemical reactions at the electrodes are: [37]

Cathode:	$6H_2O + 6e^- \rightarrow 3H_2(g) + 6OH^-$	(16)
Anode:	$W(s) + 8OH^- \rightarrow WO_4^{2-} + 4H_2O + 6e^-$	(17)
Overall:	$W(s) + 2OH^- + 2H_2O \rightarrow WO_4^{2-} + 3H_2(g)$	(18)

The material dissolution is achieved by oxidation of tungsten to the soluble tungstate anion WO_4^{2-}. The chemical reactions are complex. The tungsten reacts first to an intermediate tungsten oxide, followed by a non-electrochemical dissolution to form the tungstate anion. This anion has its greatest stability in an alkaline environment. At the cathode, hydrogen and hydroxide are formed. [37]

As already mentioned, only a re-sharpening of the needle is needed. Thus, a *Thinning* step is not required and the nanotip is fabricated by performing the *Neck-In* and the *Drop-Off* only. In Figure 39, a tip before re-sharpening is shown. It is obvious, that the tip is not only blunted but also broken off instead. Nevertheless, the diameter is small enough, so that a *Thinning* step is still unnecessary.

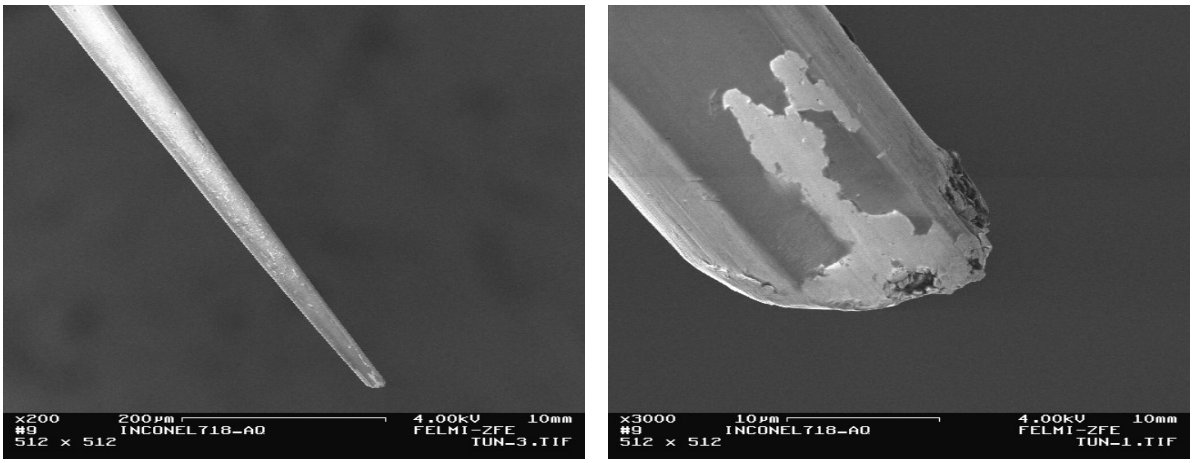

(a) Overview (scale 200 µm) *(b) Broken-off end (scale 10 µm)*

Figure 39: Initial tungsten tip, which is broken off.

The sample does not need any kind of preparation before undergoing the polishing. It is only rinsed with isopropanol, ethanol and distilled water. Then, the needle can be fixed instantly with the tweezers, as shown in Figure 40. After the etching process, the tungsten needle is rinsed again with isopropanol, ethanol and distilled water.

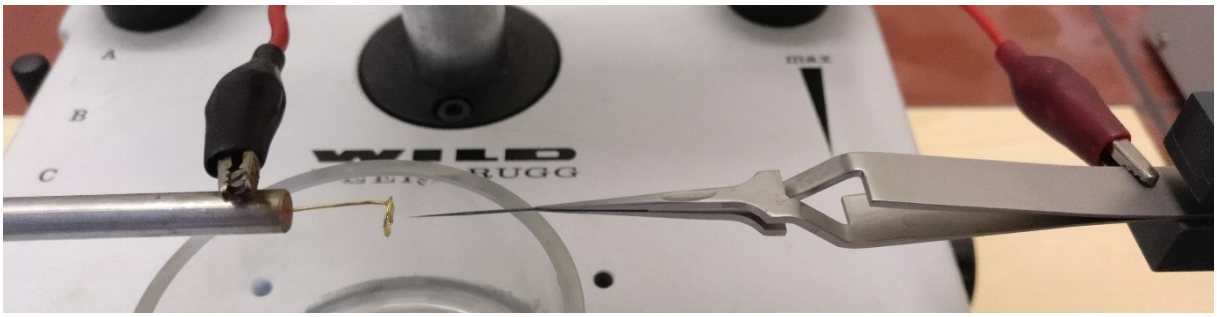

Figure 40: Mounted tungsten needle.

The re-sharpening of the tungsten needle is fast. The etching process can be finished within 5 minutes. Including the preparation and the cleaning time of the device, a nanotip can be accomplished in under 30 minutes.

After the etching process, dark precipitates are visible on the gold cathode. These residues are probably depositions of the tungstate and can be wiped away with cleaning paper.

In Table 3, the used parameters for tip preparation of each tungsten needle are listed.

Table 3: Parameters of the tungsten needle etching

No.	Material	Dimension	Electrolyte	Age	*Neck-In*	*Drop-Off*	Pulls	Duration
1	Tungsten needle	Ø 500 µm	caustic potash 1 $\frac{mol}{l}$	0 d	4 V	1 V	6	5 min
2	Tungsten needle	Ø 500 µm	caustic potash 1 $\frac{mol}{l}$	4 d	4 V	1 V	7	5 min
3	Tungsten needle	Ø 500 µm	caustic potash 1 $\frac{mol}{l}$	32 d	6 V	6 V	20	5 min

5. Results

5.1. Inconel 718

In the following, the influence of the cross section, the *Drop-Off* voltage and the thinning voltage on the tip quality is investigated in detail. First, some general observations of the etching process are given.

During the etching with the electrolyte 1 (solution of perchloric acid with acetic acid), a current could be observed of about 150 mA at an applied voltage of 20 V, which heats the electrolytic cell due to the ohmic resistance. The current also depends on the immersed area of the anode as well the temperature of the electrolyte. A simple estimation of the temperature increase is given in the next paragraphs.

As this is only a rough estimate, the calculation considers the electrolyte as a pure acetic acid solution. Further losses by the resistance of electric wires and connections as well as consumed chemical energy are neglected. Therefore, the total electrical power contributes to the thermal energy in the electrolyte droplet. Equation (19) gives the temperature rise per second. With the applied voltage U, the observed current I, the volume of the droplet V, the density ρ and heat capacity of acetic acid c_p.(18)

$$\Delta T = \frac{P}{\rho V c_p} = \frac{UI}{\rho V c_p} \left[\frac{K}{s}\right] \tag{19}$$

A current of about 150 mA is present at an applied voltage of 20 V. The volume of a droplet is approximated with 50 µl. The density of acetic acid is 1.05 gml^{-1} and the heat capacity is 2.05 $Jg^{-1}K^{-1}$. [49] These values result in a temperature rise of about 28 Ks^{-1}. An average etching time with a single droplet takes around 3 s until it is highly saturated, and the reaction stops. The total temperature rise is then about 84 K. The real temperature rise will be smaller due to heat dissipation, especially to the gold wire and due to the losses in the electrical wires and connections.

The higher temperature can be beneficial for a higher current density. Furthermore, the boiling point of perchloric acid is higher than that of acetic acid, which leads to an increase in concentration of the electrolyte during the etching process. Both effects, increasing temperature and concentration, change the U-I curve as well as the range of the polishing regime, and can have an unwanted impact on the specimen.

The electrolyte instantly begins to vaporise at the anode at an applied voltage of 35 V. This results in a spraying electrolyte from the droplet. Due to these turbulences, the solution droplet cannot be held by the microloop and drips into the beaker. Although the electrolyte is not saturated this way, it has to be renewed more often than at lower voltages.

The colour of the electrolyte changes with the saturation grade from transparent to orange, and finally to green. The saturation also reduces the current. Therefore, the electrolyte should be frequently renewed, if it does not drip by itself into the beaker.

The power supply can only display currents above 1 mA. During the etching process with electrolyte 2 (perchloric acid in 2-butoxyethanol), the current was below the sensitivity. Hence, a temperature rise of the solution is not expected. Nevertheless, high convection in the droplet occurs.

During the characterisation of the nanotip with the SEM, already some precipitates could be observed. These can be seen in Figure 41 (a) and match with the δ-phase, which is described in [44]. It seems that the etching rate is higher around those precipitates. The δ-phase is very stable against the dissolution. The valleys around the precipitates are internally connected. The δ-phase forms primarily at grain boundaries, which are also more electroactive, being the potential reason for the valleys. On the

reference specimen in Figure 41 (b), many small precipitates can be observed, but they cannot be allocated to the specific phases by only looking at the SE image. Such precipitates are observed exclusively at the reference specimens.

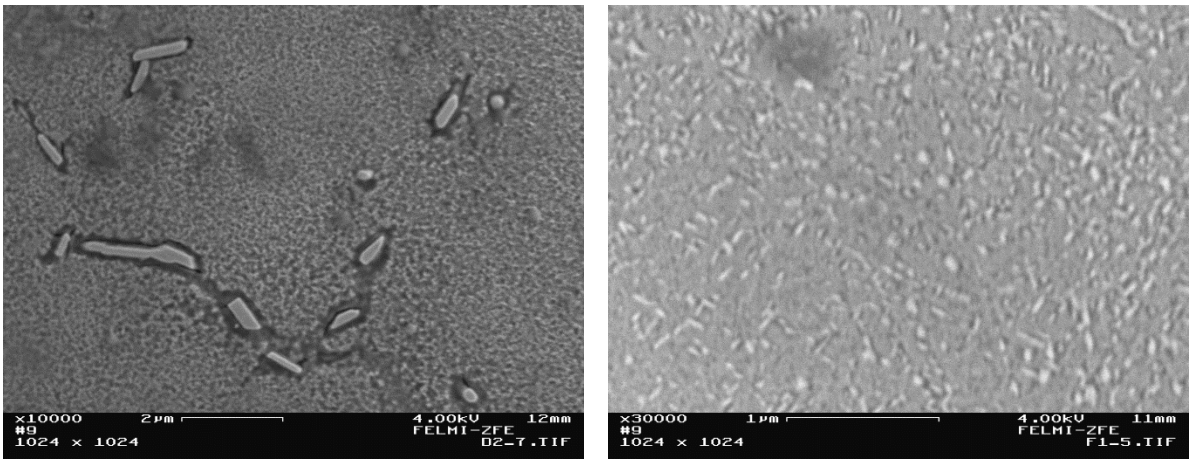

(a) Alloy718_AC *(b) Alloy718 (Ref)*

Figure 41: Precipitates of the Inconel samples.

In the subsequent sections, the influence of the following parameters will be discussed:

- Symmetry of the initial cross section
- Applied voltage during the *Thinning* step
- Applied voltage at the last *Drop-Off*

Influence of the cross section

A symmetric cross section is very important for a rotationally symmetric nanotip. Otherwise, the initial asymmetry will lead to blade-shaped tips. This shape distorts the ion trajectory to the detector at the APT. [26] For electron tomography the requirement of a rotation symmetric nanotip is not that important. Nevertheless, the thickness of the specimen has to be smaller than the maximum allowed length from any tilt angle, and must not to exceed the measured area.

Figure 42 shows the results of etching an asymmetric sample. The specimen was not polished mechanically and had a rectangular cross section of (290 x 480) µm² before the electrochemical polishing process.

The resulting nanotip is blade-shaped. At higher magnification, the nanotip seems to be fine from one direction. However, if the nanotip is observed from a perpendicular direction, it is obvious, that it is neither round nor straight. The tip cannot be used for nanoscale tomography.

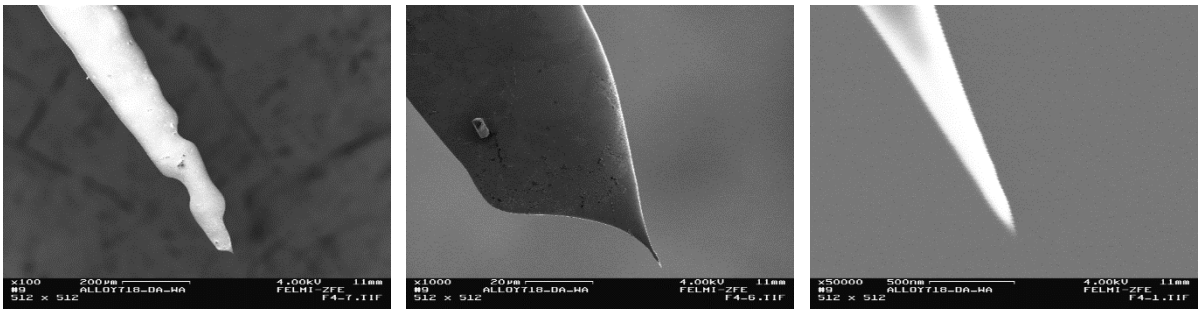

(a) 0° tilt angle, at 200 µm *(b) 0° tilt angle, at 20 µm* *(c) 0° tilt angle, at 500 nm*

(d) 90° tilt angle, at 200 µm *(e) 90° tilt angle, at 20 µm* *(f) 90° tilt angle, at 500 nm*

Figure 42: Nanotip from the asymmetric specimen (290 x 480) µm². The images in the second row are rotated 90° to the images in the first row. Scales left to right: 200 µm – 20 µm – 500 nm.

The asymmetry of the sample before the etching process was significant. Therefore, two less symmetric samples were investigated additionally. The first sample had a cross section of (190 x 200) µm² and the second one of (210 x 240) µm². The boundaries of the finished tips are shown from two perpendicular directions in Figure 43. The deviation of 10 µm from a square cross section leads to a good circular shape of the nanotip, but an elliptical shape can already be observed at an initial deviation of 30 µm. These two tips are etched with the same electrolyte and voltages. The initial more symmetrical tip has a *critical length* of 166 nm and 127 nm, depending on the observation perspective. The other tip has a *critical length* of only 41 nm and 27 nm. There could also be a dependency on the sharpness of the tip from the starting cross section.

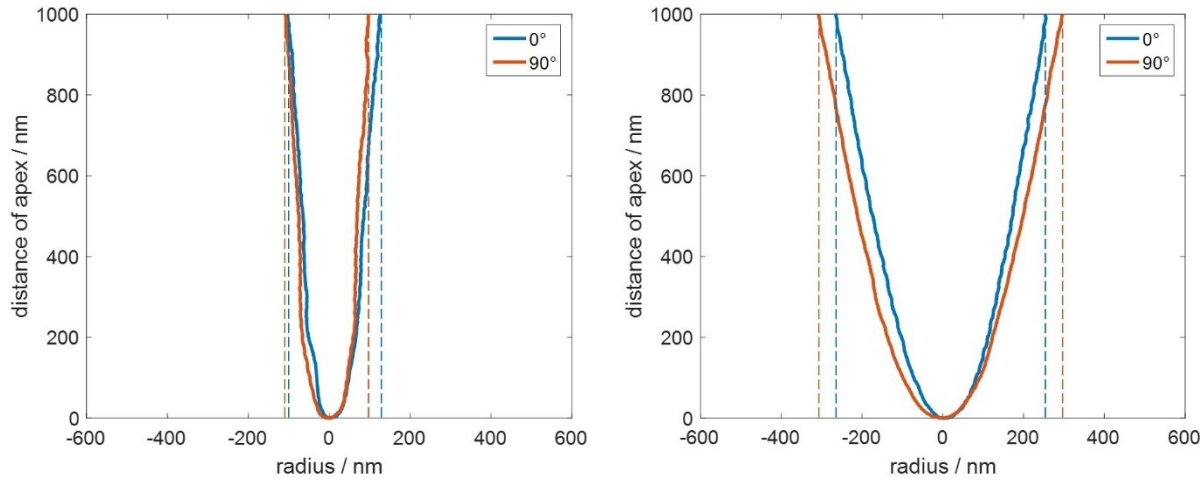

(a) (190 x 200) µm² specimen *(b) (210 x 240) µm² specimen*

Figure 43: Comparison of two tips, (a) has an initial cross section of (190 x 200) µm² and (b) a primary cross section of (210 x 240) µm². The blue curve shows the boundary of the tip, which is 90° rotated to the orange curve.

The final symmetry of the nanotip does not only depend on the initial dimension. During the etching with electrolyte 1, a layer is formed on the polished surface. This is discussed in the next section in detail. This layer can also have influence on the symmetry of the finished tip. In Figure 44, a nanotip with an initial dimension of (185 x 190) µm² is shown. Some residues of the layer are observed on the surface, which disturbed the etching process. Despite the good symmetry of the initial shape, the achieved nanotip is highly asymmetric.

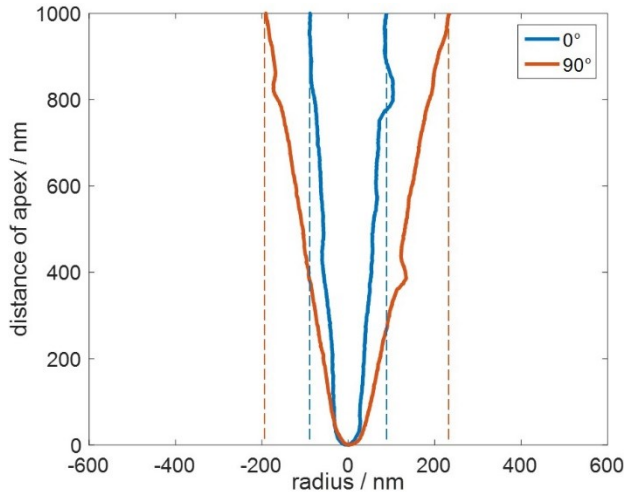

Figure 44: Boundary of the specimen with initial dimension of (185 x 190) µm².

Influence of the thinning-potential

The formation of a non-uniform layer is observed during etching with the electrolyte 1. This layer appears under the transmitted light microscope as a brown layer and slowly vanishes during etching with the electrolyte 2. However, the layer seems rather to detach than to dissolve. Thereby, big pieces of this layer accumulate in the electrolyte droplet. The non-uniformity of the layer could cause artefacts to the final tip shape, like the deviation from the square cross section.

The growth of the layer depends on the applied voltage. At 20 V, a thick layer can already be observed with the light microscope, while at 35 V almost no layer is visible. Figure 45 shows two samples, which are etched with the electrolyte of perchloric acid in acetic acid at 35 V and at 20 V. With the high potential, only small islands are formed with a size of a few microns on the surface. Lowering the potential increases the size of these islands, and especially their height increased. At 20 V, the dimension of the islands is in the range of a few ten microns.

The formed layer seems to be non-conductive, as charging occurs in the SEM.

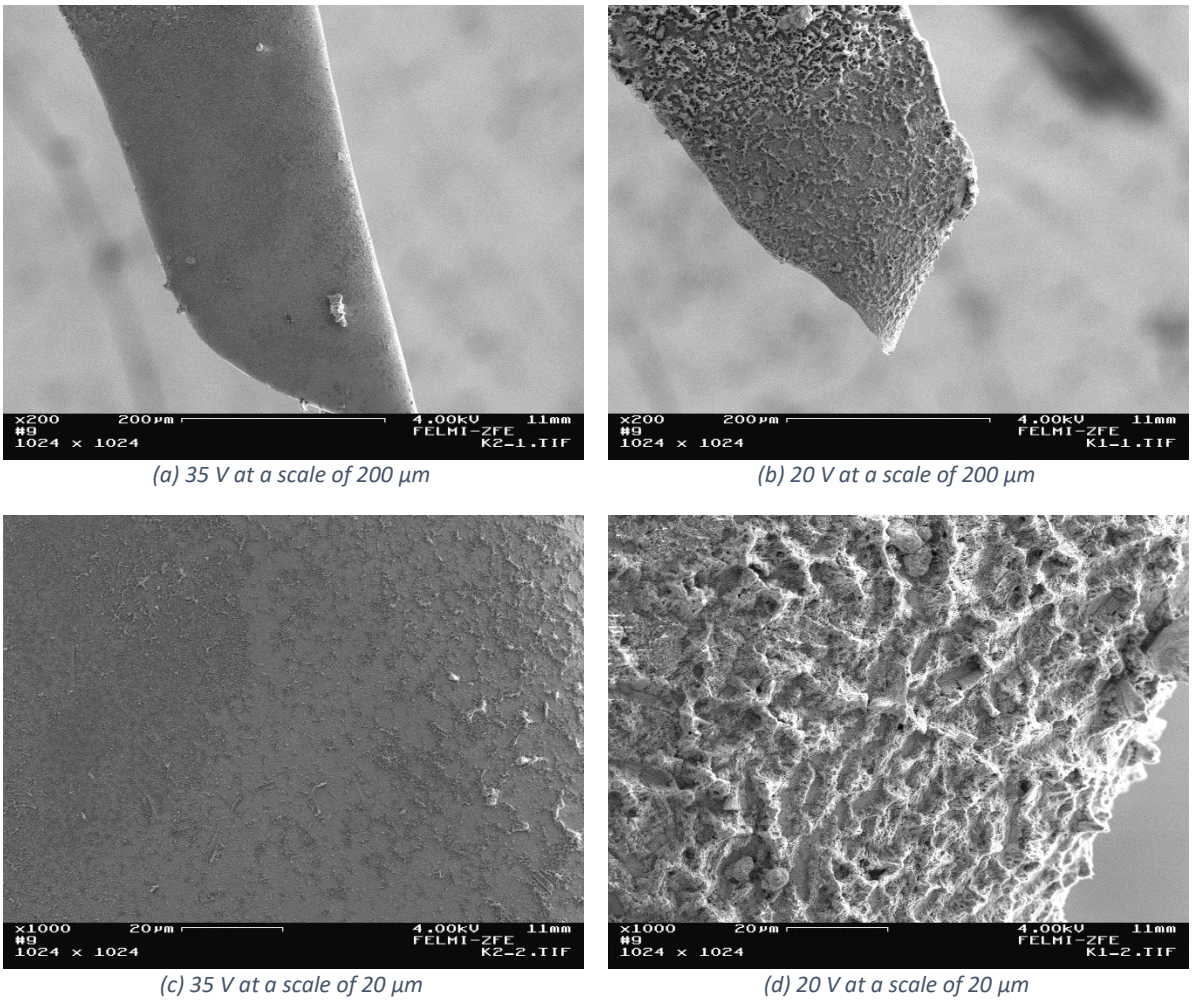

(a) 35 V at a scale of 200 µm

(b) 20 V at a scale of 200 µm

(c) 35 V at a scale of 20 µm

(d) 20 V at a scale of 20 µm

Figure 45: Two Inconel 718 samples, which are etched with the electrolyte of perchloric acid in acetic acid with different potentials. In the two images on the left side, a voltage of 35 V was applied, on the right side 20 V.

As already mentioned, the high voltage induces enough thermal energy for the electrolyte to vaporise instantly at the anode. The induced vibration causes the droplet in the microloop to fall. The two samples above were etched approximately for the same amount of time. Nevertheless, during that time span, a tip was accomplished only for the sample prepared at the lower voltage, because the bubbles replace the electrolyte at the anode surface and reduce the etching rate.

In the following, EDX-analysis were carried out to determine the elements of the observed layers.

Figure 46 and Figure 47 show the composition map of a small area of the samples, which are etched with an applied voltage of 20 V and 35 V. Two phases can be detected in both samples; the generated layer and the specimen underneath. The chemical composition of the layers of both specimens is almost the same. The layers consist of chlorine, oxygen and carbon, which stem from the electrolyte. Furthermore, high amounts of niobium and molybdenum are observed in the layers. These elements are not as well dissolved from the specimen surface as nickel, iron and chromium. This effect can be counteracted by increasing the applied voltage. The layer of the specimen, which is etched at 20 V, consists of a higher amount of copper than the second layer. That is because the electrolyte came in contact with the copper sleeve, which dissolved a part of it and then deposited it in the layer. The origin of the sodium, especially at the specimen etched at low voltage, cannot be explained. This is most probably due to contamination during the etching process.

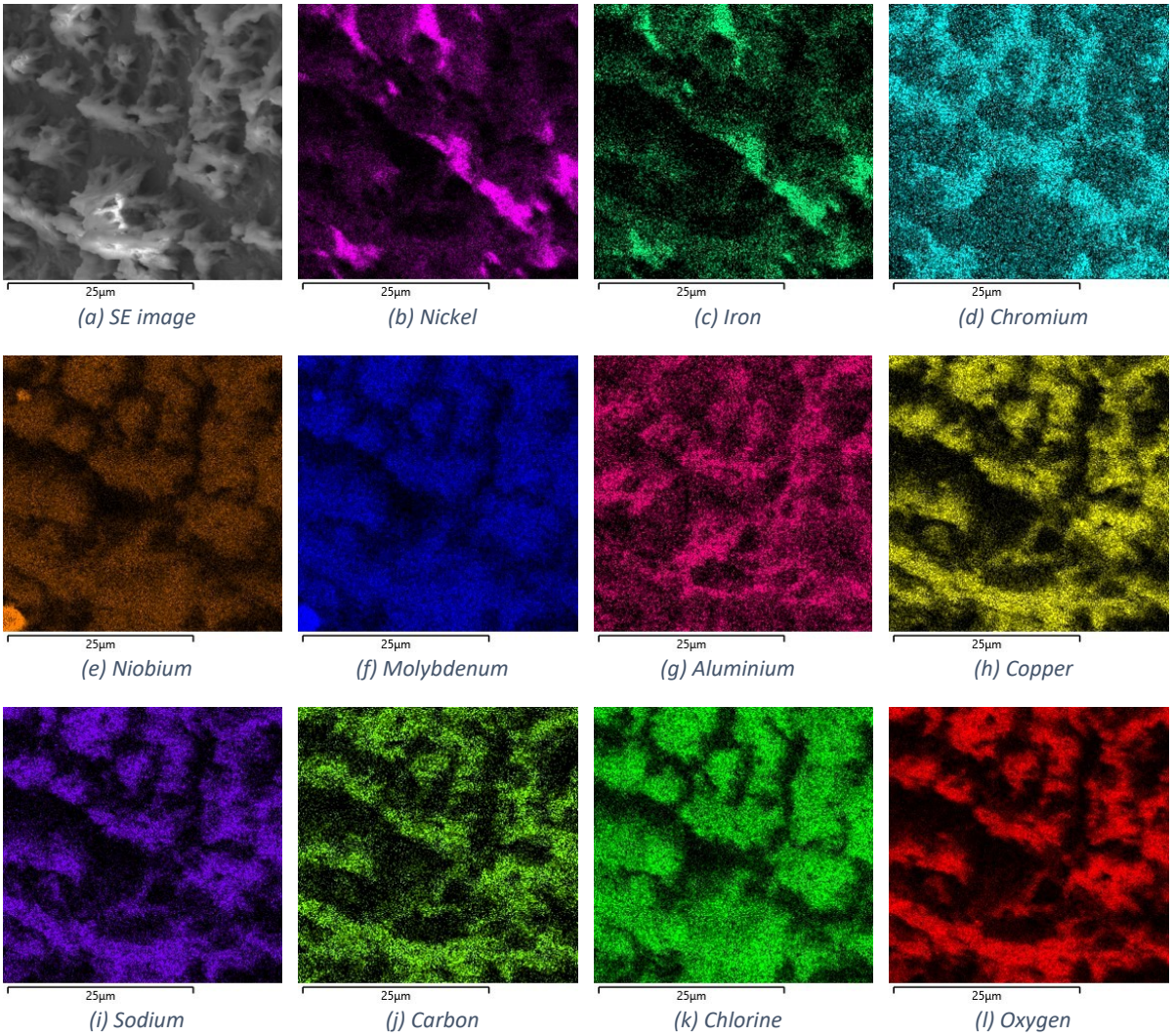

Figure 46: Composition map of the Alloy718 (Ref) sample, which is etched wit 20 V.

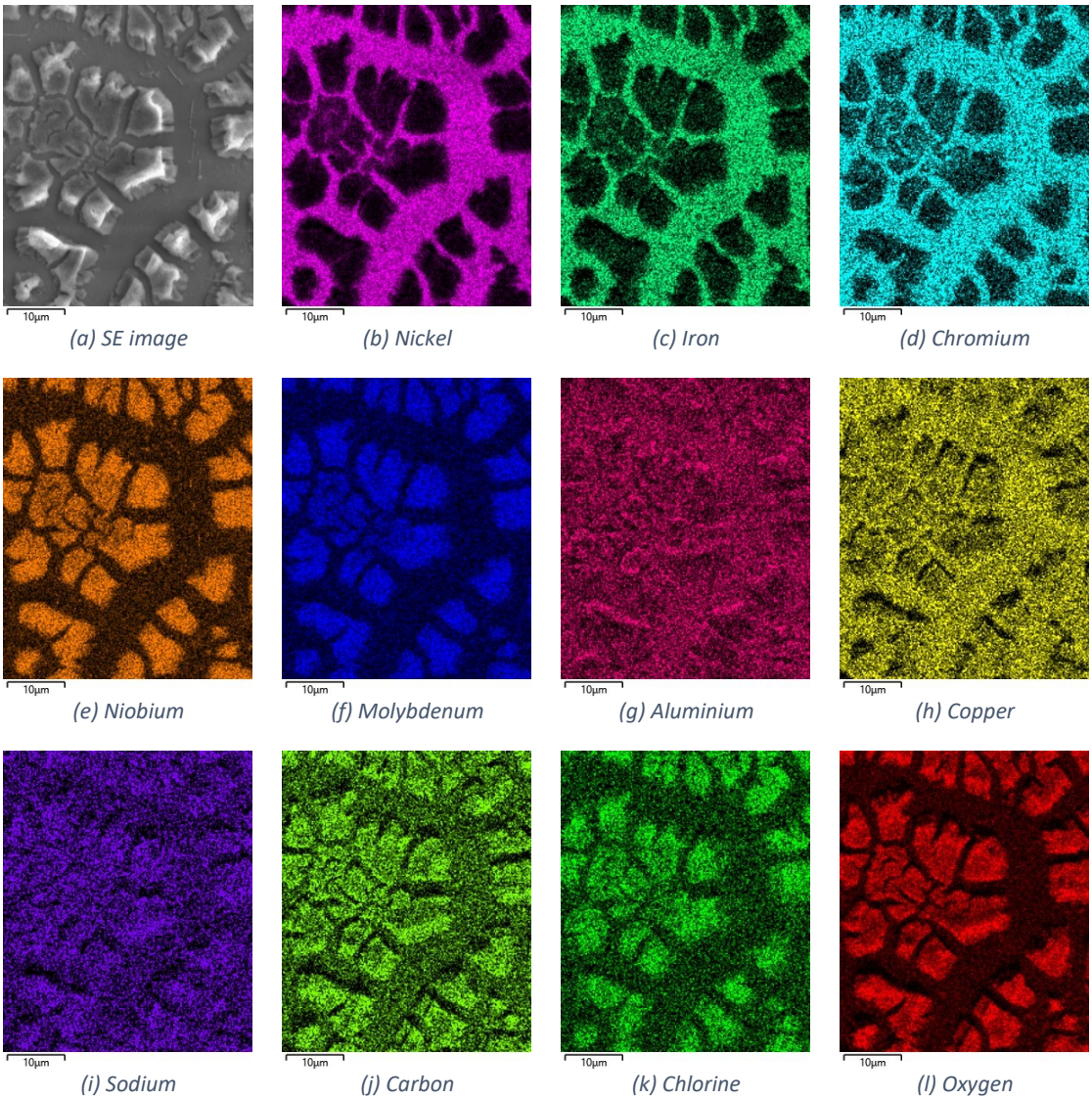

(a) SE image (b) Nickel (c) Iron (d) Chromium

(e) Niobium (f) Molybdenum (g) Aluminium (h) Copper

(i) Sodium (j) Carbon (k) Chlorine (l) Oxygen

Figure 47: Composition map of the Alloy718 (Ref) sample, which is etched wit 35 V.

In Table 4, the quantitative results of the EDX-analysis are listed. Three different regions are investigated, which are shown in Figure 48. The areas are layers from the low voltage specimen (L20, marked in red), from high voltage specimen (L35, marked in blue) and from the specimen underneath (Valley, marked in green). In both cases, the layer consists mainly of oxides and salts of niobium and molybdenum. Copper, which is dissolved from the specimen mount, is also found in the layers. However, the same formations of the layers were observed, even though the electrolyte did not come in contact with copper.

(a) Specimen, which is etched at 20 V (b) Specimen, which is etched at 35 V

Figure 48: Selected area for the quantitive EDX-analyse, which is listed in Table 4.

Table 4: Chemical composition of the areas which are red (L20), blue (L35) and green (Valley) marked in Figure 48.

	L20 / wt%	L35 / wt%	Valley / wt%
Ni	2.5	6.1	48.5
Fe	1.5	3.1	15.3
Cr	6.5	5.1	16.2
Nb	21.5	28.5	5.2
Mo	4.6	8.4	2.7
Al	1.3	1.7	1.7
Ti	1.1	2.2	1.0
Si	0.4	0.3	0.1
Cu	15.0	4.3	---
C	11.5	14.5	7.8
Cl	7.0	3.8	---
O	25.1	21.7	1.5
Na	1.8	0.3	---

Additionally, one sample was etched with an applied voltage of 4 V. At this specimen, the layer formation was far smaller than for samples etched with an applied voltage of 20 V. However, the surface exhibits several spikes, which can disturb the final shape of the tip. At a potential of 4 V, the etching rate is very small and the corresponding current is around 1 mA. Saturation is achieved only after a few minutes compared to a few seconds with voltages of 20 V or 35 V. The etching at 4 V was performed until the electrolyte was fully saturated, but no increased layer formation was observed at higher saturation. Due to the slow etching, the process can be better controlled compared to higher voltages, but the duration of the *Thinning* step increases quickly with a bigger initial cross section.

The reason for the formation of the layer could be described by the salt film model, but the niobium products are not dissolved as well as the other elements generating a layer with higher amount of niobium. The disappearance of the layer at higher potential could be explained by the pitting regime of the general polarisation curve. At this regime, the oxide layer is pulled off frequently. This process could also remove the salt film, before it grows to a large size. The absence of the layer at 4 V could be due to the low voltage, which is below the passivation regime where no salt film is formed. In this etching regime a non-uniform etching occurs, which leads to the spikes.

However, the chemically reactions and kinetics in such an electrolytic cell are too complex to be fully described within the scope of this work.

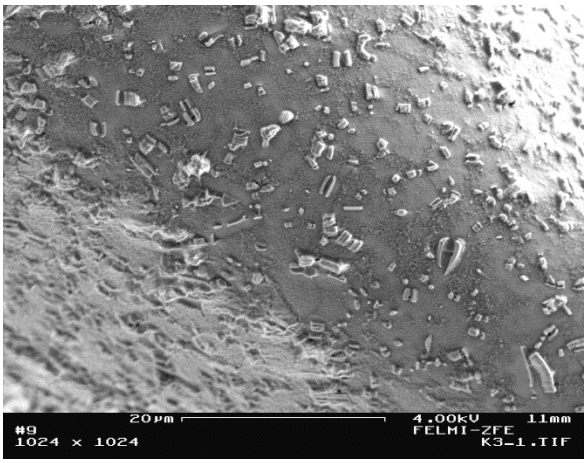

(a) Applied voltage of 35 V (scale 20 µm)

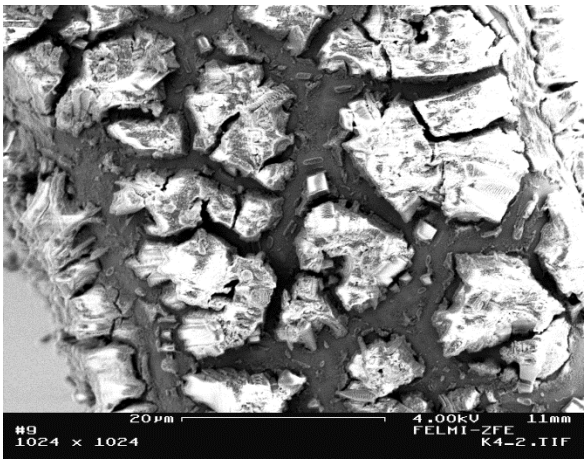

(b) Applied voltage of 20 V (scale 20 µm)

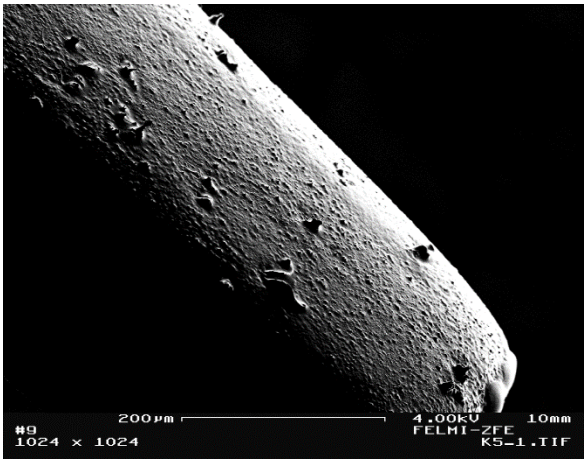

(c) Applied voltage of 4 V (scale 200 µm)

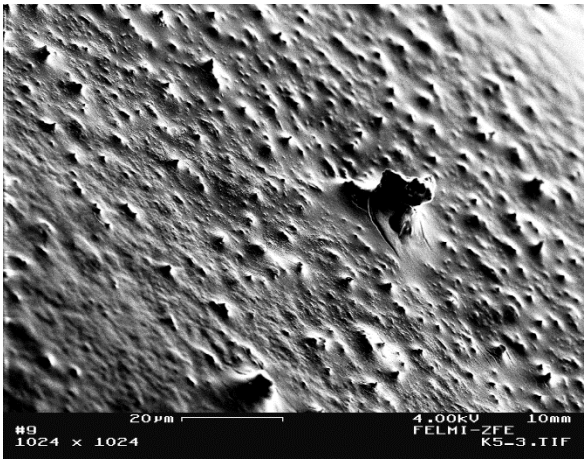

(d) Applied voltage of 4 V (scale 20 µm)

Figure 49: Layer formation at different applied voltages of 35 V, 20 V and 4 V without any contact of the electrolyte to the copper sleeves.

Influence of the Drop-Off potential

With electrolyte 2 (perchloric acid in 2-butoxyethanol), no layer formation is observed. The *Neck-In* is always done at a voltage of 15 V, because it offers a high enough etching rate. However, the most important setting is the potential at the *Drop-Off*. In references [12], [19] and [24], a dependency of the applied voltage to the ROC is observed. The lower the voltage, the smaller the ROC. A much higher aspect ratio at lower applied voltages can also be found in [28]. Nevertheless, in these references, the material for the nanotips are always tungsten. The different noble metals in the nickel-based superalloy can cause problems. Therefore, the plateau in the polarisation curve is even more important to be found, since a stable diffusive layer is formed there. This ensures a smooth surface by a constant etching rate of all elements of the sample. Unfortunately, a polarisation curve of Inconel 718 in 2% perchloric acid in 2-butoxyethanol could not be found in any literature for this thesis.

The *Drop-Off* voltage is varied in a range from 2 V to 24 V to find the optimal voltage. Additionally, the dependency of the *critical length* to the applied voltage should be verified. Since the nanotip is removed from the electrolyte immediately after the *Drop-Off*, the higher blunting effect at higher voltages could be reduced or even avoided. This correlation is observed in the references [22], [28], [33].

Figure 50 shows some nanotips with different *Drop-Off* voltages, and Table 5 lists the *critical length*s of them. The finest tip is achieved at a *Drop-Off* voltage of 4 V. Generally, the *critical length*s of the tips become shorter with higher voltages. Especially the nanotip with a *Drop-Off* voltage of 16 V has a bad quality. The *critical length* of the nanotips does not depend only on the *Drop-Off* voltage. As already mentioned, the asymmetry of the starting cross section and the formation of the layer could have led to the bad tip.

Table 5: Critical lengths of the nanotips, which are shown in Figure 50.

***Drop-off* voltage**	***Critical length***
4 V	247 nm
8 V	132 nm
12 V	146 nm
16 V	34 nm
24 V	87 nm

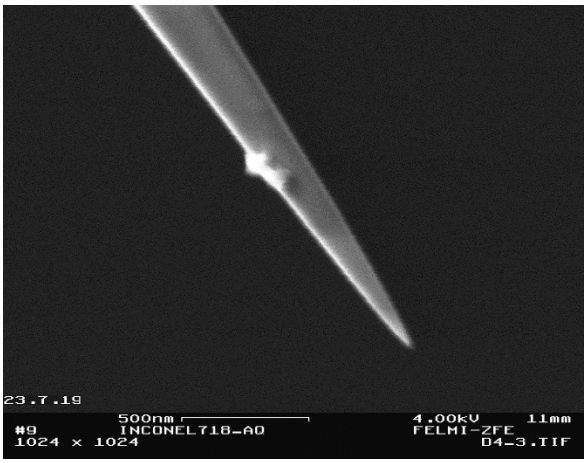

(a) Drop-Off voltage of 4 V

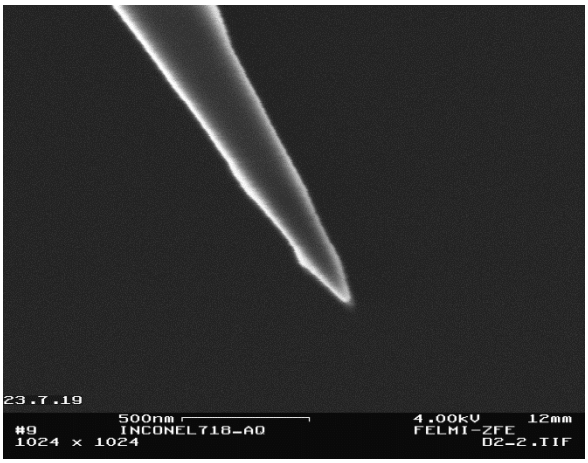

(b) Drop-Off voltage of 8 V

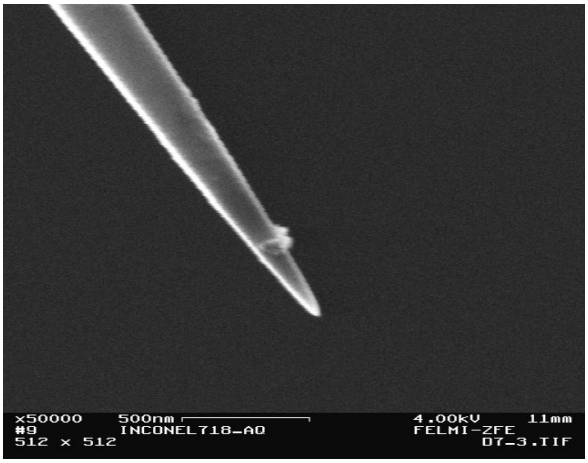

(c) Drop-Off voltage of 12 V

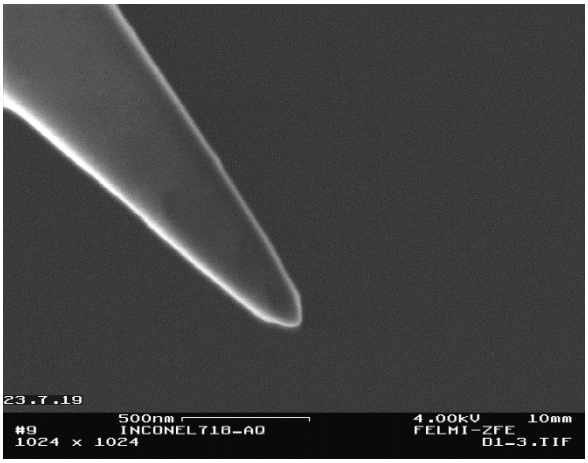

(d) Drop-Off voltage of 16 V

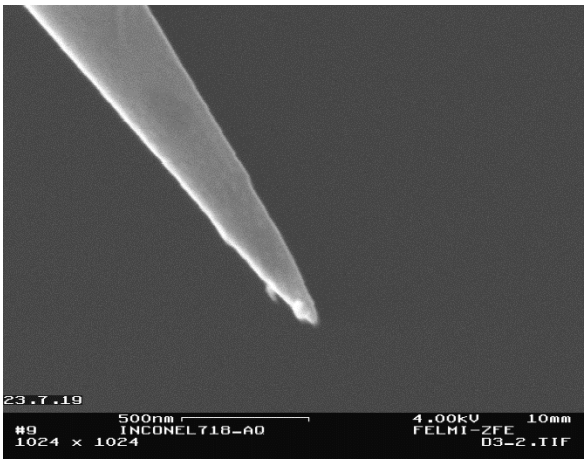

(e) Drop-Off voltage of 24 V

Figure 50: Nanotips with different Drop-Off voltages.

The *critical length* of the nanotip with the *Drop-Off* voltage of 4 V was the best tip observed. If the *Drop-Off* voltage is reduced further, the domain of the selective dissolution is reached. This can be seen in the tip prepared with a *Drop-Off* voltage of 2 V, shown in Figure 51. Several holes are visible on this tip, and in the image taken at the highest magnification, an irregularly shaped tip is observed. This voltage is in the etching regime, where no diffusive layer is formed, which smoothens the surface by the location-dependent ohmic resistance. Therefore, dissolution only depends on how electroactive the surface atoms are. This depends on the kind of element and its position (e.g. edge-sites). [18]

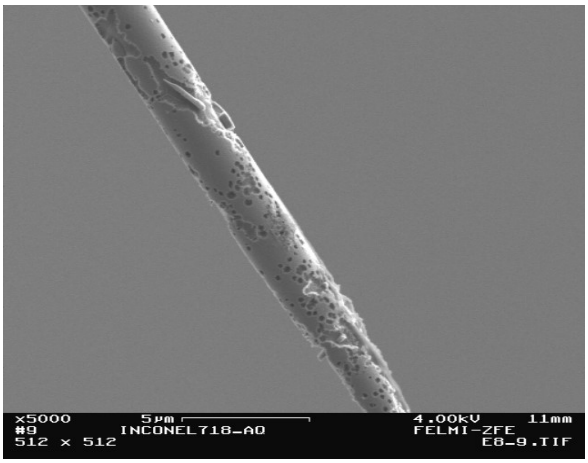

(a) Scale 5 µm

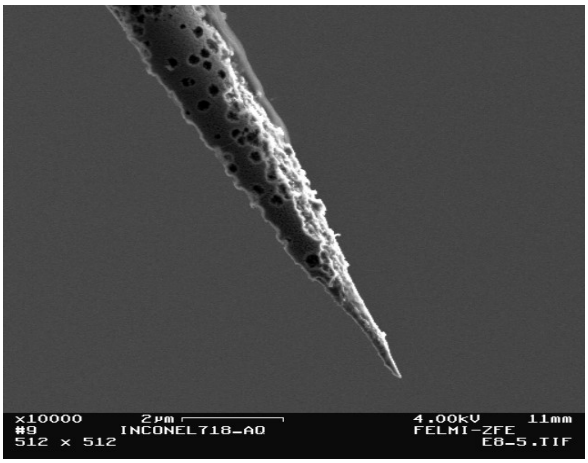

(b) Scale 2 µm

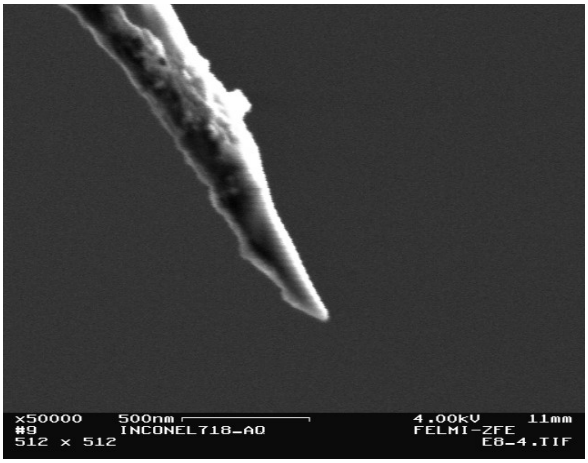

(c) Scale 500 nm

Figure 51: Nanotip with a Drop-Off voltage of 2 V.

The composition of the tip is almost identical to the ideal nanotip (see Table 6). The reason could be that some grains with specific orientation are dissolved completely, and therefore cannot change the composition of the remaining material. Furthermore, the interaction volume of EDX is too big to measure the composition of the selectively dissolved surface and hence, the bulk material is also analysed. Only small reductions are observed for the elements nickel, iron and chromium. These elements are well soluble in both solutions.

Precipitates, as shown in Figure 52, are often observed at the nanotip. This kind of precipitates contains a large amount of niobium. Further components are titanium, carbon and oxygen (see Table 6). A small amount of chlorine can also be found. Such irregularities and protrusions near the end of the nanotip might make it unusable for APT and electron tomography.

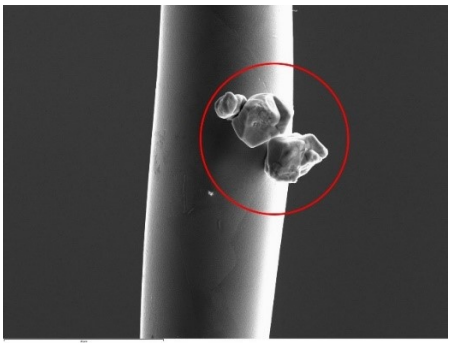

Figure 52: Precipitates in the red circle, which can often be found on nanotips.

Table 6: Chemical composition of the nanotips etched at 4 V (T4), 2 V (T2) and the precipitate (P), which is marked in Figure 52.

	T4 / wt%	T2 / wt%	P / wt%
Ni	51.6	50.6	0.5
Fe	16.0	14.8	0.5
Cr	16.7	15.6	0.6
Nb	5.2	5.4	61.1
Mo	2.8	2.7	0.1
Al	0.6	1.7	0.1
Ti	1.0	0.9	5.6
Si	0.1	0.1	---
Co	0.2	0.2	---
C	4.6	6.7	13.6
O	1.3	1.3	17.1

Re-sharpening

If the nanotip fabrication is not successful or the tip does not contain the region of interest, it can be re-sharpened. The *Neck-In* and the *Drop-Off* steps are repeated with electrolyte 2 (perchloric acid in 2-butoxyethanol). Such a re-sharpening process takes only around 5-10 minutes. In Figure 53, re-sharpened nanotips are shown. The reasons, why a re-sharpening of these nanotips was necessary; were bluntness of the tip, protrusions on the nanotip or a bent tip. Each of these problems could be eliminated with an additional *Neck-In* and *Drop-Off* step. This process can be repeated until the length of the tip is too short.

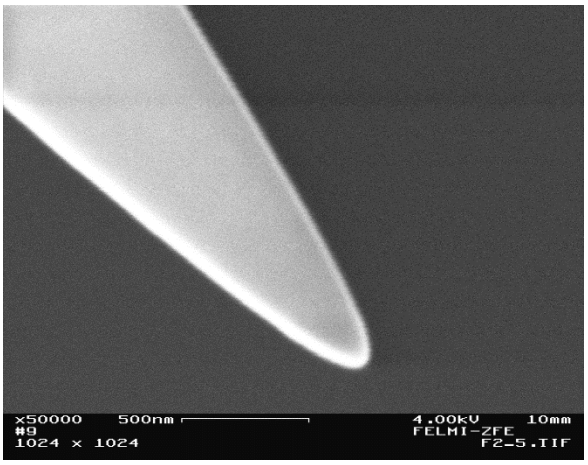

(a) Blunt nanotip

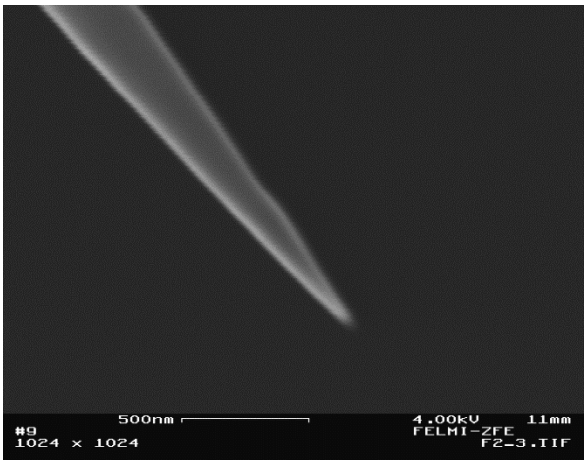

(b) Re-sharpened nanotip: finer

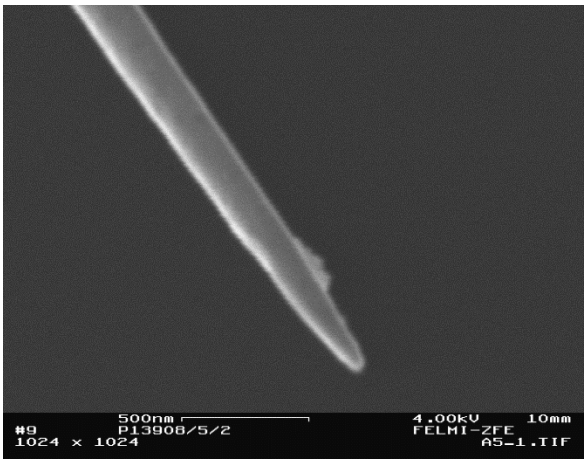

(c) Protrusion on the nanotip

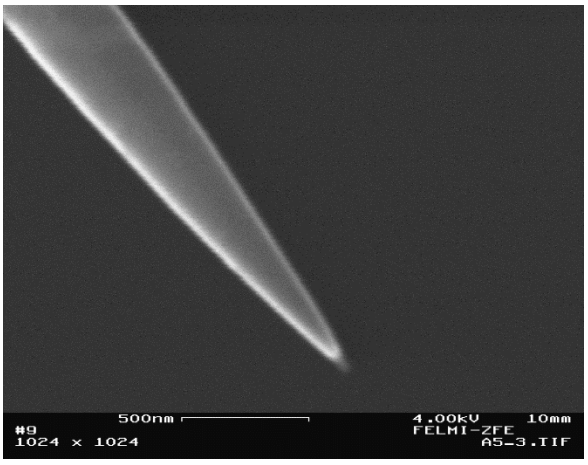

(d) Re-sharpened nanotip: free from protrusions

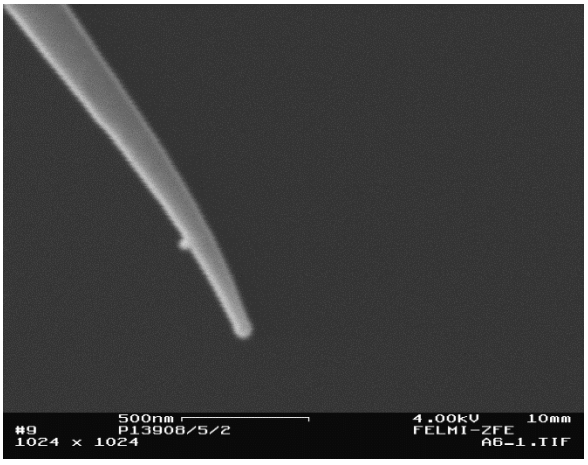

(e) Bent nanotip (caused by recoil)

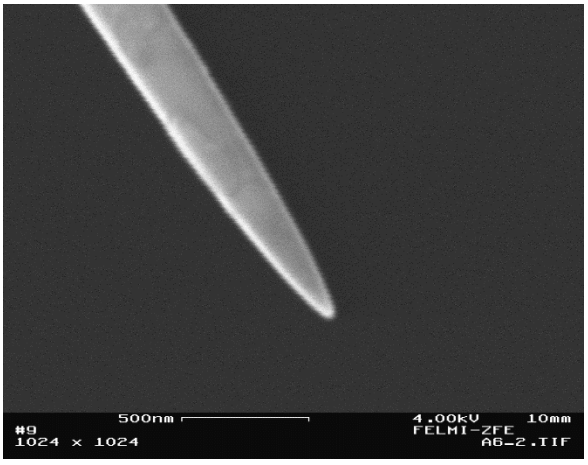

(f) Re-sharpened nanotip: straight

Figure 53: Re-sharpening of tips. Left column: before the sharpening processes; Right:Re-sharpened nanotips.

Trends

This section attempts to give some trends for the dependence of the tip quality on different parameters. The parameters, which are considered, are the aspect ratio of the initial cross section, the *Drop-Off* voltage and the number of pulls for finishing the *Drop-Off* step. A trend line, which is calculated by the least square method, is placed in all plots to show potential tendencies for the nanotip quality.

The *critical length* is always measured from two directions, which are perpendicular to each other. The mean of these values is calculated for the plots and correlations. The length is estimated with the MATLAB-file from the appendix 9.1.

First, the asymmetry is considered in Figure 54. The aspect ratio is the relation of the longer side to the shorter side of the cross section. Each nanotip is finished with a *Drop-Off* voltage of 4 V. The slope of the correlation curve is only small for the low sample size. The dependence of the *critical length* on the asymmetry of the cross section is not clear. However, the deviations should be kept small, because otherwise the nanotip gets blade-shaped and cannot be used for APT or electron tomography.

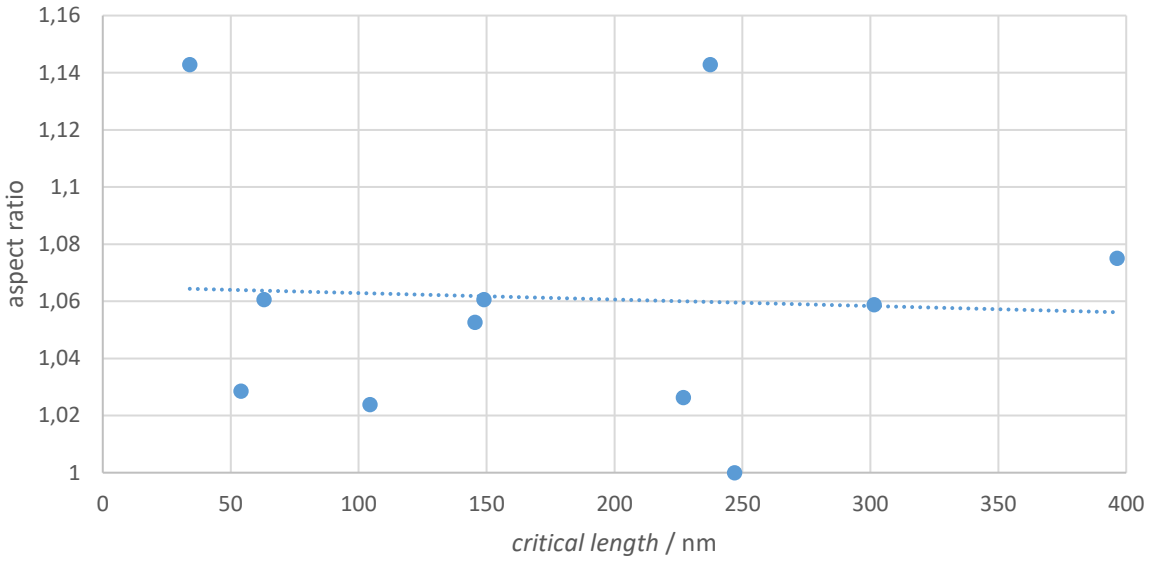

Figure 54: Critical length in dependence of the asymmetry of the initial cross section (aspect ratio). The used nanotips are taken from Table 7 with the numbers: 6, 11, 12, 14, 17, 18, 20, 21, 23, 24 and 26.

Next, the voltage at the *Drop-Off* with the second electrolyte is considered. Here, a clear dependence of the *critical length* on the *Drop-Off* voltage can be seen in Figure 55, even at a low sample size. Good nanotips are achieved with a voltage of 4 V. If the potential is decreased slightly further, the tip quality could be enhanced a little bit. However, selective dissolution was observed at 2 V, which makes the tips unusable. This limits the applied voltage. Although the nanotip is removed fast from the electrolyte, this trend of finer nanotips with decreasing voltage corresponds still with references [15], [22] and [27].

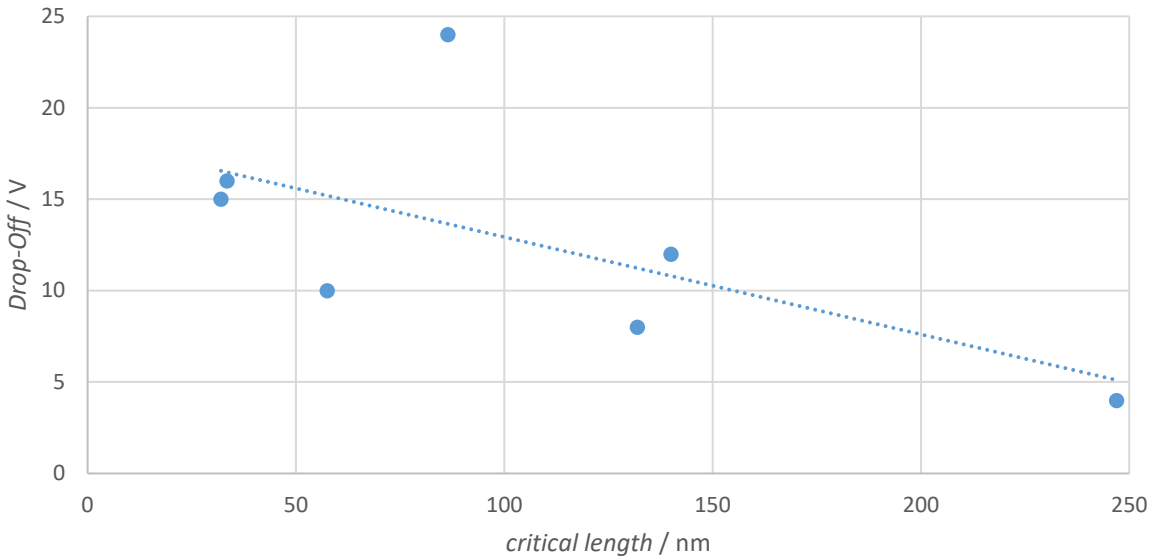

Figure 55: Critical length in dependence of the last Drop-Off voltage. The used nanotips are taken from Table 7 with the numbers: 1, 2, 3, 4, 5, 6 and 9.

The last parameter is the number of pulls to accomplish the *Drop-Off* with electrolyte 2. The *critical length* is shown in Figure 56 in dependence of the number of pulls for the *Drop-Off*. It indicates a decreasing *critical length* with the number of pulls. For a possible explanation of this effect, we assuming that the electrolyte-air interface is placed at the exact same position, the thinnest point at the *Neck-In*, for each pull. Now, if it does not break on the first try, the *Drop-Off* step is repeated. In this case, only the front end is etched, and the diameter of the shaft stays constant. This decreases the aspect ratio and thus also the *critical length*.

If a high number of pulls is needed, the nanotip can be re-sharpened instantly by producing a new *Neck-In* and re-doing the *Drop-Off*. This takes less than 10 minutes.

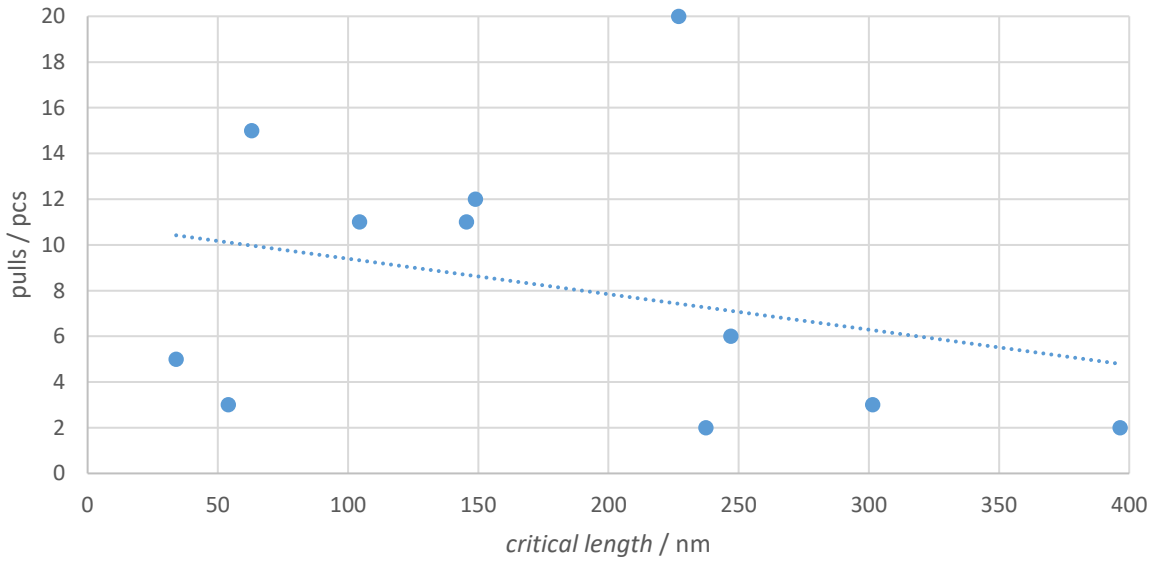

Figure 56: Critical length in dependence of the number of pulls at the Drop-Off. The used nanotips are taken from Table 7 with the numbers: 6, 11, 12, 14, 17, 18, 20, 21, 23, 24 and 26.

Table 7: Determined critical lengths from the nanotips fabricated according to ***Error! Reference source not found.****.*

					Critical length	
No.	**Material**	**Deviation of the cross section**	***Drop-Off***	**Pulls**	**First side**	**Second side**
1	Alloy718_HT	20 µm	15 V	1	31 nm	33 nm
2	Alloy718_HT	10 µm	10 V	3	75 nm	40 nm
3	Alloy718_AC	5 µm	16 V	40	33 nm	34 nm
4	Alloy718_AC	10 µm	8 V	21	132 nm	---
5	Alloy718_AC	15 µm	24 V	13	132 nm	41nm
6	Alloy718_AC	0 µm	4 V	6	160 nm	334 nm
7	Alloy718_AC	0 µm	2 V	31	Broken	
8	Alloy718_AC	0 µm	20 V	23	Bent	
9	Alloy718_AC	10 µm	12 V	9	164 nm	116 nm
10	Alloy718_AC	30 µm	2 V	5	Dealloyed	
11	Alloy718 (Ref)	10 µm	4 V	11	164 nm	127 nm
12	Alloy718 (Ref)	30 µm	4 V	5	41 nm	27 nm
13	Alloy718_DA_WA	190 µm	4 V	5	Blade-shaped	
14	Alloy718 (Ref)	5 µm	4 V	20	356 nm	98 nm
15	Alloy718 (Ref)	---	---	---	Only thinning	
16	Alloy718 (Ref)	---	---	---	Only thinning	
17	Alloy718 (Ref)	10 µm	4 V	15	33 nm	93 nm
18	Alloy718 (Ref)	15 µm	4 V	2	426 nm	367 nm
19	Alloy718(Ref)	10 µm	4 V	5	Bent	93 nm
20	Alloy718(Ref)	10 µm	4 V	12	143 nm	155 nm
21	Alloy718(Ref)	15 µm	4 V	11	118 nm	91 nm
22	Alloy718(Ref)	5 µm	4 V	18	Bent	
23	Alloy718(Ref)	30 µm	4 V	2	225 nm	250 nm
24	Alloy718(Ref)	10 µm	4 V	3	403 nm	200 nm
25	Alloy718(Ref)	5 µm	15 V	4	187 nm	45 nm
26	Alloy718_HT	5 µm	4 V	3	59 nm	49 nm

5.2. Tomography

The preliminary TEM investigation of each specimen offered, that precipitates are only present at the reference sample. Thus, electron tomography was only performed on this sample. The precipitates could be observed already in Figure 41.

The tip investigated by tomography had a large *critical length* of around 400 nm. However, the front end of the nanotip is melted by the released energy at the *Drop-Off*. This causes the ball-shaped end, which makes the tip unusable for APT. The high tension and the temperature increase, even if the material is not melted, can have an impact on the material at the front end.

It could be observed, that the specimen does not have a perfectly circular cross section. The shape is elliptical with a nearly constant eccentricity of 0.7 over the whole imaged length of the tip. Nevertheless, an electron tomography experiment was performed. The signal, which was recorded during the tilt series, is the HAADF signal and therefore, only a mass contrast is obtained. Due to this, the visible precipitates cannot be allocated to the different phases. The reconstructed nanotip is shown in Figure 57.

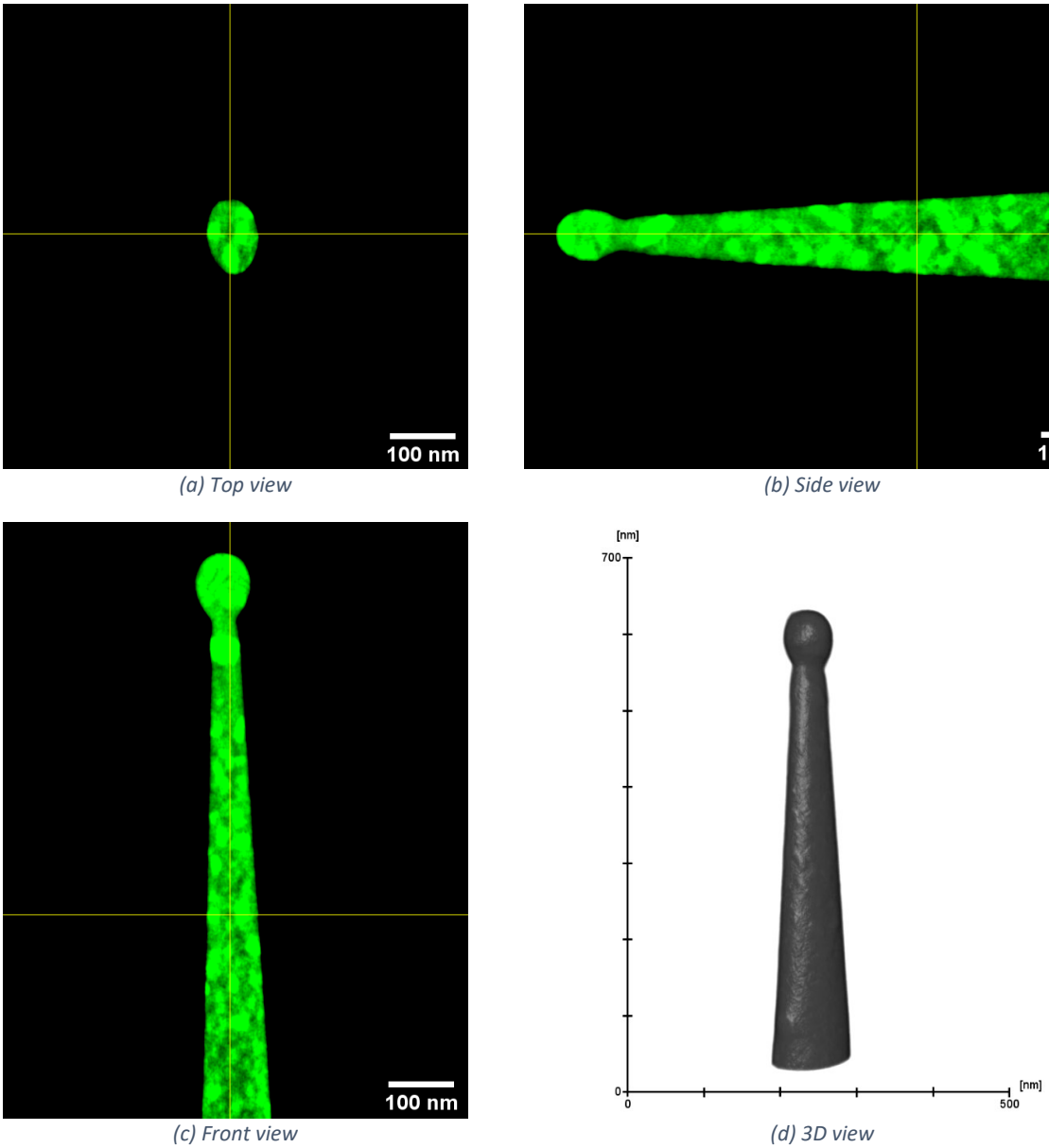

(a) Top view *(b) Side view*

(c) Front view *(d) 3D view*

Figure 57: Reconstructed nanotip from the HAADF signal.

By adjusting contrast and brightness, the carbon layer around the tip can be made visible, as shown in Figure 58. Such carbon layers are often deposited during SEM investigations due to the electron beam. Even though the electron dose was kept as small as possible during the SEM investigation, a thick layer of around 30 nm developed. The formation depends on the material, but it can also be enhanced by residues of the electrolyte on the specimen. Such a carbon layer does not significantly disturb the electron tomography investigation. Nevertheless, the tip is also unusable for the APT due to this layer.

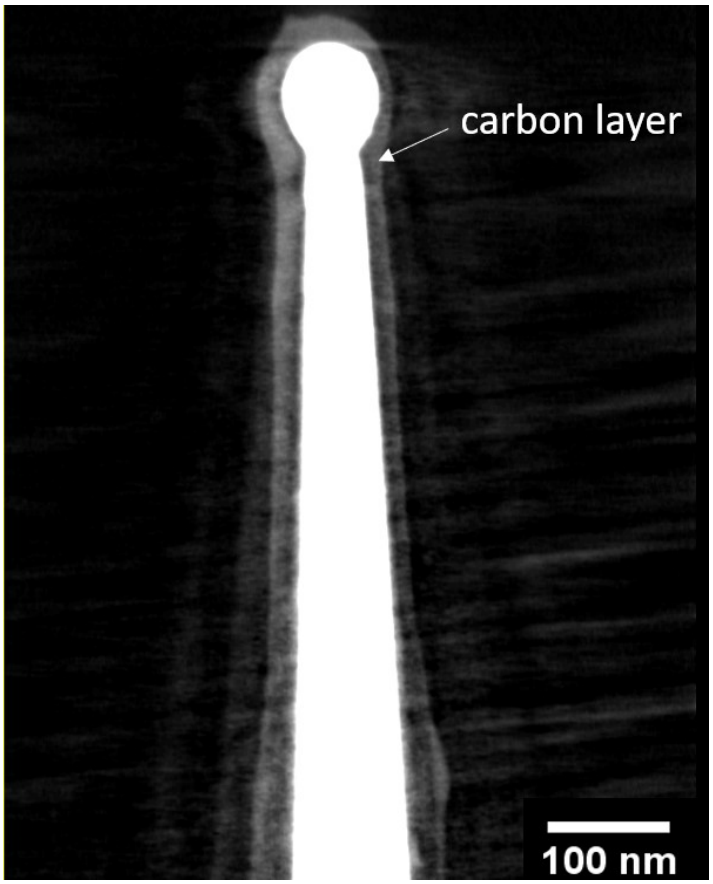

Figure 58: Nanotip image used for the tomography with high contrast to image the carbon layer.

5.3. Tungsten

The re-sharpening of the tungsten needle does not cause as many problems as the nickel-based superalloy due to the single species of material, in addition the sample must not fulfil the strict requirements for nanoscale tomography.

Since the specimen is already needle-shaped, a *Thinning* step was not necessary. The results of the etching processes are shown in Figure 59. The quality of the nanotip did not change with an increased applied voltage, and also the surface roughness could not be enhanced, as mentioned in [21]. The nanotip in Figure 59 (a) was bent mechanically. The diameter of the needle increases quickly, making it mechanically more stable, and it should be suitable for the usage as micromanipulator.

(c) 1 V (No. 1)

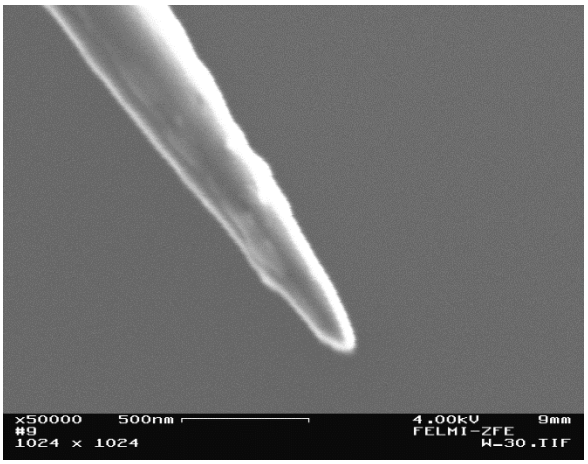

(d) 1 V (No. 2)

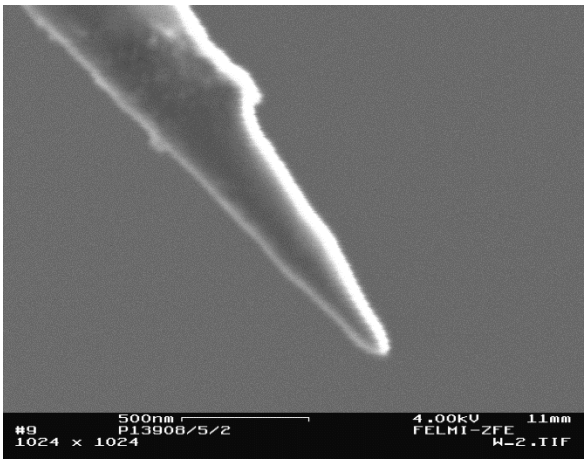

(e) 6 V (No. 3)

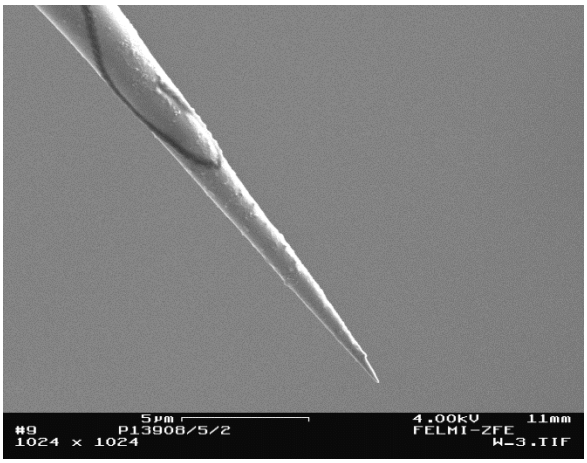

(f) Overview of the nanotip (No. 3)

Figure 59: Tungsten nanotips, which are etched with the parameters according to Table 3.

6. Summary

In this master thesis, a workflow has been developed for the preparation of nanotips for electron tomography by electrochemical polishing.

The process was tested with two different materials. First, a nickel-based superalloy (Inconel 718) is used. The finished nanotip has to fulfill the strict requirements for electron tomography, for example in order to use EELS, the typical diameter of a tip should be below 100 nm over a large length. Therefore, the parameter to quantify the quality of the nanotips in this thesis is defined as the length of the tip with a diameter below 100 nm, which we called the *critical length*.

The requirement on the specimen before starting the electrochemical polishing is that its cross section is symmetric, in order to avoid blade-shaped nanotips. A square cross section is applicable to avoid blade-shaped nanotips. The initial shape of the alloy are cylinders with a diameter of around 1 cm and a length of around 1 cm. First, a disk is cut out of the cylinder with a rotating saw. From this disk, pins are cut out with the wire saw. The square cross section is then achieved by a mechanical polishing process.

These symmetric specimens are crimped in commercial copper sleeves to fix them at the electrochemical polishing device and the TEM specimen holder during the measurement of the tomography.

The polishing process includes three different steps:

- *Thinning*
- *Neck-In*
- *Drop-Off*

For the nickel-based alloy, two electrolytes were used:

- Electrolyte 1: 20 vol% perchloric acid (60 wt%) in acetic acid
- Electrolyte 2: 2 vol% perchloric acid (60 wt%) in 2-butoxyethanol

With the first electrolyte, all three steps are executed. A major problem at his stage is a non-uniform layer formation on the specimen. This layer consists mainly of niobium and molybdenum. These residues can disturb the further etching steps due to the asymmetry caused by the layer. It was observed that at a low voltage of 4 V no layer is formed. At an intermediate voltage of 20 V, a thick layer is formed. At 35 V, the formation of the layer is again reduced.

The nanotip is finished with the second electrolyte. The *Neck-In* step and the *Drop-Off* step are repeated with the solution of perchloric acid in 2-butoxyethanol on the same tip, which was previously made with the first electrolyte. Single precipitates are also formed on the surface during the *Neck-In* and the *Drop-Off*. These residues contain niobium and titanium and they are often found near the finished nanotip. Such irregularities can eliminate the usage of the nanotip for electron tomography or APT.

The asymmetry of the starting cross section does not have or has only a small influence on the final thickness of the nanotip. Deviations from an ideal square cross section between 0 µm and 30 µm show no great influence on the final quality of the tip. However, large deviations of the cross section can lead to blade-shaped tips. Thus, the mechanical polishing step during the sample preparation is still necessary.

The *Drop-Off* voltage with the second electrolyte has a big influence on the quality of the nanotip. The *critical length* decreases with increasing voltage. The potential for the *Drop-Off*, with which the best nanotips were fabricated, is a voltage of 4 V. At even lower voltages, selective dissolution is observed, which leads to an irregularly shaped nanotip with holes.

Another influence, which affects the quality of the nanotips, is the numbers of attempts required for a successful *Drop-Off*. The *critical length* shortens with a higher number of attempts.

Every tip can be re-sharpened, if the tip is long enough. For the re-sharpening, the *Neck-In* and *Drop-Off* steps have to be repeated.

*Critical length*s of a successful electrochemical polishing process are in the range of 100 nm up to 400 nm. However, due to the large number of influences, several attempts might be necessary to achieve this. With re-sharpening, several preparation attempts are possible for a single specimen, where each attempt takes only 5 to 10 minutes.

Tomography of a nanotip is performed, whose end is ball-shaped by the recoil at the *Drop-Off*. In addition, a carbon layer of around 30 nm is formed at the surface, which makes the tip unusable for APT. Nevertheless, the tip is successfully reconstructed by using the HAADF signal. The precipitates are clearly visible, but to allocate them to the correct phase, an EELS or EDX analysis is needed. This is outside the scope of this thesis, but such experiments will be performed in the near future.

The re-sharpening process is also used for the second material on a tungsten needle, which is used for micromanipulation. Because of its fine-shaped end, a *Thinning* step is not necessary. The used electrolyte is an aqueous base with potassium hydroxide, called caustic potash. The concentration is kept small, because high etching rates are not necessary and better nanotips are accomplished with lower concentrations. Nanotips are obtained within 5 minutes.

7. Outlook

Electrolyte

A major problem for the nanotip fabrication of the nickel-based superalloy Inconel 718 occurs at the *Thinning* step. During the etching, a layer forms with the electrolyte of the perchloric acid in acetic acid. This layer consists mainly of oxides or salts of niobium and molybdenum, which can disturb the further etching process. Precipitates are also often observed during the etching process with the electrolyte of perchloric acid in 2-butoxyethanol. These residues contain oxides of niobium and titanium. Such precipitates are often found near the finished nanotip. Niobium does not dissolve as well as the other elements in the used electrolytes.

Such problems can be reduced by modifying the electrolyte to increase the solubility of niobium. According to [9] (see appendix), a solution of hydrofluoric acid in nitric acid can be used to etch niobium. Instead of using only perchloric acid in acetic acid or 2-butoxyethanol, an additional percentage of hydrofluoric acid could be added to the solutions. This could reduce the formation of the niobium layer and precipitates. However, hydrofluoric acid is a contact poison and it should be handled very carefully.

Pulsed-Etching

The electric circuit could be modified to enable pulsed etching. A pulsed voltage could reduce strong bubble formation at high voltages, which is caused by the electric resistance heating. Furthermore, instead of the used *Drop-Off* method, the specimen is immersed in the electrolyte and single pulses can be used until the front end breaks off. This can enhance the reproducibility, and reduces the recoil at the *Drop-Off*, because the surface tension does not pull the front end. If the region of interest is not in the front end of the nanotip, or the nanotip needs a bigger tip angle for the use as micromanipulator needle, single pulses can be used as post-treatment for a controlled blunting of the tip. Such experiments with pulsed etching were already done in reference [21].

The modification for pulsed etching can be achieved for instance with an Arduino board. A possible configuration is shown in Figure 60. For this purpose, an N-channel MOSFET is used to control the electric etching circuit. The Arduino can switch the etching current by setting the gate voltage on high or low. A similar electric circuit is used in reference [35]. Instead of using a differentiator and flip-flop to cut off the circuit once, an Arduino is used to pulse the etching current.

Two modes can be implemented. The first mode is triggered by a switch (S1). As long as the switch is pressed, the output of the Arduino frequently gives pulses with pre-specified pulse-on and pulse-off durations. The second mode can be achieved with a button (S2). If the button is pressed, the Arduino gives a single pulse with a pre-defined duration. This can be controlled by detecting the positive flank of input D2.

Both switches are connected to a pulldown resistor. This means, if the switch is open, the input signal is zero. The pulldown resistor is necessary, because the input would be “floating” at opened switches without it. This is a non-defined state, where the voltage is between the maximum and minimum value. The resistor before the MOSFET is protecting the Arduino of inrush current, because the MOSFET has a small capacitance. The digital output of the Arduino can switch between high (+5 V) and low (0 V). Therefore, the MOSFET should be a logical transistor. The transistor also has to be selected in accordance to the dissipated power. The resistor, which is parallel to the electrolytic cell, is again preventing the “floating” of the output. [50]

A suitable program needs to be written for pulsing the Arduino output.

The button for DC-etching can be still used by connecting it parallel to the MOSFET (drain and source). Both etching modes, pulsed and DC, could be used with this setup.

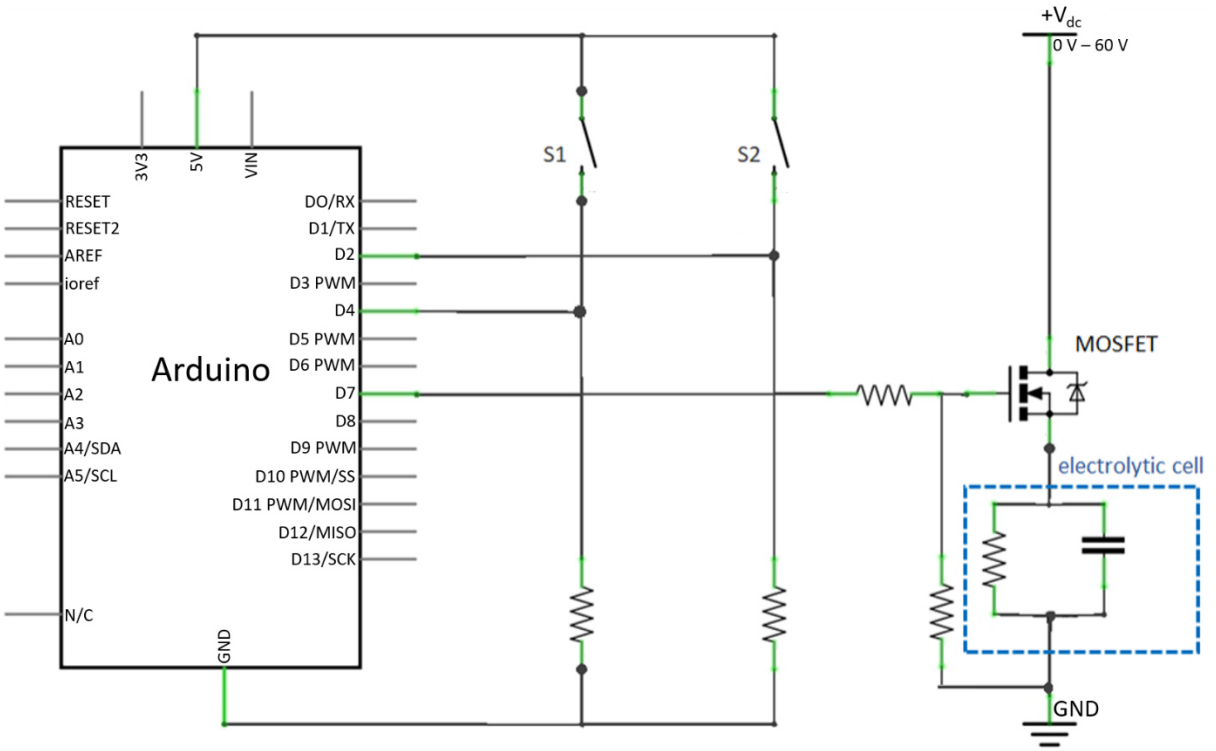

Figure 60: Electric circuit for pulse etching, which is controlled by an Arduino.

Reverse voltage

Due to the oxidation at the anode, an oxide layer is always present at the finished nanotip. The thickness of the oxide layer can be reduced by a controlled reversed bias, like in reference [29]. However, re-deposition must be avoided. The suitable parameters of the amplitude of the bias and the duration of the reverse process have to be adjusted for each material and electrolyte as well.

8. Bibliography

[1] S. Wischnitzer, *Introduction to electron microscopy*. Elsevier, 2013.

[2] H. Kohl and L. Reimer, *Transmission electron microscopy: physics of image formation*. Springer, 2008.

[3] S. J. Pennycook and P. D. Nellist, *Scanning transmission electron microscopy: imaging and analysis*. Springer Science & Business Media, 2011.

[4] J. I. Goldstein, D. E. Newbury, J. R. Michael, N. W. M. Ritchie, J. H. J. Scott, and D. C. Joy, *Scanning electron microscopy and X-ray microanalysis*. Springer, 2017.

[5] B. Hafner, "Scanning electron microscopy primer," *Charact. Facil. Univ. Minnesota-Twin Cities*, pp. 1–29, 2007.

[6] A. J. Schwartz, M. Kumar, B. L. Adams, and D. P. Field, *Electron backscatter diffraction in materials science*. Springer, 2000.

[7] M. L. Rivers and S. R. Sutton, "A wavelength dispersive detector for synchrotron x-ray fluorescence microprobe analysis," *Rev. Sci. Instrum.*, vol. 66, no. 2, p. 1454, 1995.

[8] M. Weyland and P. A. Midgley, "Electron tomography," *Mater. Today*, vol. 7, no. 12, pp. 32–40, 2004.

[9] B. Gault, M. P. Moody, J. M. Cairney, and S. P. Ringer, *Atom probe microscopy*, vol. 160. Springer Science & Business Media, 2012.

[10] W. R. McKenzie, E. A. Marquis, P. R. Munroe, and A. M. V Díaz, "Focused ion beam sample preparation for atom probe tomography," *Microsc. Sci. Technol. Appl. Educ.*, vol. 3, pp. 1800–1810, 2010.

[11] C. G. Zoski, *Handbook of electrochemistry*. Elsevier, 2006.

[12] A. J. Bard, L. R. Faulkner, J. Leddy, and C. G. Zoski, *Electrochemical methods: fundamentals and applications*, vol. 2. wiley New York, 1980.

[13] G. Yang, B. Wang, K. Tawfiq, H. Wei, S. Zhou, and G. Chen, "Electropolishing of surfaces: theory and applications," *Surf. Eng.*, vol. 33, no. 2, pp. 149–166, 2017.

[14] W. Plieth, "4 - Ad-Atoms and Underpotential Deposition," W. B. T.-E. for M. S. Plieth, Ed. Amsterdam: Elsevier, 2008, pp. 101–142.

[15] W. Han and F. Fang, "Fundamental aspects and recent developments in electropolishing," *Int. J. Mach. Tools Manuf.*, vol. 139, pp. 1–23, 2019.

[16] S.-J. Lee, Y.-M. Lee, and M.-F. Du, "The polishing mechanism of electrochemical mechanical polishing technology," *J. Mater. Process. Technol.*, vol. 140, no. 1–3, pp. 280–286, 2003.

[17] A. J. Melmed, "The art and science and other aspects of making sharp tips," *J. Vac. Sci. Technol. B Microelectron. Nanom. Struct. Process. Meas. Phenom.*, vol. 9, no. 2, pp. 601–608, 1991.

[18] K. Sieradzki, "Curvature effects in alloy dissolution," *J. Electrochem. Soc.*, vol. 140, no. 10, pp. 2868–2872, 1993.

[19] R.-D. Grimm and D. Landolt, "Salt films formed during mass transport controlled dissolution of iron-chromium alloys in concentrated chloride media," *Corros. Sci.*, vol. 36, no. 11, pp. 1847–1868, 1994.

[20] C. A. Huang, Y. C. Chen, and J. H. Chang, "The electrochemical polishing behavior of the Inconel 718 alloy in perchloric–acetic mixed acids," *Corros. Sci.*, vol. 50, no. 2, pp. 480–489, 2008.

[21] W.-T. Chang, I.-S. Hwang, M.-T. Chang, C.-Y. Lin, W.-H. Hsu, and J.-L. Hou, “Method of electrochemical etching of tungsten tips with controllable profiles,” *Rev. Sci. Instrum.*, vol. 83, no. 8, p. 83704, 2012.

[22] Y. Wang, Y. Zeng, X. Wang, N. Qu, and D. Zhu, “Liquid Membrane Electrochemical Etching: Twin Nano-Tips Fabrication for Micromachining,” *Int. J. Electrochem. Sci*, vol. 11, pp. 4174–4185, 2016.

[23] A. Chandra, M. Sumption, and G. S. Frankel, “On the mechanism of niobium electropolishing,” *J. Electrochem. Soc.*, vol. 159, no. 11, pp. C485–C491, 2012.

[24] S. Magaino, M. Matlosz, and D. Landolt, “An impedance study of stainless steel electropolishing,” *J. Electrochem. Soc.*, vol. 140, no. 5, pp. 1365–1373, 1993.

[25] K. Popov, B. Grgur, and S. S. Djokić, *Fundamental aspects of electrometallurgy*. Springer, 2007.

[26] D. J. Larson, T. J. Prosa, R. M. Ulfig, B. P. Geiser, and T. F. Kelly, “Applications of the Local Electrode Atom Probe,” in *Local Electrode Atom Probe Tomography*, Springer, 2013, pp. 201–247.

[27] M. Fotino, “Tip sharpening by normal and reverse electrochemical etching,” *Rev. Sci. Instrum.*, vol. 64, no. 1, pp. 159–167, 1993.

[28] B.-F. Ju, Y.-L. Chen, and Y. Ge, “The art of electrochemical etching for preparing tungsten probes with controllable tip profile and characteristic parameters,” *Rev. Sci. Instrum.*, vol. 82, no. 1, p. 13707, 2011.

[29] J. Lindahl, T. Takanen, and L. Montelius, “Easy and reproducible method for making sharp tips of Pt/Ir,” *J. Vac. Sci. Technol. B Microelectron. Nanom. Struct. Process. Meas. Phenom.*, vol. 16, no. 6, pp. 3077–3081, 1998.

[30] O. L. Guise, J. W. Ahner, M.-C. Jung, P. C. Goughnour, and J. T. Yates, “Reproducible electrochemical etching of tungsten probe tips,” *Nano Lett.*, vol. 2, no. 3, pp. 191–193, 2002.

[31] A. Bani Milhim and R. Ben Mrad, “Electrochemical etching technique: Conical-long-sharp tungsten tips for nanoapplications,” *J. Vac. Sci. Technol. B, Nanotechnol. Microelectron. Mater. Process. Meas. Phenom.*, vol. 32, no. 3, p. 31806, 2014.

[32] R. Hobara, S. Yoshimoto, S. Hasegawa, and K. Sakamoto, “Dynamic electrochemical-etching technique for tungsten tips suitable for multi-tip scanning tunneling microscopes,” *e-Journal Surf. Sci. Nanotechnol.*, vol. 5, pp. 94–98, 2007.

[33] Y. Zeng, Y. Wang, X. Wu, K. Xu, and N. Qu, “Note: Buoyant-force assisted liquid membrane electrochemical etching for nano-tip preparation,” *Rev. Sci. Instrum.*, vol. 85, no. 12, p. 126105, 2014.

[34] Y. Wang, Y. Zeng, N. Qu, and D. Zhu, “Note: Electrochemical etching of cylindrical nanoprobes using a vibrating electrolyte,” *Rev. Sci. Instrum.*, vol. 86, no. 7, p. 76103, 2015.

[35] Y. Khan, H. Al-Falih, Y. Zhang, T. K. Ng, and B. S. Ooi, “Two-step controllable electrochemical etching of tungsten scanning probe microscopy tips,” *Rev. Sci. Instrum.*, vol. 83, no. 6, p. 63708, 2012.

[36] M. Kulakov, I. Luzinov, and K. G. Kornev, “Capillary and surface effects in the formation of nanosharp tungsten tips by electropolishing,” *Langmuir*, vol. 25, no. 8, pp. 4462–4468, 2009.

[37] J. P. Ibe *et al.*, “On the electrochemical etching of tips for scanning tunneling microscopy,” *J. Vac. Sci. Technol. A Vacuum, Surfaces, Film.*, vol. 8, no. 4, pp. 3570–3575, 1990.

[38] W. X. Sun, Z. X. Shen, F. C. Cheong, G. Y. Yu, K. Y. Lim, and J. Y. Lin, “Preparation of cantilevered W tips for atomic force microscopy and apertureless near-field scanning optical microscopy,” *Rev. Sci. Instrum.*, vol. 73, no. 8, pp. 2942–2947, 2002.

[39] N. Otsu, “A Threshold Selection Method from Gray-Level Histograms,” *IEEE Trans. Syst. Man. Cybern.*, vol. 9, no. 1, pp. 62–66, 1979.

[40] Q. Zhang and I. Couloigner, “Accurate Centerline Detection and Line Width Estimation of Thick Lines Using the Radon Transform,” *IEEE Trans. Image Process.*, vol. 16, no. 2, pp. 310–316, 2007.

[41] T. J. Atherton and D. J. Kerbyson, “Size invariant circle detection,” *Image Vis. Comput.*, vol. 17, no. 11, pp. 795–803, 1999.

[42] S. R. Deans, “Hough Transform from the Radon Transform,” *IEEE Trans. Pattern Anal. Mach. Intell.*, vol. PAMI-3, no. 2, pp. 185–188, 1981.

[43] Special Metals Corporation, “Datasheet INCONEL® alloy 718,” 2007.

[44] R. Lawitzki *et al.*, “Differentiation of γ’- and γ’’- precipitates in Inconel 718 by a complementary study with small-angle neutron scattering and analytical microscopy,” *Acta Mater.*, vol. 163, pp. 28–39, 2019.

[45] Royal Society of Chemistry (ChemSpider), “Perchloric acid ID 22669.” [Online]. Available: http://www.chemspider.com/Chemical-Structure.22669.html. [Accessed: 17-Sep-2019].

[46] Royal Society of Chemistry (ChemSpider), “Acetic acid ID 171.” [Online]. Available: http://www.chemspider.com/Chemical-Structure.171.html. [Accessed: 17-Sep-2019].

[47] D. C. Harris, C. A. Lucy, U. of N. C. at C. Hill., and D. of Chemistry., *Quantitative chemical analysis*. New York, NY: Freeman Custom Publishing, 2016.

[48] C. A. Huang and Y. C. Chen, “The effect of water content on the electropolishing behavior of Inconel 718 alloy in perchloric–acetic acid mixtures,” *Corros. Sci.*, vol. 51, no. 9, pp. 1901–1906, 2009.

[49] J. R. Rumble, D. R. Lide, and T. J. Bruno, *CRC handbook of chemistry and physics : a ready-reference book of chemical and physical data.* 2017.

[50] “Arduino Description: Digital Pins.” .

9. Appendix

9.1. Nanotip evaluation

This section contains the MATLAB code, which is used for the nanotip characterisation.

```
%% Nanotips_detection
% This script loads the image of the nanotip (tif-file) and analyze it. The
% part of the tip, which should be analyzed, can be cropped out. Results are
% the radius of curvature, tip angle and the length of the tip, where the
% diameter is below 100 nm. The boundary of the tip is saved as an image and
% a MATLAB-cell file. A txt-file is saved, which contains the evaluated
% values. Additionally, an image, that contains the original image with the
% calculated values is saved.

%% Script
close all; clear all;clc;

boundary = 1;             % tip angle and radius only with boundary
                          % calculated, instead of the original image

%% Settings
% scales
scale = 500;              % scale of the image
resolution = 1024;        % size of the image (1024 or 512)

% Reading image (path and name)
path = 'Nr8_D4_Alloy718_AQ';
name = 'D4_3';

%% Calculation

if scale == 500
    if resolution == 1024
        scale_I = 500/281;  % 500 nm scale [nm/px]
    elseif resolution == 512
        scale_I = 500/141;
    end
elseif scale == 200
    scale_I = 200/223;      % 200 nm scale [nm/px]
end

RGB = imread([path,'\',name,'.tif']); % loading image

% Check image size for correct scales
RGB_size = size(RGB);
disp(['Size of image: ',num2str(RGB_size(1)),' x ',num2str(RGB_size(2))])

% Cropping image
RGB_size = size(RGB);
I2 = imcrop(RGB);
close
RGB_size = size(I2);

% Increasing contrast
I4 = imadjust(I2);

% Creating binary image through intensity difference from tip to background
level = graythresh(I4);
bw = im2bw(I4,level); % Adjust threshold (level)
bw_i = imcomplement(bw);
```

```
bw_i = bwareaopen(bw_i, 1000);
A_i = bwconncomp(bw_i,4);
for j = 1: A_i.NumObjects
   length_area(j) = length(A_i.PixelIdxList{j});
end
jj = 1:A_i.NumObjects;
jj = jj(length_area ~= max(length_area));
for jjj = 1:length(jj)
    bw_i(A_i.PixelIdxList{jj(jjj)}) = 0;
end
bw_finish = imcomplement(bw_i);

% Smoothing edges
windowSize = 10;
kernel = ones(windowSize)/windowSize^2;
blurryImage = conv2(single(bw_finish),kernel,'same');
bw_finish = blurryImage > 0.5;

% Tip angle and radius by boundary image
if boundary == 1
    [b l] = bwboundaries(bw_finish);
    I_boundary = zeros(RGB_size);
    a = b{1};
    index_boundary = sub2ind(RGB_size,a(:,1),a(:,2));
    I_boundary(index_boundary) = 1;
    I_boundary = I_boundary(2:end,2:end);
    I4 = I_boundary;
end

% Radon transformation
theta = 0:0.1:180;
[R,xp] = radon(I4,theta);

% Finding maxima
R_size = size(R);
k = 0;
for i = 1:R_size(1)
    [pks, loc] = findpeaks(R(i,:));
    if ~isempty(pks)
        k = k+1;
        [pks_theta(k), index] = max(pks);

    end
end

[pks_total loc_x] = findpeaks(pks_theta);
[pks_sorted index_sorted] = sort(pks_total,'descend');

pks_finish = pks_sorted([1 2]); % Assumption 1. and 2. maxima are the tip
                                % angles
L = R == pks_finish(1);
L = L + (R == pks_finish(2));
[row col] = find(L);
theta_finish = theta(col);
x_finish = xp(row);

% Plotting radon-transformation
figure
imagesc(theta,xp,R); colormap(hot);
xlabel('\theta (degrees)');
ylabel('x^{\prime} ( pixes from center)');
```

```
title('R_{theta} (x^{prime})');
colorbar


% Finding the critical length
A = imrotate(bw_finish,-abs(theta_finish(1)+theta_finish(2))/2,'crop');
B = bwboundaries(A,8,'noholes');
C = B{1};
y_B = C(:,1);
x_B = C(:,2);

[y_Bmax loc_y] = max(y_B);

for i= 1:max(y_Bmax)
    x_i = x_B(y_B == y_Bmax-i);
    x_length = (x_i(1) - x_i(2))*scale_I;
    if x_length > 100
       y_i = y_Bmax-i;
       break
    end
end
z_bw = y_Bmax-y_i;
I_log = zeros(size(A));
I_log(y_i,x_i(1)) = 1;
I_log(y_i,x_i(2)) = 1;
A_log =
imrotate(I_log,abs(theta_finish(1)+theta_finish(2))/2,'bilinear','crop');
[y_A x_A] = find(A_log);
if numel(x_A) > 2 % Rotation of image can produce problems
   I_vec = (abs(y_A-circshift(y_A,1)) > 2);
   y_A = y_A(I_vec);
   x_A = x_A(I_vec);
end

% Measuring tip radius
[centers_0,radii_0] = imfindcircles(I4,[10 30],'ObjectPolarity','bright',
...
    'Sensitivity',1/100);
j = 2;
while isempty(centers_0) && j < 100
    [centers_0,radii_0] = imfindcircles(I4,[10
30],'ObjectPolarity','bright', ...
    'Sensitivity',j/100);
    j = j + 1;
end

if isempty(centers_0)
   disp('Tip/Circle not detected')
end

[radii loc] = max(radii_0);
centers = centers_0(loc,:);

% Line calculation for plotting
k = tan((theta_finish)*pi/180);
d_1 = max(x_A)-k(1)*min(y_A);
d_2 = min(x_A)-k(2)*max(y_A);

y_11 = 1;
y_12 = centers(2)-radii*sin(min(theta_finish)*pi/180);
x_11 = k(1)*1+d_1;
```

```
x_12 = k(1)*y_12+d_1;

y_21 = 1;
y_22 = centers(2)+radii*sin(max(theta_finish)*pi/180);
x_21 = k(2)*1+d_2;
x_22 = k(2)*y_22+d_2;

% Plotting

h_boundary = figure;
imshow(I2)
hold on
for kk = 1: length(b)
   boundary = b{kk};
   plot(boundary(:,2),boundary(:,1),'g','LineWidth',2)
end

figure
subplot(2,2,1)
imshow(RGB)
title('original image')
subplot(2,2,2)
imshow(I2)
title('cropped image')
subplot(2,2,3)
imshow(I4)
title('image for further calculations')
subplot(2,2,4)
I2_plot = insertShape(I2,'Line',[x_11 y_11 x_12
y_12],'LineWidth',2,'Color','blue');
I2_plot = insertShape(I2_plot,'Line',[x_21 y_21 x_22
y_22],'LineWidth',2,'Color','blue');
I2_plot = insertShape(I2_plot,'Line',[x_A(1) y_A(1) x_A(2)
y_A(2)],'LineWidth',2,'Color','yellow');
I2_plot = insertShape(I2_plot,'Circle',[centers
radii],'LineWidth',2,'Color','red');
imshow(I2_plot)
title('finished calculation')

figure
subplot(2,2,1)
imshow(I4)
title('image for further calculations')
subplot(2,2,2)
imshow(bw)
if edge_detection == 1
    title('binary image with edge detection')
else
    title('binary image with intensity detection')
end

subplot(2,2,3)
imshow(bw_finish)
title('finished image')
subplot(2,2,4)
imshow(A)
hold on
line([x_i(1) x_i(2)],[y_i y_i])
title('rotated image with 100nm marker')
hold off
```

```
disp('*************************************************')
disp('*************************************************')
disp(['tip radius: ',num2str(ceil(radii*scale_I)),' nm'])
disp('*************************************************')
disp(['tip angle: ',num2str(abs(theta_finish(1)-theta_finish(2))),' °'])
disp('*************************************************')
disp(['tip length with diameter below 100 nm:
',num2str(ceil(z_bw*scale_I)),' nm'])
disp('*************************************************')
disp('*************************************************')

% saving results in the results folder
[parentFolder deepestFolder] = fileparts('results');
newSubFolder = sprintf(['%s/',path,'-%s'],'results',deepestFolder);
if ~exist(newSubFolder,'dir')
    mkdir(newSubFolder)
end

fileID = fopen([newSubFolder,'/',path,'_',num2str(scale),'.txt'],'w');
fprintf(fileID,['tip radius: ',num2str(ceil(radii*scale_I)),' nm\n']);
fprintf(fileID,['tip angle: ',num2str(abs(theta_finish(1)-
theta_finish(2))),' °\n']);
fprintf(fileID,['tip length with diameter below 100 nm:
',num2str(ceil(z_bw*scale_I)),' nm']);
fclose(fileID);

imwrite(I2_plot,[newSubFolder,'/Calculated_',num2str(scale),'.png'])
print(h_boundary,[newSubFolder,'/Boundary_',num2str(scale),'.png'],'-dpng')

B = b{1};
B(B(:,1)==1,:) = [];
B(B(:,2)==1,:) = [];
b{1} = B;
b{2} = (theta_finish(1)+theta_finish(2))*pi/(2*180);

save([newSubFolder,'/',path,'_boundary_',num2str(scale),'.mat'],'b')
```